DOI 10.1007/s10778-019-00954-2
International Applied Mechanics, Vol. 55, No. 3, May, 2019

NONCLASSICAL PROBLEMS OF FRACTURE/FAILURE MECHANICS: ON THE OCCASION OF THE 50TH ANNIVERSARY OF RESEARCH (REVIEW). II

A. N. Guz

The principal results of research on some nonclassical problems of fracture/failure mechanics have been analyzed. These results have been obtained by the author and his followers at the Department of Dynamics and Stability of Continua of the S. P. Timoshenko Institute of Mechanics of the National Academy of Sciences of Ukraine (the NAS of Ukraine) during the last 50 years.

The nonclassical problems of fracture/failure mechanics are problems to which the approaches and criteria of classical fracture mechanics are not applicable. A distinguishing feature of the results obtained by the author and his followers is application of three-dimensional theories of stability, dynamics, and statics of solid mechanics to study the nonclassical problems of fracture/failure mechanics. The majority of other researchers have been using various approximate theories of shells, plates, and rods as well as other approaches to studying the nonclassical problems of fracture/failure mechanics.

The main scientific results of solving the eight nonclassical problems of fracture\failure mechanics obtained in the framework of the above mentioned approach (three-dimensional theories of solid mechanics) have been presented very briefly, with focus on the statement of problems, the analysis of corresponding experiments, the development of methods for their solution within the framework of approach under consideration, and the discussion of final results. The mathematical aspects of the methods for solving the mentioned problems and their computer-aided implementation have not been discussed in this review, with information on this subject briefly presented as annotation.

The following eight nonclassical problems of fracture\failure mechanics (results by the author and his followers) are considered in this review:

– first problem is fracture of composites compressed along the reinforcement;

– second problem is short-fiber model in stability and fracture of composites under compression;

– third problem is end-crush fracture of composites under compression along the reinforcement;

– fourth problem is brittle fracture of cracked materials with initial (residual) stresses acting along the cracks;

– fifth problem is shredding fracture of composites stretched or compressed along the reinforcement;

– sixth problem is fracture of materials under compression along parallel cracks;

– seventh problem is brittle fracture of cracked materials under dynamic loads (with contact interaction of the crack faces);

– eighth problem is fracture of thin-walled cracked bodies under tension with prebuckling.

About 523 monographs and papers published by the author and his followers on the eight nonclassical problems of fracture mechanics have been included in the references to this review.

This review consists of three parts. The first part is General Problems; it is published in *Prikladnaya Mekhanika* (55, No. 2, 2019). The second part is Compressive Failure of Composite Materials; it is

S. P. Timoshenko Institute of Mechanics, National Academy of Sciences of Ukraine, 3 Nesterova St., Kyiv, Ukraine 03057; e-mail: guz@carrier.kiev.ua. Translated from Prikladnaya Mekhanika, Vol. 55, No. 2, pp. 5–91, May–June, 2019. Original article submitted March 26, 2018.

published in *Prikladnaya Mekhanika* (55, No. 3, 2019). The third part deals with other nonclassical problems of fracture mechanics.

Keywords: nonclassical problems of fracture/failure mechanics; research during the last 50 years; author and his students; S. P. Timoshenko Institute of Mechanics; department of dynamics and stability of continuum

Preface. This review gives a brief description and analysis of the principal results on nonclassical problems of fracture/failure mechanics obtained by the author and his followers during the last 50 years at the Department of Dynamics and Stability of Continuum of the S. P. Timoshenko Institute of Mechanics of the National Academy of Sciences of Ukraine.

The review is divided into three parts. The first part is General Problems; it is published in *Prikladnaya Mekhanika* (55, No. 2, 2019) and includes Introduction and Secs. 1 and 2. The second part is Compressive Failure of Composite Materials; it is published in *Prikladnaya Mekhanika* (55, No. 3, 2019) and contains Secs. 3–5. The third part deals with others nonclassical problems of fracture/failure mechanics and comprises Secs. 6–10 and a list of references, which is common for all the parts.

Throughout the review (Secs. 1–10), for all formulas, figures, remarks, and tables, double numeration is used (within each section) so that the first number denotes section and the second one (separated from the first with a dot) corresponds to object's number in the current section. Thus, it is possible to consider the results of each section almost independently of the other sections, navigating by the list of references, which is common for the whole article and presented in the third part.

3. Problem 1. Fracture of Composites Compressed along the Reinforcement. We will briefly (omitting the mathematical aspects, as mentioned in the Introduction) the basic results on the problem obtained at the Department Dynamics and Stability of Continua of the S. P. Timoshenko Institute of Mechanics over the period from 1967 to 1968. We will also discuss some historical aspects, including some relevant experimental results.

The major results on the problem obtained at the Department of Dynamics and Stability of Continua are presented in the monographs [30, 31, 54, 57, etc.]. Originally, these results were published in articles included in the lists of references to the monographs [30, 31, 54, 57]. The problem discussed here was addressed in the following papers: [8, 10, 11, 20, 25, 26, 29, 42, 50, 53, 55, 61, 62, 75, 80–82, 91–100, 132–138, 167–170, 175, 213–220, 241–246, 278, 290–293, 302, 307, 310, 311, 313, 319, 321, 326, 347, 350, 354–361, 374–376, 396, 400–406, 409, 410, 425–429, 440–443, 448, 485, 487–491, 503, 505–507, 512–516, 518, 524–527, 534, 538, 539, 559, 566–571] and the following conference proceedings: [318, 320, 323, 329, 335, 445, 446, 460, 469, 471–475, 477–480, 517, 519–523].

Five doctoral dissertations related to this problem were defended by I. Yu. Babich, V. N. Chekhov, Yu. N. Lapusta, I. A. Guz, and E. A. Tkachenko. It should be noted that I. A. Guz's dissertation also included results on the sixth problem 6 (fracture of materials compressed along parallel cracks).

3.1. General Concept and Main Research Areas. The literature on the fracture mechanics of composites currently recognizes the paper [271] published in 1960 to be the first to describe the phenomenon of microbuckling of fibers as a mechanism of fracture of a fibrous composite under compression. This phenomenon was repeatedly validated by experiments in a number of research centers (see Sec. 3.2). This allows us to accept the following general concept.

3.1.1. General Concept. The initial stage (start) of fracture of composites modeled, in continuum approximation, by orthotropic materials and compressed along the axes of material symmetry is microbuckling. The propagation of fracture, which originates near macro- and microinhomogeneities, is determined by the behavior of perturbations in the theory of stability used. The theoretical ultimate compressive strength and theoretical ultimate compressive strain are critical load and critical strain predicted by the theory of stability.

Remark 3.1. The basic concept in the fracture mechanics of composites compressed along the axes of material symmetry is similar to the situation in the mechanics of structural members (rods, plates, shells, etc.) where buckling is the initial stage of structural failure of structural members compressed along their axes of symmetry.

Thus, we will consider unidirectional fibrous (Fig. 3.1) and laminated (Fig. 3.2) composites, composites made of them by cross winding or laying up, and other composites compressed along the axes of symmetry. For consistent and rigorous application of the general concept, we will formulate the existence condition for the microbuckling phenomenon in a structural member made of a certain composite. Denote:

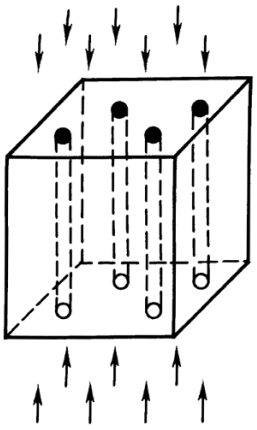

Fig. 3.1

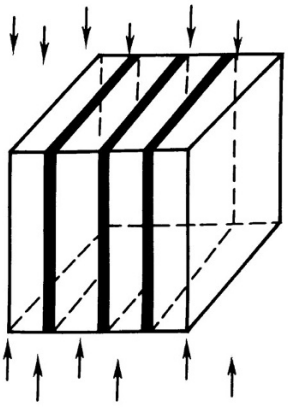

Fig. 3.2

p_{cr} is the critical load causing microbuckling in the composite;
p_{cr}^{sm} is the critical load causing buckling of the structural member;
L is the typical (minimum) size of the structural member;
l_{cr} is the microbuckling half-wavelength in the composite.
With this notation, the microbuckling conditions are expressed as

$$p_{cr} < p_{cr}^{sm}, \quad l_{cr} << L. \tag{3.1}$$

If one of conditions (3.1) fails, then the failure mechanism defined by the general concept does not occur under continuously changing load in a specific case being considered (shape of structural member + properties of composite).

The concept of microbuckling was for the first time introduced in the paper [224] published in 1963 and studied in the plane case of theory 5 (theory of incremental deformation [222]), which was analyzed in Sec. 2.2. Later, microbuckling was studied in the spatial and plane cases for compressible and incompressible materials with general constitutive equations in a unified general form for theories 1, 2, and 3 (as termed in Sec. 2.2). Specific results were obtained for both piecewise-homogeneous medium and continuum. The above-mentioned results on microbuckling are presented in the monographs [30, 31, 49, 54, 57, 334]. Preliminarily, these results were published in papers that are partially included in the list of references to these monographs and the present review. For the continuum model of composites, various cases of microbuckling (internal instability) were addressed in [57, Vol. 2, Ch. 2, Sec. 4].

When the piecewise-homogeneous material model is used, the critical load and microbuckling modes are usually analyzed, considering the second inequality in (3.1), for composites of specific structure that occupies an infinite space. After solving the appropriate eigenvalue problems for "infinite" composite, the dependence of the load parameter p on the wave number α is determined:

$$p = p(\alpha), \quad \alpha = \pi \frac{h}{l}, \tag{3.2}$$

where h is the typical geometrical parameter of the composite (h is the minimum thickness of plies in a composite laminate (Fig. 3.2) or the fiber radius in a unidirectional fibrous composite (Fig. 3.1)); l is the microbuckling half-wavelength (along plies and fibers) in the composite.

We may now conclude that microbuckling in a composite cannot occur for arbitrary relationship (3.2). As an illustration, the curves A and B in Fig. 3.3 represent two types of relationship (3.2). Since the curve A has a well-defined minimum, the value of p_{cr} can be found by minimizing the first expression in (3.2), and the values of α_{cr} can be found from the expression $p_{cr} = p(\alpha_{cr})$. Thus, if (3.2) is represented by the curve A in Fig. 3.3, we can determine the critical load p_{cr} and the buckling mode corresponding to the wave number $\alpha_{cr} = \pi h l_{cr}^{-1}$. Note that for the curve A, the following relations hold:

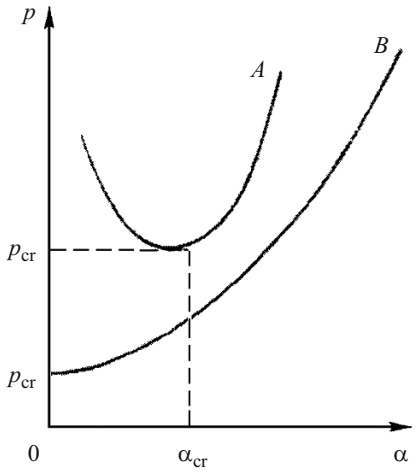

Fig. 3.3

$$\alpha_{cr} \neq 0, \quad l_{cr} \neq \infty. \tag{3.3}$$

With (3.3) and (3.2) represented by the curve *A* in Fig. 3.3, conditions (3.1) are used for those structural members (their dimensions) in which microbuckling occurs in the composite they are made of.

The curve *B* in Fig. 3.3 is a monotonic curve; hence, by minimizing expression (3.2) we get the formula $p'_{cr} = p(0)$, and

$$\alpha_{cr} = 0, \quad l_{cr} = \infty. \tag{3.4}$$

From expressions (3.4) it follows that if (3.2) is represented by the curve *B* in Fig. 3.3, it is impossible to determine the microbuckling mode in the composite. Thus, if (3.4) is represented by the curve *B* in Fig. 3.3, then microbuckling does not occur in the composite. According to the second expression in (3.4) and the curve *B* in Fig. 3.3, the second condition in (3.1) is satisfied for no structural member; hence, only the whole structural member can buckle.

Thus, microbuckling in the composite does not occur if the dependence of the load parameter p on the wave number α (the first expression in (3.2)) is represented by the curve *B* in Fig. 3.3. For the curve *A* in Fig. 3.3 and α_{cr} slightly different from zero, microbuckling in structural members does not occur too because of the second condition in (3.1) since $l_{cr} \to \infty$. This should be taken into account in analyzing this phenomenon in specific composites.

The general concept and procedure of its application make discussed above allow us to obtain (using the TLTSDB) and analyze results related to problem 1 (fracture in composites compressed along reinforcement) and other nonclassical problems of fracture/failure mechanics of composites. For example, such an approach is applicable to the infinite-fiber model in the mechanics of composites with buckling modes periodic along reinforcement (fibers, plies). There are two approaches to the solution of problem 1 using the general concept. They are briefly discussed below (in Secs. 3.1.2 and 3.1.3).

3.1.2. First (Approximate) Approach. The first approach employs various approximate design models and assumptions in studying microbuckling in composites, which is the initial stage (start) of fracture of composites under compression. This approach has not been analyzed appropriately in the basic problems, if at all possible. In this connection, any results obtained with the first approach should be treated with caution because they are results of theoretical studies based on approximate design models and assumptions used without appropriate analysis and discussion.

The author of the present review, as well as the authors of the review [65] published in 2016 did not intended to provide a systematic review and analysis of publications related to the first approach because there are many published results on the mechanics of composites and fracture mechanics obtained with the first approach. The objective of the present section (Sec. 3.1.2) as well as Sec. 1.2.2.1 in [65] is to classify results obtained with the first approach, to formulate the basic assumptions typical for the first approach, and to review the first publications on the first approach.

The assumptions widely used by the first approach can be divided into five groups.

1. A fibrous composite is modeled by a composite laminate, and the plane case is considered.

2. To analyze the stability of reinforcement (fibers, plies), wide use is made of applied one- and two-dimensional theories of stability of thin-walled systems (rods, plates) based on the Bernoulli hypotheses, Kirchhoff–Love hypotheses, etc. Such theories are known to be applicable only to the description of relatively long-wave buckling modes.

3. As a rule, the fact that the matrix (binder) also takes up a compressive load is ignored. This assumption can be made because the reinforcement is much stiffer than the matrix. Thus, the matrix can be considered unloaded. For some composites, including those with low concentration of reinforcement, this assumption is very approximate.

4. The interaction between the matrix (binder) and the reinforcement (fibers, plies) is described approximately. To describe the interaction between the matrix and a fiber, the matrix is frequently modeled by a coaxial cylinder (a part of the matrix). A one-dimensional model of the matrix can be used as well.

5. The interface conditions between the reinforcement and the matrix are satisfied approximately, frequently without any explanation.

If one of these assumptions is made, other assumptions are introduced automatically. To illustrate this situation, we will consider the following example. For example, if it is assumed that compression of a composite does not affect the matrix and induces stresses in the reinforcement (third group of assumptions), then it is also assumed that the interface conditions between the matrix and the reinforcement (fifth group of assumptions) are satisfied approximately. The matter is that the initial assumption automatically means that the matrix and reinforcement can freely slip relative to each other along the fibers in the subcritical state (before buckling) and are perfectly bonded during buckling.

Certainly, the assumptions of the five groups and other assumptions used by the first approach can be further analyzed, but such an analysis is not intended here. Let us discuss some historical aspects related to the use of the first approach.

It is currently agreed that the first theoretical results on the phenomenon mentioned in the publication [271] in 1960 were reported in the paper [551] published in English in 1965 and in Russian as [161] in 1967. It should be noted that the papers [551, 161] use in one way or another approximate assumptions from the five groups mentioned above. The papers [551, 161] are well-known and recognized in the world's literature on the mechanics of composites and fracture mechanics, despite the approximateness of the results reported in them. For example, these results were included as the paper [162] in the first part of the seventh volume of the seven-volume treatise on fracture [160]. Moreover, these results were included in the eight-volume treatise on composites [127] and in the collective monograph [163] published in Russian in 1970.

It should be noted that these results had not been planned to be included in the collective multivolume monographs [247, 248], which had been planned to be published by Elsevier in 2006. This followed from promotional materials available to the author at the end of 2006. Also, the results reported in [551, 161] were not included in the four-volume book on fracture mechanics [146] published in 1988–1990.

Currently, in addition to the paper [551] published in 1965, many articles on the first approach have been published, of which noteworthy are the papers [556] of 1966, [553] of 1967, [493] of 1966, [494] of 1970, and [162] of 1976. These articles and others are included in the lists of references to [54, 57, 64, 65]. In the monograph [174] with reference to [162], these results are called the Dow–Gruntfest–Rosen–-Schuerch theory (as the authors of the publications [271] of 1960, [551] of 1965, and [556] of 1966). Some results on the first approach are reviewed in [557] published in 1996.

This completes the brief discussion of the results on the first approach.

3.1.3. Second (Rigorous and Consistent) Approach. The second approach involves studies of the first phenomenon (microbuckling) of composites and the second phenomenon (surface or near-surface instability (buckling in surface or near-surface layers)) of composites, which are the initial stage (start) of fracture of compressed composites according to the general concept, which was formulated in Sec. 3.1.1 for the first phenomenon and will be formulated in Sec. 3.1.3 for the second phenomenon. To study the first and second phenomena, the second approach employs the three-dimensional linearized stability theory of deformable bodies (TLTSDB), briefly outlined in Sec. 2.

It should be noted that the second phenomenon was not studied with the first approach. Apparently, with the approximate models and assumptions 1–5 specified in Sec. 3.1.2 and used in the first approach, it is very difficult to construct any theory adequately describing so small-scale phenomenon as surface or near-surface instability in a compressed composite.

3.1.3.1. Internal Fracture (Microbuckling). The second approach employs rigorous and consistent methods based on the TLTSDB rather than approximate design models and assumptions 1–5 used by the first approach (Sec. 3.1.2). Thus, specific results obtained with the second approach can be used to validate the results obtained with the first approach.

The second approach made it possible to obtain specific results for a series of classes spatial and plane problems of the fracture mechanics of compressed composites using piecewise-homogeneous material and continuum models. Brief comments

on the first approach (piecewise-homogeneous material model) and the second approach (homogeneous material model with effective parameters resulting from the application of homogenization) will be given in Sec. 1.4.1.

The first approach (piecewise-homogeneous material model) applies the basic relations of the TLTSDB to each element of the reinforcement and matrix, at the interface between which the stress and displacement vectors are continuous. Numerous results were obtained for unidirectional fibrous composites under uniaxial compression (along fibers) (Fig. 3.1) and for composite laminates (Fig. 3.2) under uniaxial or biaxial compression along plies.

The second approach (homogeneous material model with effective parameters) applies to composites of various structure with one symmetry plane, two or three mutually perpendicular planes of material symmetry along the normals to which uniaxial, biaxial, or triaxial compressive forces act. For these conditions (material properties + loading conditions), a continuum theory of fracture of composites (identification of nonlocal disturbances in the material) was constructed, and methods for determining the theoretical ultimate strength under uniaxial loading and for plotting surfaces of theoretical ultimate strength under biaxial and triaxial loading were developed.

3.1.3.2. Near-Surface Fracture (Microbuckling of Near-Surface Plies of Composite). The concept of surface instability was for the first time introduced in the paper [223] published in 1963 and studied in the plane case of theory 5 (theory of incremental deformation [222]), which was analyzed in Sec. 2.2. When a half-plane is compressed along its boundary, its equilibrium state undergoes instability [223] near the surface, the buckling modes decaying with distance it. In the author's opinion, this phenomenon should be called near-surface instability rather than surface instability because buckling occurs in plies near the surface and the amplitude of the buckling modes decreases with distance from the surface. In this connection, we will use the term "near-surface fracture" ("near-surface instability," microbuckling in near-surface plies).

Later, near-surface instability was studied in the spatial and plane cases for compressible and incompressible materials with general constitutive equations in a unified general form for theories 1, 2, and 3 (as termed in Sec. 2.2). Specific results were obtained for both piecewise-homogeneous medium and continuum. The above-mentioned results on near-surface instability are presented in the monographs [30, 31, 49, 54, 57, 334]. Preliminarily, these results were published in papers that are partially included in the list of references to these monographs and the present review.

In the general case, we consider composites of different structure modeled by orthotropic materials, assuming that these materials have free surface that is parallel to one of the planes of orthotropy. When compression is parallel to the free surface and along one or two perpendicular axes, microbuckling can occur in near-surface plies of the composite with buckling modes decaying with distance from the free surface. This phenomenon is called surface instability or near-surface instability. The above results make it possible to formulate the general concept for near-surface fracture (taking into account the presence of the free surface) similar to the general concept formulated in Sec. 3.1.1 for compressed composites (regardless of the free surface).

General Concept. In composites that are modeled by orthotropic materials, that have free surface (parallel to one of the planes of orthotropy), and are compressed in parallel to the free surface in one or two mutually perpendicular directions, the initial stage (start) of near-surface fracture is near-surface instability. In analyzing the further development of this failure mechanism, it is necessary to consider its possible interaction with other failure mechanisms. The theoretical ultimate compressive strength and theoretical ultimate compressive strain are critical load and critical strain predicted by the TLTSDB.

The general concept allows developing the mechanics of near-surface fracture of composites under compression, studying near-surface instability near the free boundary of the composite using the TLTSDB (second approach according to Sec. 3.1.3). This type of study cannot be effectively made with the first approach (Sec. 3.1.2).

This completes the brief discussion of the second approach (see the two remarks below for additional details).

Remark 3.2. The above reviews of the first approach (Sec. 3.1.2) and the second approach (Sec. 3.1.3) are far from being even very brief. The discussions in Secs. 3.1.2 and 3.1.3 are should be regarded as brief characteristics of the approaches. The basic results obtained with the second approach will be briefly reviewed in Sec. 3.3. Section 3.2 will present experimental results on microbuckling of composite under compression and fracture of composites compressed along reinforcement (Problem 1 as termed in Sec. 1.3).

Remark 3.3. The monographs [90, 423] and the papers [348, 424] and other papers from the list references to the monographs outline the foundations of the mechanics of polymer-matrix nanocomposites, including the principles of the mechanics of polymer-matrix composites and some divisions on the dynamics, stability, and statics of nanocomposites. For example, foundations of the fracture mechanics of polymer-matrix nanocomposites under compression, which is based on the TLTSDB and can be considered as a development of the results related to the second approach (Sec. 3.1.3) are outlined in [90, 423].

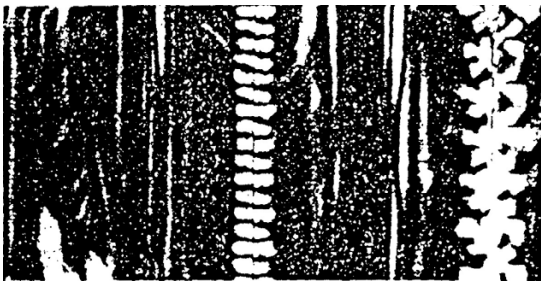

Fig. 3.4

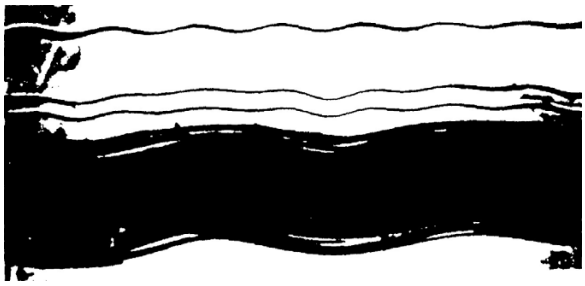

Fig. 3.5

3.2. Analysis of Experimental Results on Compression of Composites. There have been many experimental and theoretical studies on the compression of composites, which follows from the list of references to the present review. An example is the review [572] published in English in 1996 in the journal Prog. Aerospace Sciences and having a list of 133 references. Experimental results on the fracture of composites under compression are reviewed in [572]. Interestingly, the paper [271] is considered in the review [572] as a pioneering publication on the effect of the microbuckling mechanism on the fracture of a composite under compression.

The goal of this section is to review experimental results confirming the existence of the phenomenon (microbuckling of compressed composite) and to review experimental results characterizing the fracture composites compressed along the reinforcement. Such an analysis was performed in the monographs [30] in 1971, [54] in 1990, [57] in 2008, [64] in 2015, and in [65] in 2016, with different coverage of publications. The monograph [57] provides the greatest amount of evidences on the two issues. Note that the monographs [90, 423], which formulate the principles of the mechanics of with polymer-matrix nanocomposites, also present experimental results on the stability of nanotubes in polymer matrix under compression.

3.2.1. Experimental Results on Microbuckling in Compressed Composites. It should be noted that microbuckling is not observed in homogeneous materials. It is only typical for composites (as for structurally inhomogeneous materials whose internal structure is described at different scales during analysis). The structural homogeneity or inhomogeneity of a material is mainly determined by the scale of the processes, which, in turn, is determined by the variability of fields of mechanical variables (stresses, strains, etc.) with the space variables.

In analyzing experimental results on microbuckling in composites, it is necessary to take into account the following. It is very difficult to experimentally observe (record) pure microbuckling in composites compressed along reinforcements (fibers, filler) because insignificant or significant fracture also occurs at the very beginning of microbuckling. In this connection, the existence of microbuckling in a compressed composite is usually proved by conducting special experiments.

Fibers (reinforcement) are placed in epoxy (or other) resin that is allowed to polymerize at certain temperature; after that the resin cools down to certain temperature and sets. In almost all cases, compression occurs as the matrix (resin, binder) shrinks upon setting or as the composite cools down. Since the thermal-expansion coefficient of the fibers and matrix, which are coupled, are different, the fibers are subject to compressive loads.

These experiments were conducted at various centers of science at various times. The results of such experiments have been published.

These experimental results were, apparently, reported for the first time in [161] in Russian (in 1967) and in [551] in English (in 1965). In this connection, we will discuss the results from [161, 551]. For example, Fig. 3.4 shows a photoelastic pattern for three E-glass fibers (diameters 0.13, 0.09, 0.013 mm) in an epoxy resin matrix polymerized at a temperature of 120 °C. The photoelastic pattern in Fig. 3.4 is periodic (with a great number of periods), which is indicative of a sinusoidal (along the fibers) buckling mode. Note that Fig. 3.4 corresponds to [161, Fig. 3.20]. These results were obtained by the photoelastic method.

Later, related experimental results were obtained at many centers of science, using also other resin (matrix) curing methods.

We will now discuss, as an example, experimental results for thermochemically setting resin (matrix) in which glass fibers and strands floated before curing. These results for 0.01 mm glass fibers were published in [290] in 1982. Figure 3.5 [290] shows (50x magnification) results for separate fibers and a fiber strand after thermochemical curing of resin (matrix). It can be seen that the entire strand and individual fibers take on a well-defined periodic sinusoidal (along the fibers) shape after curing of the resin (matrix).

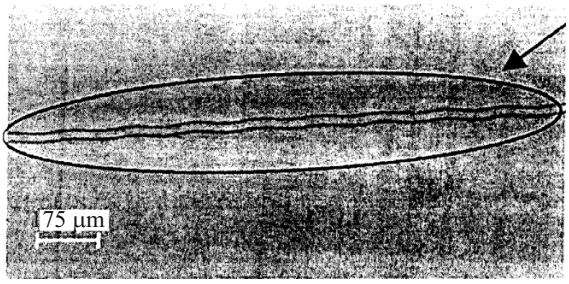

Fig. 3.6

It should be noted that Figs. 3.4 and 3.5 (published in the second half of the 20th century) represent the microbuckling of composites reinforced with glass fibers 0.13, 0.09, 0.013, and 0.01 mm in diameter. Related experimental studies for composites reinforced with fibers made of other materials and compressed after shrinkage of resin (matrix) due to its curing or cooling have also been conducted now (in the beginning of the 21st century).

An example of experimental results for carbon fibers in a polymer matrix (epoxy resin) is the paper [498] published in 2004. Figure 3.6 [498] shows a periodic sinusoidal buckling mode with a great number of periods. The buckling mode in Fig. 3.6 (the scale in μm is indicated in the lower left corner) was recorded in [498] at the 68th second of cooling of the polymer matrix.

Along with the results for glass and carbon fibers in Figs. 3.4–3.6, experimental results on microbuckling in various composites have been published recently.

Thus, the above and related experimental results for quite long fibers in a matrix (binder) confirm that the phenomenon of microbuckling can occur in composites. The buckling modes in Figs. 3.4–3.6 are periodic (along the fibers) sinusoidal and have a great number of periods. In this connection, the boundary conditions at the ends of reinforcements (fibers) cannot strongly affect buckling modes and critical loads and strains. The above experimental results validate the long-fiber model.

Remark 3.4. The experimental studies represented in Fig. 3.4–3.6 were specially set up (i.e., are model experiments) to prove the existence of the microbuckling phenomenon in composites. Taking a close look at Fig. 3.4–3.6, we can observe microbuckling in pure form, i.e., without signs of failure, because no separation of the fibers from the matrix can be seen. This situation appears quite important and should be given appropriate attention in analyzing the experimental results on the fracture of compressed composites in the next section.

Remark 3.5. Here we address various processes in mainly unidirectional composites compressed mainly, along the fibers, i.e., in the direction of preferential reinforcement. In continuum approximation, these composites, as well as cross-ply composites, are modeled by orthotropic homogeneous materials. Thus, we will use the orthotropic model to study compression along the axes of symmetry of materials. A similar situation occurs under loading of other types, as in compressed zones of various bent structural members and in other cases. When various structural members (rods, plates, and shells) are compressed along the axes of (geometrical and material) symmetry, the basic mechanism of structural failure is buckling.

3.2.2. Experimental Results on the Fracture of Composites Compressed along Fibers. Here we will analyze experimental results on compressed composites after fracture. These results are images of an already destroyed material that, naturally, do not show the initial stage (start) of fracture. Hence, no experimental studies have yet been made of the entire fracture process under compression, from microbuckling (initial stage (start) of fracture) in the composite to the fragmentation of the composite (final stage of fracture). Such studies have not also been made of most fracture processes in other materials under other types of loads.

Thus, we will analyze the fracture behavior of compressed composites using scaled-up images of an already destroyed composite. The experimental studies to be discussed are focused on composites the compressed along the axes of material symmetry (along fibers in unidirectional composites, in the direction of preferential reinforcement in cross-ply composites, and in the perpendicular direction to the plane of preferential reinforcement in cross-ply composites). We will analyze specific features of fracture behavior under loading of the type being considered.

It should be noted these specific features are observed in compression not only in the direction of preferential reinforcement, but also in the perpendicular direction. The above situation can be illustrated by results from the paper [21] published in 1968, such as Fig. 3.7 from [21]. In [21], a glass-fiber laminate uniaxially compressed in the perpendicular direction to the reinforcement plane was considered. Figure 3.7 shows that fracture occurred in planes perpendicular to the load direction,

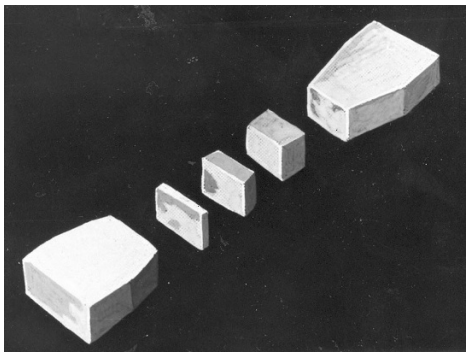

Fig. 3.7

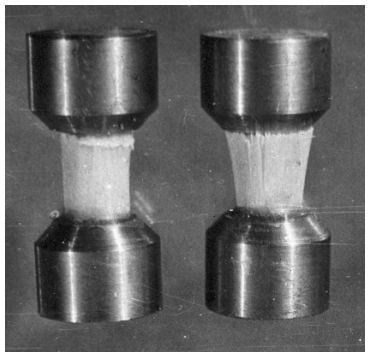

Fig. 3.8

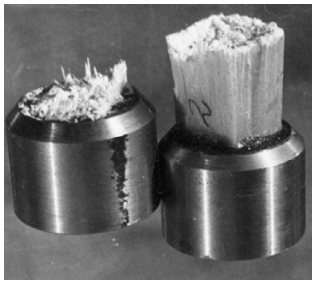

Fig. 3.9

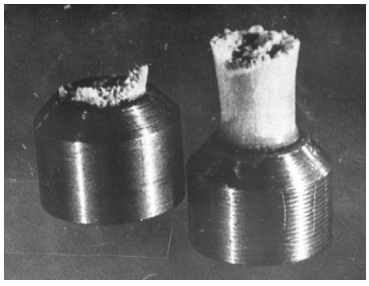

Fig. 3.10

causing the material to fragment. Fracture of such composites along planes almost perpendicular to the uniaxial compressive load is a specific feature.

Results on the fracture behavior of unidirectional fiberglass-reinforced plastic specimens compressed along the fibers are presented in [396] published in 1969. These results were obtained at the Institute of Mechanics of the Academy of Sciences of the USSR (currently the S. P. Timoshenko Institute of Mechanics).

Cylindrical specimens 10 mm in diameter and 45 mm in height and 15×15×70 mm prismatic specimens (Fig. 3.8) were cut out from glass-fiber-reinforced plastic plates made by winding over a metal mandrel followed by hardening under a press at a specific pressure of 1 MPa. NS-55/6 alkali-free glass fibers with wax emulsion as a sizer were used as reinforcements (filler), and EFB-4 epoxy-phenolic binder was used as a matrix. The fraction of the matrix by weight was 26.6%, the degree of polymerization being 89.9%. The techniques of making and testing the specimens are detailed in [57, Vol. 1, pp. 189–191; 396].

It should only be noted that the crushing of the ends of compressed specimens was avoided by putting metal rings on the specimens at their ends and filling them with cold-setting epoxy resin. As a result, the specimen length not covered by the rings was 1.5 to 2 of the linear dimension of the cross-section. Figures 3.9 and 3.10 show the fracture behavior of specimens of circular and square cross-sections, respectively. After fracture, the specimens were easily split into the two fragments shown in the figures. Note that fracture commonly occurred near the metal rings, which is possibly due to the initial local fracture caused by cutting extreme fibers.

The fracture (Fig. 3.8) of unidirectional fiberglass-reinforced plastic specimens compressed along the fibers propagates along planes almost perpendicular to the fibers and to the line of action of the compressive load.

Thus, the fracture of unidirectional fiberglass-reinforced plastic compressed along the fibers and compressed glass-fiber laminate compressed in the perpendicular direction to the reinforcement planes propagates along planes almost perpendicular to the line of action of the uniaxial compressive load. This situation is a specific feature of the type of fracture under consideration. Note that in both cases (Figs. 3.7–3.10), the specimens are compressed along the axes of material symmetry. Additional considerations on the fracture process can be found in [57, Vol. 1, p. 191].

Note that the experimental results in Figs. 3.7–3.10 represent fiberglass-reinforced plastics with polymer matrix. Related experimental studies were also conducted for other composites.

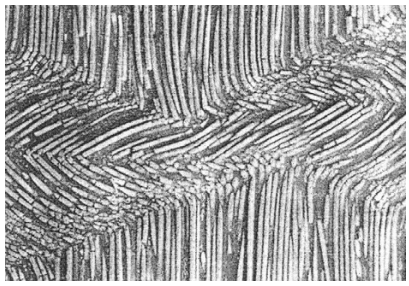

Fig. 3.11

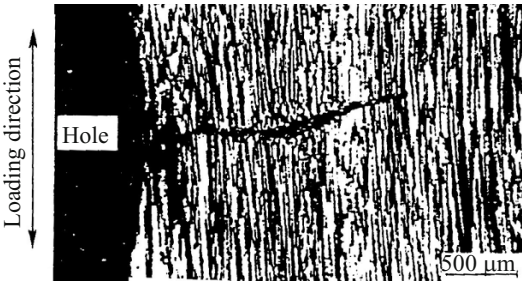

Fig. 3.12

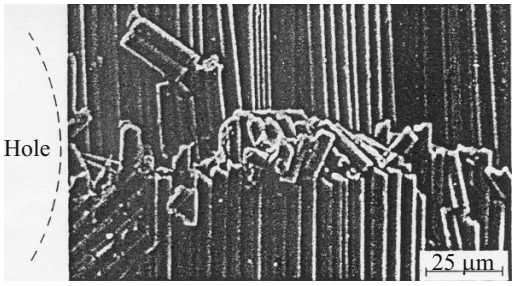

Fig. 3.13

The paper [558] published in 1985 reports experimental results for a composite with an aluminum matrix reinforced with and compressed along unidirectional sapphire fibers. Figure 3.11 [558] shows a scaled-up image of fracture in the metal-matrix composite (sapphire fibers + aluminum) uniaxially compressed along unidirectional sapphire fibers. The fracture is localized in a relatively narrow zone. A plane drawn through the middle of the fracture zone in Fig. 3.11 is almost perpendicular to the line action of the compressive load.

Thus, when both fiberglass-reinforced plastics with polymer matrix (Figs. 3.8–3.10) and metal-matrix composites (Fig. 3.11) are compressed along reinforcement, fracture occurs or propagates almost transversely to the line of action of the compressive load, which is a specific feature of this type of fracture. However, fracture of this type does not occupy the entire volume of the material instantaneously though it begins with microbuckling in the composite. It is quite natural that this type of fracture may arise near any microinhomogeneity (discontinuity) and then proceed as describe above. In this connection, it is of interest to study the propagation of fractures near a macroinhomogeneity in a composite compressed along the fibers.

The paper [362] published in 1991 reports experimental results (Figs. 3.12–1.15) on the propagation of fractures from a circular hole in a composite plate compressed along the reinforcement.

Figure 3.14 shows a design model and the axes of coordinates (compression is along the vertical axis 0y). The plates are composite laminates, each ply being a unidirectional fibrous material (epoxy resin matrix reinforced with carbon fibers).

The plies were laid up (along the 0z-axis in Fig. 3.14) so that the 0x- and 0y-axes (Fig. 3.14) were the axes of material symmetry (cross-ply laminate).

Hence, this composite can be approximated by an orthotropic material compressed along the 0y-axis, the 0x-, 0y- and 0z-axes (Fig. 3.14) being the axes of material symmetry. In the cross-ply laminates, the unidirectional fibers within most plies are aligned with the 0y-axis (Fig. 3.14). In this connection, the laminated plates can be considered to be mainly reinforced along the 0y-axis along which they are compressed.

In these experiments, fracture began at two points on the edge of the hole along the horizontal line in Fig. 3.14, i.e., the points at which the concentration of compressive macrostresses is maximum (stresses predicted by the orthotropic model). The fracture was further developed as two almost straight cracks filled with destroyed material, originated at points with maximum concentration of compressive stresses (Fig. 3.14) on the edge of the hole, and propagating almost transversely to the line of action of the compressive load. The behavior of cracks (fracture) is demonstrated by the electron microscope images in Figs. 3.12, 3.13, and 3.15 [558], where the scale in μm is indicated in the right lower corner. Figures 3.12, 3.13, and 3.15 show fracture propagating from the right point on the hole edge on the horizontal axis in Fig. 3.14. For example, Fig. 3.12 shows a crack

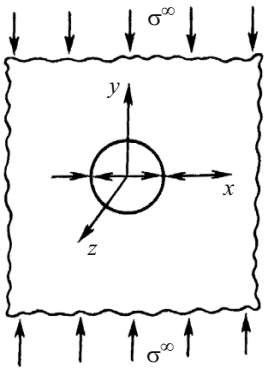

Fig. 3.14

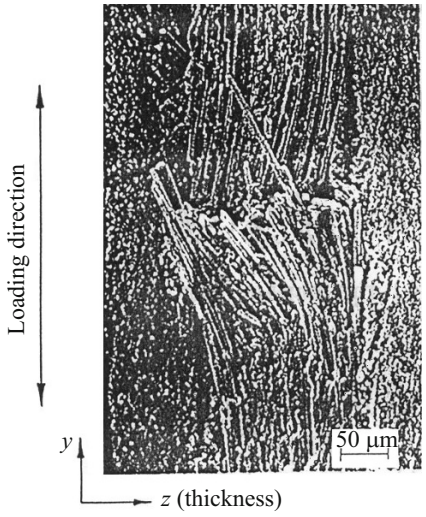

Fig. 3.15

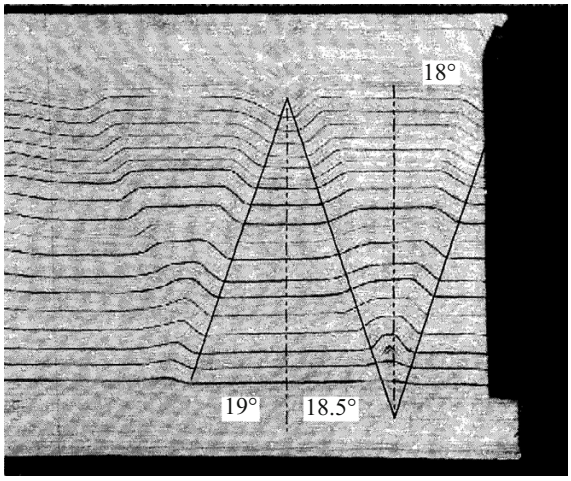

Fig. 3.16

propagating from the hole almost transversely to the line of action of the compressive load. Figure 3.13 shows (at 20× magnification) the damaged portion of the material in an extending narrow band, which can be modeled by a filled crack. In Figs. 3.12 and 3.13, the compressive load is on the order of 95% of the ultimate load for the plate with a hole. Figure 3.15 shows the structure of the damaged portion of the material on the edge of the hole throughout the thickness (along the 0*z*-axis in Fig. 3.14) of the plate. The following types of fracture can clearly be seen: breaking of fibers, bending of broken fibers toward the hole, delamination of the laminated material. In Fig. 3.15, the compressive load is on the order of 80–85% of the ultimate load for the plate with a hole.

It should be noted that in analyzing fracture in the internal structure of composites (as in Figs. 3.8–3.13 and 3.15), many authors mention only microbuckling and delamination. Actually, as can be seen from Fig. 3.13, there are much more failure mechanisms in the microstructure of a compressed composite such as breaking of a fiber within a crack, bending of a broken fiber, breaking of a fiber outside the crack, separation of a fiber from the matrix, fracture of the matrix, etc. These and similar failure mechanisms in the microstructure of a composite compressed along the axes of material symmetry manifest themselves only at subsequent stages of fracture, while the initial stage (start) of fracture is, apparently, microbuckling in the composite.

Fracture can, naturally, start near local inhomogeneities (such as cuts of fibers caused by the metal rings in Figs. 3.8–1.10) in the internal structure of the composite and near macroinhomogeneities (near the hole in Figs. 3.12–1.15). The local fracture in Figs. 3.7–3.15 then propagates along planes and surfaces that are almost perpendicular to the line of action of the compressive load. As repeatedly mentioned, this is a specific feature of the type of fracture under consideration.

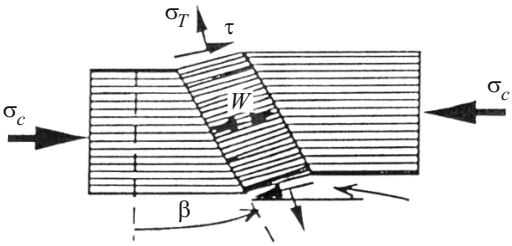

Fig. 3.17

The experimental results represented in Figs. 3.7–3.15 and related ones were published in 1968–1991. Such experimental studies are also conducted in the 21st century. Let us discuss, as an example, the experimental results published in [573] in 2004. These are results of experiments on a composite laminate consisting of 628 plies and subjected to compression along them. The number of plies is so great that we may assume that this material consists of an "infinite" number of plies. In this connection, the results in [573] may be considered to represent phenomena that occur in the internal structure of a composite laminate and do not depend on the boundary conditions for the whole laminate. It is, however, hardly possible to neglect the effect of boundary conditions, especially at the edges of the laminate, on all phenomena. Since the laminate was compressed along plies in [573], it may be assumed that the compression is along the axes of orthotropic symmetry (continuum approximation). Figure 3.16 [573, p. 1074, Fig. 2] shows the shapes taken by plies under different compressive loads. The figure demonstrates narrow bands of destroyed material (shown by slanting solid lines in Fig. 3.16) that are periodic along the horizontal axis along which the material is compressed. It should be noted that the narrow bands are inclined to the vertical axis through angles of 19°, 18.5°, and 18°, i.e., they are almost perpendicular to the horizontal axis. Thus, and the experimental results [573] presented in Fig. 3.16 confirm the conclusion drawn from the experimental results in Figs. 3.7–3.15. This conclusion is that uniaxial compression causes fracture propagating along planes and surfaces that are almost perpendicular to the line of action of the compressive load. As repeatedly mentioned, this is a specific feature of the type of fracture under consideration.

This completes the analysis of experimental results on the fracture of composites compressed along reinforcements (or along the axes of symmetry).

3.2.3. On Study of the Kinking Phenomenon. We will briefly discuss the kinking phenomenon following from the analysis of experimental results on compressed composites.

The paper [240] published in 1983 was the first to address the kinking phenomenon. Later, the kinking concept became popular, especially among English-speaking researchers, and was addressed in numerous articles of which noteworthy is the review [274] published in 1997 in Advances in Applied Mechanics published in the USA.

Kinking is manifested as narrow kink bands of destroyed material occurring in a composite compressed along the reinforcement. The kinking phenomenon is schematized in Fig. 3.17 (included in most publications on kinking), where W is the width of the kink band. Kink bands are usually analyzed using quite approximate design model and formulas.

The author briefly discussed the kinking phenomenon in the paper [383] published in 2006, the monograph [57] (Vol. 1, pp. 73–74) published in 2008, the monograph [64, pp. 94–96] published in 2015, and the review [65, pp. 46–47] published in 2016. Below, we will briefly formulate the conclusions made in these publications and correct typing errors and discrepancies.

Figure 3.17 represents an already destroyed specimen; in this connection, the start of fracture is not determined here. Thus, it is not inconceivable that the start of fracture, which resulted in a kink band, was determined by microbuckling of composite according to the general concept (Sec. 3.1.1). The above situation provides grounds for assigning the discussion of the kinking phenomenon to the first approach (Sec. 3.1.2). It should also be noted that kinking caused by compression along the horizontal axis (Fig. 3.17) is accompanied by displacement of the material on both sides of the kink band along the vertical axis (Fig. 3.17), which is a typical feature of the phenomenon.

Following [57, 64, 65, 383], we will make three remarks on kinking.

1. Kinking (Fig. 3.17) can occur if the boundary conditions at the ends of a specimen compressed along the horizontal axis allow displacements along the vertical axis.

2. An isolated kink band cannot occur during internal fracture in an unbounded material compressed along the axes of material symmetry. Inside a composite compressed along the axes of material symmetry, only alternating kink bands can exist to balance the disturbed stress–strain state.

3. By analyzing the kinking phenomenon, it is, apparently, impossible to uniquely identify the mechanisms responsible for the beginning (start) of fracture. One of the mechanisms responsible for the beginning (start) of fracture may be microbuckling according to the general concept (Sec. 3.1.1). It can be studied using the TLTSDB (Sec. 3.1.1).

As already mentioned in the above-mentioned publications, these remarks are just the point of view of the authors, and there may be other points of view.

The second remark is in a sense validated by the experimental results reported in [573] and presented in Fig. 3.17. The experimental results from [573] are briefly discussed here, near Fig. 3.17.

This completes the discussion of experimental results on the fracture of composites compressed along the axes of material symmetry.

3.3. Basic Results of the Second (Rigorous and Consistent TLTSDB-based) Approach. The second approach to the theoretical studies on the fracture mechanics of composites compressed along the axis of material symmetry was briefly characterized in Sec. 3.1.3. Main features of studies made with the second approach are as follows.

1. Approximate design models and assumptions (such those in Sec. 3.1.2) are not used.

2. The TLTSDB (Sec. 2) is used, which leads to results as accurate as those in other divisions of solid mechanics.

3. Due to feature 2, the results obtained with the second approach can be used to validate more approximate theories, including the first approach.

4. The foundations of the mechanics of near-surface fracture were developed using the second approach only.

5. The results of the second approach rigorously and consistently define the beginning (start) of either internal fracture or near-surface fracture of compressed composites.

3.3.1. Introductory Remarks. It was mentioned in Sec. 1.3 in describing Problem 1 that it is the author of the present paper and his followers who mainly used the second approach. The papers [25, 26] published in 1969 were the first to address the second approach. The publications (monographs, articles, and conference reports) that are included in the list of references to the present review and were prepared based on studies of the Department of Dynamics and Stability of Continua of the S. P. Timoshenko Institute of Mechanics are presented in the prologue of Sec. 3.

In what follows, we will discuss the basic results of the second approach that were originally reported in the papers and international conferences cited above and then included in the above and other monographs. The second approach was also used to study the behavior of elastic and elastoplastic, compressible and incompressible, isotropic, transversely isotropic, and orthotropic materials under compression along the axes of material symmetry. General results were obtained using elastic models for hyperelastic materials with arbitrary elastic potential and using elastoplastic models for materials with general constitutive equations. Specific results were obtained using elastic and elastoplastic models for materials with elementary constitutive equations. For elastoplastic models (of matrix and reinforcement), use is made of the generalized concept of increasing load outlined in Sec. 2.3.2. In this connection, results are formulated in a unified general form for elastic and elastoplastic models.

The second approach is used to study internal instability and near-surface instability in composites under an external "dead" load, which is typical for all publications on fracture mechanics. For the second approach based on elastic and elastoplastic models (including the generalized concept of increasing load), it was strictly proved that the sufficient conditions for the applicability of the static method of stability analysis (Sec. 2.4.2) are satisfied; therefore, the buckling problems are reduced to eigenvalue problems, i.e., the Euler method is used. This proof is also valid in the cases of near-surface instability under compression along reinforcements and near-surface instability near loaded ends. Thus, using the second approach is fully consistent with the standard and rigorous method of studying buckling by analyzing the behavior of small perturbations in linearized three-dimensional dynamics. The above conclusion, proof, and approach hold for elastic and elastoplastic models (including the generalized concept of increasing load) and do not hold for rheological models.

Remark 3.6. The present review (Sec. 3.3) does not include results for rheological models because of the following.

1. As indicated in Remark 2.9, for bodies with rheological properties, there are no general method and strict criterion that allow studies with the same generality and rigor as for elastic and elastoplastic bodies.

2. Recently, results have been obtained using three-dimensional equations for bodies with rheological properties that were derived using static method and an approximate failure criterion (Sec. 2.3.3). Since the criterion is approximate, it is not clear how general and reliable the results are.

3. The above conclusion, proof, and approach do not apply to bodies with rheological properties.

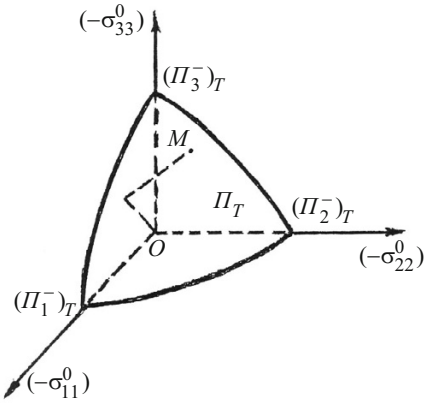

Fig. 3.18

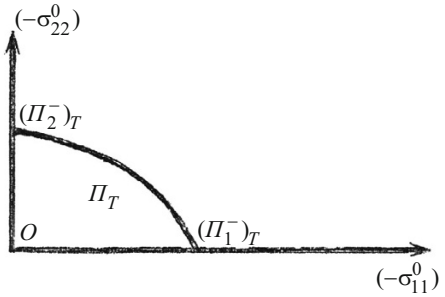

Fig. 3.19

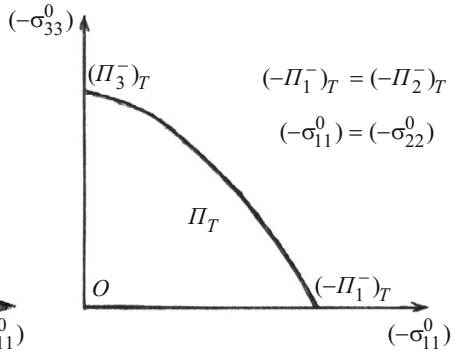

Fig. 3.20

Remark 3.7. Results of the second approach are intended for composites with polymer and metal matrix. For polymer-matrix composites, brittle fracture is analyzed by modeling the matrix by an elastic body, which is typical for composites at moderate temperatures and under relatively short-term load because the viscosity effects can be neglected in this case. For metal-matrix composites, ductile fracture is analyzed (using the generalized concept of increasing load) considering the stage of loading in which the entire matrix deforms plastically.

Remark 3.8. When the second approach is used to study microbuckling and near-surface buckling in a composite, it is assumed that the reinforcement and the matrix deform by equal amount along the line of compression (along the fibers in Fig. 3.1 for an unidirectional fibrous composite and along the plies in Fig. 3.2 for a laminated composite). The above is, apparently, the only condition that allows analyzing phenomena inside a composite. In experiments, such conditions are provided by compressing the composite with quite hard disks along the vertical axis in Fig. 3.2 with minimum friction along the horizontal axis in Fig. 3.2. In theoretical studies, the displacements of the reinforcement and the matrix along the vertical axis are assumed equal, and the shear stresses along the horizontal axis are assumed zero.

The second approach was used to develop the continuum theory of the fracture of composites based on a homogeneous material model with effective characteristics and the TLTSDB and the three-dimensional theory of fracture of unidirectional fibrous and laminated composites based on a piecewise-homogeneous material model with exact interface conditions and the TLTSDB. We will follow the monographs [54, 57] and the experience of brief discussion of these results in the review [65, pp. 27–45] published in 2016.

3.3.2. Continuum Fracture Theory. We will briefly discuss the main elements of the continuum theory of the fracture of compressed composites based on the continuum model with effective parameters and the TLTSDB. Brittle and ductile fracture will be addressed, taking into account Remark 3.7 for ductile fracture. The major results were obtained for internal fracture (microbuckling, internal instability) and near-surface fracture (near-surface microbuckling, near-surface instability).

3.3.2.1. Internal Fracture. Internal fracture should be studied for an unbounded composite. The propagation of fracture is described by a system of static TLTSDB equations (Sec. 2), which is elliptic for a compressible material under no load. In continuum approximation, the compressibility of a composite is due to the compressibility of either the reinforcement or the matrix.

Since the material under consideration is unbounded, internal fracture is considered as buckling of a microvolume. Thus, changes in a microvolume must be somehow manifested in a macrovolume, and they must not be local because only in this case, fracture of the whole specimen (macrofracture) will be observed. Such changes in a microvolume must manifest themselves in the properties that are independent of the boundary conditions because it is the fracture of the material (internal fracture corresponds to an "infinite" material) that is studied rather than the influence of the testing machines, the shape of the cross section, etc. It is obvious that changes in a macrovolume are determined by perturbed displacements that are described by the system of static TLTSDB equations (Sec. 2).

Thus, fracture may be considered to start when the solutions (except for homogeneous stress–strain states) of the system of static TLTSDB equations (Sec. 2) for a compressible material become independent of the boundary conditions (the material is unbounded) and nonlocal. This condition for the system of static TLTSDB equations (Sec. 2) can be satisfied only when this system is hyperbolic.

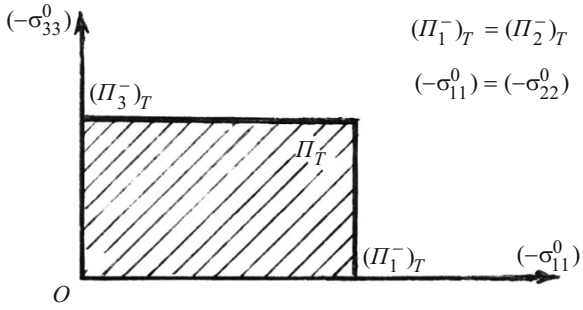

Fig. 3.21

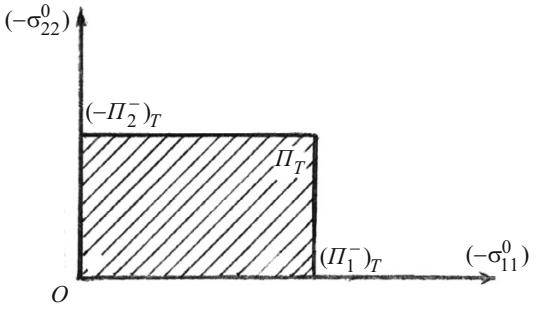

Fig. 3.22

Considering the foregoing, we can formulate the basic concept underlying the continuum theory of internal fracture of compressed composites as follows.

Basic Concept. The fracture onset can be identified with that instant in the history of loading when the system of static TLTSDB equations (for compressible materials) changes over from elliptic into hyperbolic, i.e., the system loses the property of ellipticity. The theoretical ultimate strength is determined from the same condition. The fracture of compressed composites occurs along characteristic planes and surfaces.

More details can be found in [57, Vol. 1, Ch. 2]. We will consider only some results.

Following the basic concept, we introduce the concept of surface Π_T of theoretical ultimate compressive strengths in the three-dimensional space of principal compressive stresses $((-\sigma_{11}^0), (-\sigma_{22}^0), (-\sigma_{33}^0))$. Π_T-surfaces are schematized in Figs. 3.18–3.20: Fig. 3.18 corresponds to the general case, Fig. 3.19 to the axisymmetric case, and Fig. 3.20 to the plane case. In Figs. 3.18–3.20, $(\Pi_j^-)_T$ denotes the theoretical ultimate uniaxial compressive strengths along the corresponding axes. Figure 3.19 shows a meridional section of the theoretical ultimate compressive strength surface because the Π_T-surface is a surface of revolution in this case. In three-dimensional space $((-\sigma_{11}^0), (-\sigma_{22}^0), (-\sigma_{33}^0))$ in Fig. 3.18, the loading path is shown by the dashed line *OM*. If the point *M* (Fig. 3.18) for the first time visits the Π_T surface during loading, the theoretical ultimate strength is achieved under triaxial compression.

In the case of brittle fracture (polymer-matrix composites), the surface Π_T was constructed explicitly for axisymmetric three-dimensional (Fig. 3.21) and two-dimensional (Fig. 3.22) problems.

Figure 3.21 for brittle fracture and Fig. 3.19 for the general case show a meridional section of the theoretical ultimate strength surface of revolution in the axisymmetric case. The hatched areas in Figs. 3.21 and 3.22 are the ellipticity domains of the static TLTSDB system of equations (Sec. 2); As the load parameters are varied within the ellipticity domain, no fracture occurs at certain values of the load parameters (see [57, Vol. 1, pp. 182–185] for more details).

In the case of ductile fracture, additional numerical studies are needed to draw theoretical ultimate compressive strength surfaces.

Also, it was strictly proved that brittle fracture propagates along planes perpendicular to the line of action of compressive loads. This theoretical fact is in agreement with the experimental results in Figs. 3.7–3.12.

We will now compare, following [57, Vol. 1, Ch. 2], the theoretical ultimate compressive strengths and theoretical ultimate compressive strains calculated with the continuum theory of internal fracture (Sec. 3.3.2.1) and found experimentally. We will consider a unidirectional fibrous composite (Fig. 3.1) that has no clearly defined fibrous structure in the cross-sectional plane ($x_3 = \text{const}$) and is subject to uniaxial compression along fibers (along the $0x_3$-axis). In this connection, such a composite is modeled by a transversely isotropic material with axis of isotropy directed along fibers (along the $0x_3$-axis). The indices "r" and "m" will be used to refer to the reinforcement and the matrix.

Brittle Fracture. Let us consider a unidirectional fibrous composite with epoxy resin matrix and quite stiff fibers, for which

$$E_r >> E_m . \tag{3.5}$$

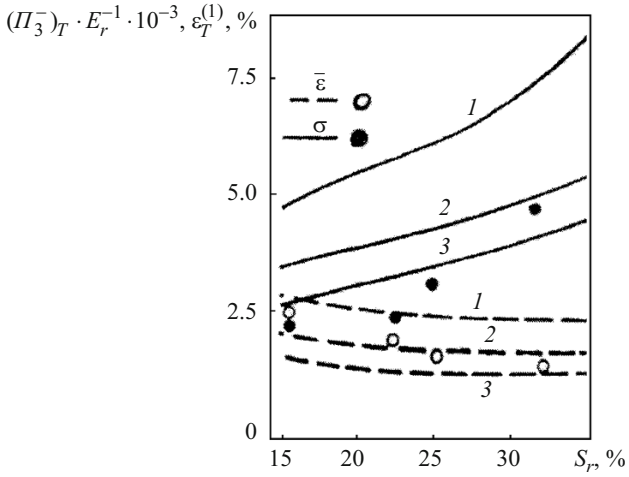

Fig. 3.23

We introduce the following notation: $(\Pi_3^-)_T$ is the theoretical ultimate strength in compression along one axis (in our case, the $0x_3$-axis); $(\Pi_3^-)_{ex}$ is the experimental ultimate strength in compression along the same axis. In the case of (3.5), the theoretical ultimate compressive strength (found using the continuum theory of fracture) for a composite with 50% volume fraction of unidirectional fibers ($S_r = S_m = 0.5$) was given in [57, Vol. 1, p. 192]:

$$(\Pi_3^-)_T = 2.09\text{–}3.00 \text{ GPa} \tag{3.6}$$

taking into account the spread in the properties of the epoxy resin specified in [57, Vol. 1, Table 0.1, p. 67]. The handbook [153] published in Russian in 1981 (and translated into English in [492] in 1978) gives (on p. 656) experimental ultimate strengths for various composites (different fibers for $S_r = S_m$). These results were also presented in [57, Vol. 1, p. 192] in the form

$$(\Pi_3^-)_{ex} = \begin{cases} 3.10\,\text{GPa} & \text{for boron fibers,} \\ 1.38\,\text{GPa} & \text{for high-strength carbon fibers,} \\ 1.03\,\text{GPa} & \text{for high-modulus carbon fibers.} \end{cases} \tag{3.7}$$

Comparing (3.6) and (3.7), we see that the theoretical ultimate compressive strengths and experimental ultimate uniaxial compressive strengths of polymer-matrix composites are in quite good agreement.

Ductile Fracture. Let us consider a unidirectional fibrous material with pure aluminum matrix and stainless-steel wire reinforcement using the experimental results from [548]. The theoretical ultimate strength and theoretical ultimate compressive strain (calculated using the continuum theory of internal fracture (Sec. 3.3.2.1)) were determined in the first approximation in the monograph [57, Vol. 1, Ch. 2, pp. 193–202] where the reinforcement was modeled by a linear elastic isotropic compressible body and the matrix was modeled by an elastoplastic isotropic incompressible body with power relationship between intensities of stresses and strains:

$$\sigma_u^m = A_m \varepsilon_u^{mk_m}, \quad A_m, k_m = \text{const}. \tag{3.8}$$

In [548], the experimental results were given for different concentrations in % of the reinforcement ($S_r = 4.1$, 11, 15.3, 21.2, 24.8, 32.8). To save space, Fig. 3.23 shows (in contrast to [57, Vol. 1, Ch. 2, Fig. 2.9, p. 206)] results only for the following values of S_r (%): 15.3, 21.2, 24.8, 32.8. In [57, Vol. 1, Ch. 2, Fig. 2.9, p. 206], the factor E_r^{-1} (E_r is Young's modulus of the reinforcement (stainless steel wire) according to (3.5)) was left out. This is corrected in Fig. 3.23.

In describing the plastic deformation of pure aluminum using formula (3.8), the following three approximations for A_m and k_m in (3.8) were used:

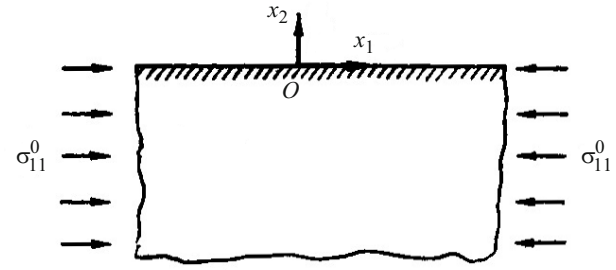

Fig. 3.24

$$1 \sim A_m = 100\,\text{MPa}, \quad k_m = 0.1,$$
$$2 \sim A_m = 100\,\text{MPa}, \quad k_m = 0.25,$$
$$3 \sim A_m = 68\,\text{MPa}, \quad k_m = 0.25. \tag{3.9}$$

The monograph [57, Vol. 1, Ch. 2, p. 207] cites publications that used approximations (1.10).

Figure 3.23 shows the dependence of the following quantities on S_r (volume fraction of stainless steel wire): dimensionless normalized theoretical ultimate compressive strength $(\Pi_3^-)_T^{(1)} \cdot E_r^{-1} \cdot 10^{-3}$ calculated in the first approximation (solid lines) and theoretical ultimate strain $\varepsilon_T^{(1)}$ calculated in % in the first approximation (dashed lines).

The curves in Fig. 3.23 corresponding to approximations (3.9) are numbered by *1*, *2*, and *3*. The experimental results from [548] are shown in Fig. 3.23 by full circles for the ultimate strength and by open circles for the ultimate strain. Note that approximation 2 was used in [548].

Figure 3.23 indicates that the satisfactory agreement between the theoretical and experimental results is observed for ultimate strengths when approximation 3 in (3.9) is used and for ultimate strains when approximation 2 in (3.9) is used.

This completes the discussion of the mechanics of internal fracture within the framework of the continuum theory of fracture (see [57, Vol. 1, Ch. 2] for more details).

3.3.2.2. Near-Surface Fracture. The continuum theory of near-surface fracture is based on the TLTSDB (Sec. 2) used to study a near-surface buckling mode within which displacements and stresses decay with distance from the boundary. Following the basic approach outlined in Sec. 3.3.1, we arrive at static TLTSDB problems (Sec. 2) for semibounded domains (eigenvalue problems in which eigenfunctions decay with distance from the boundary).

Here we discuss the continuum theory of near-surface fracture under compression along reinforcement. The continuum theory of near-surface fracture is detailed in [57, Vol. 1, Ch. 2, Sec. 2, pp. 209–224)]. As an example, Fig. 3.24 shows a design model for a plane problem, where $x_2 = 0$ is the free surface and the reinforcement is aligned with the $0x_1$-axis. The monographs [54, 57] detailed the continuum theory of near-surface fracture of composites under compression corresponding to near-surface buckling (near the free surface) under compression along the reinforcement. In this connection, this issue will not be discussed below in detail. In [54, 57], the results were presented for polymer-matrix composites (brittle fracture) and for metal-matrix composites (ductile fracture). The monograph [57, Vol. 1, Ch. 2, Sec. 2] also outlines the two-level continuum mesomechanics of fracture of compressed composites with cracks originating from the boundary of a hole.

In summary, it should be noted that the monographs [54, 57] rigorously proved the following condition for composites with polymer and metal matrix:

$$(\Pi_3^-)_T^{\Pi} < (\Pi_3^-)_T, \tag{3.10}$$

where the following notation is introduced in addition to $(\Pi_3^-)_T$ (theoretical ultimate strength in uniaxial compression): $(\Pi_3^-)_T^{\Pi}$ is the theoretical ultimate strength in uniaxial compression for near-surface fracture. Condition (3.10) is consistent with the commonly accepted fact that fracture begins on the surface of a material.

This completes the discussion of near-surface fracture within the framework of the continuum theory of fracture of compressed composites.

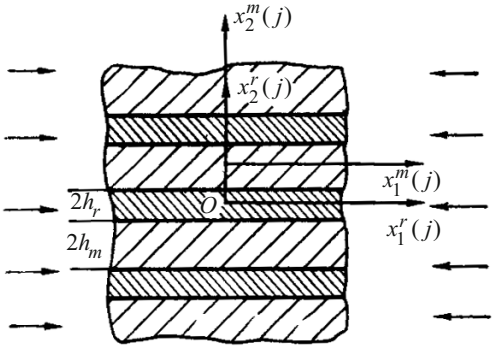

Fig. 3.25

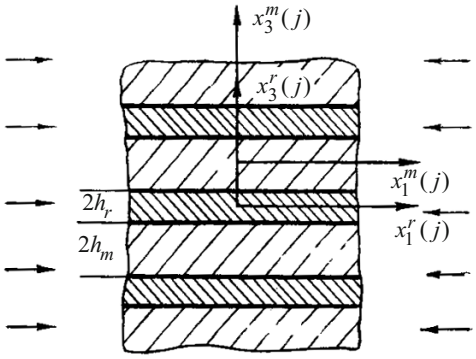

Fig. 3.26

Remark 3.9. In Sec. 3.3.2.1, it is shown that the experimental and theoretical ultimate strengths in uniaxial compression are in agreement for both brittle fracture (polymer-matrix composites) and ductile fracture (metal-matrix composites). This agreement is apparently due to the fact that the reinforcement and matrix of the composites analyzed were considered differ considerably in stiffness (conditions (3.5) are satisfied). For other composites, such good agreement is hardly achievable. It should be pointed out that the continuum theory of fracture is the most simple and convenient compared with any theories based on the piecewise-homogeneous material model for approaches. In some cases, the continuum theory appears in agreement with experiments. Historically, the paper [26] published in 1969 was the first to address the continuum theory of fracture.

This completes the discussion of the continuum theory of fracture of composites compressed along the axes of material symmetry.

3.3.3. Laminated Composite. Piecewise-Homogeneous Material. Here we will briefly discuss the mechanics of fracture of compressed composite laminates with polymer and metal matrices based on the piecewise-homogeneous material model. The TLTSDB (Sec. 2) is applied to each ply of the reinforcement and matrix, and continuity conditions for stresses and displacements are prescribed at the interfaces. The basic results were obtained for brittle and ductile fracture. In the latter case, the generalized concept of increasing load was used. In line with the basic approach outlined in Sec. 3.3.1, it is necessary to analyze the static equations and boundary conditions of the TLTSDB (Sec. 2) for a piecewise-homogeneous material (eigenvalue problem). The basic results were obtained for microbuckling [57, Vol. 1, Ch. 3] and for near-surface buckling [57, Vol. 1, Ch. 5]. These results were partially included in the monographs [30, 31, 54], and briefly in the review [65]. The results for composite laminates being discussed were preliminarily published in articles most of which are included in the list of references to the present review and in the list of papers related to second approach given in the prologue to Sec. 3 (see [30, 31, 54, 57] for more details on the published articles). Note that the results (characteristic determinants) for laminated composites are formulated in a unified general form for theories 1, 2, and 3 as termed in Secs. 2.2 and 2.3.

We will briefly discuss (following the brief review [65]) the basic results on the fracture mechanics of compressed composites obtained using the piecewise-homogeneous material model and the TLTSDB.

3.3.3.1. Internal Fracture. The internal fracture (internal instability) of an unbounded composite laminate (Fig. 3.2) is analyzed using the general solutions of the static TLTSDB equations and the procedure outlined in Sec. 3.1.1, taking into account the approach corresponding to Fig. 3.3. It should be noted that here we discuss results for composites with no defects at the interfaces (continuity of stresses and displacements at the interfaces).

Two- and three-dimensional problems were solved for laminated composites with polymer and metal matrices consisting of reinforcement plies (of equal thickness) and matrix plies (of equal thickness) that periodically alternate along the $0x_2$-axis (Fig. 3.25) in the case of plane problems and along the $0x_3$-axis (Fig. 3.26 corresponding to the plane $x_2 = 00$) in the case of spatial problems. In Figs. 3.25 and 3.26, the index "r" refers to reinforcement (filler, plies) and the index "m" refers to the matrix (binder, plies). The plies are made of orthotropic materials (or isotropic materials in a special case) in the plane case and of transversely isotropic materials (or isotropic materials in a special case) with the isotropy plane $x_3 = \text{const}$ (Fig. 3.26). In all cases, the characteristic determinants were obtained for materials described by general constitutive equations. Since the structure is periodic with period $2(h_r + h_m)$ along the vertical axis in Figs. 3.25 and 3.26, buckling modes with period T_k multiple of the period of the structure were analyzed,

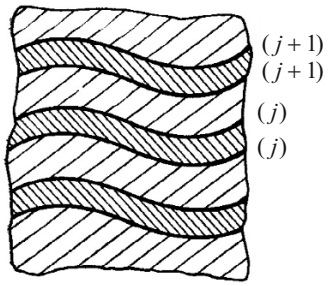

Fig. 3.27

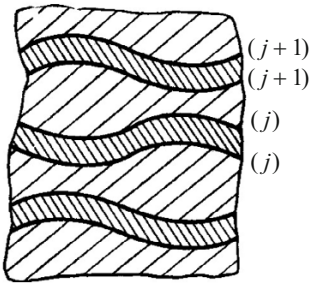

Fig. 3.28

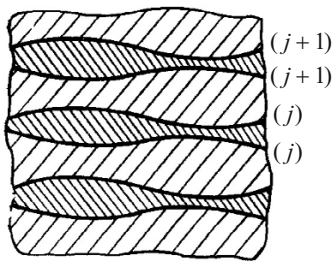

Fig. 3.29

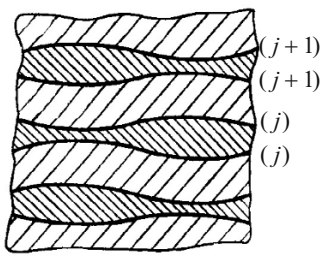

Fig. 3.30

$$T_k = 2k(h_r + h_m), \quad k = 1, 2, \ldots . \tag{3.11}$$

The method of solving plane (Fig. 3.25) and spatial (Fig. 3.26) problems of the internal fracture of composite laminates employs the static TLTSDB equations (Sec. 3.3.1) and the general solutions of the TLTSDB (Secs. 2.5.1 and 2.5.2). The following buckling modes are considered: trigonometric functions with an unknown wavelength along the lines of action of compressive loads (along the $0x_1$-axis for plane problems, Fig. 3.25; along the $0x_1$- and $0x_2$-axes for spatial problems, Fig. 3.26); solutions (based on general solutions of the TLTSDB) in x_2 for plane problems (Fig. 3.25) and in x_3 for spatial problems (Fig. 3.26) perpendicular to the plies for various types of symmetry (Figs. 3.27–3.30) and various types of periodicity according to (3.11). Applying the above solutions to satisfy the continuity conditions for stresses and displacements at the interface between the reinforcement and matrix yields characteristic determinants of the fourth order for plane problems and of the sixth order for spatial problems. Solving the characteristic equations, we obtain the dependence of load parameters on wave numbers. This dependence is minimized according to Sec. 3.1.1 and Fig. 3.5.

The first four modes called modes of the first, second, third, and fourth kinds were analyzed. These modes are schematized in Figs. 3.27–3.30. The buckling mode of the first kind has a period equal to the period of the structure ($k = 1$ in (3.11)) and is shown in Fig. 3.27; this mode corresponds to the shear mode, as termed in a number of publications.

The buckling mode of the second kind has a period equal to the double period of the structure ($k = 2$ in (3.11)) and is shown in Fig. 3.28; this mode corresponds to the tensile mode, as termed in a number of publications.

The buckling mode of the third kind has a period equal to the period of the structure ($k = 1$ in (3.11)) and is shown in Fig. 3.29.

The buckling mode of the fourth kind has a period equal to the double period of the structure ($k = 2$ in (3.11)) and is shown in Fig. 3.30.

In the plane and spatial cases, characteristic determinants were derived in closed form for the reinforcement and polymer and metal matrices of laminated composites described by general constitutive equations. The critical loads were obtained by finding numerically and minimizing the roots of the characteristic determinants. This approach helped to obtain numerous results for specific laminated composites with either polymer or metal matrix.

As an example, we will briefly discuss results for a composite laminate with isotropic plies, each modeled by a linear elastic body. These results were detailed in [57, Vol. 1, pp. 297–299]. Figure 3.31 (replicating Fig. 3.9 from [57]) shows the dependence of the load parameter on the wave number α_r (as in (3.2)) for a composite laminate with the following parameters in the plane case: $E_r \cdot E_m^{-1} = 500$, $h_m \cdot h_r^{-1} = 1$, 5, 10, 20, 30, 40, 50 (curves *1–7*, respectively), the notation corresponding to Fig. 3.25. The solid lines represent the bending mode (buckling mode of the first kind, Fig. 3.27), while the dash-dot lines represent the tension mode (buckling mode of the second kind, Fig. 3.28).

Let us briefly analyze the results in Fig. 3.31 for the bending mode. Solid curves *1* and *3* ($h_m \cdot h_r^{-1} = 1$ and 10) are curves of type *B* in Fig. 3.3; therefore, if $h_m \cdot h_r^{-1} = 1$ and 20, microbuckling in bending mode does not occur. Solid curves *4*, *5*, *6*, and *7* ($h_m \cdot h_r^{-1} = 20, 30, 40, 50$) are curves of type *A* in Fig. 3.3; therefore, if $h_m \cdot h_r^{-1} = 20, 30, 40, 50$, microbuckling occurs in bending mode. Thus, it was strictly proved that microbuckling in bending mode can or cannot occur depending on the structure of the composite laminate.

More details on the internal fracture of composite laminates can be found in [57, Vol. 1, Ch. 3].

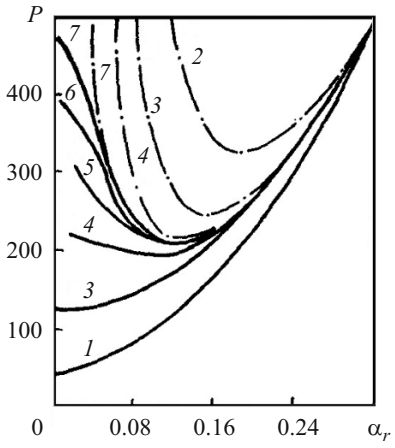

Fig. 3.31

3.3.3.2. Near-Surface Fracture. Let us briefly discuss results on the near-surface fracture of composite laminates obtained using the piecewise-homogeneous material model (see [57, Vol. 1, Ch. 5] for more details).

In studying surface instability, the composite laminate is assumed to occupy the lower half-space const $\geq x_2 > -\infty$ in the plane case (Fig. 3.25) and the lower half-space const $\geq x_3 > -\infty$ in the spatial case (Fig. 3.26). All the notation and reasoning stated in Sec. 3.3.3.1 before expression (3.11) also apply to near-surface fracture. Specific results were obtained for laminated composites with polymer or metal matrix (brittle or ductile fracture, respectively).

Two- and three-dimensional near-surface fracture problems are solved with (i) an exact method that reduces the problems to infinite systems of algebraic equations and (ii) an essentially approximate method that employs variational principles and the TLTSDB (Sec. 2).

In what follows, we will analyze results on near-surface instability in specific laminated composites with either polymer or metal matrix. We will restrict ourselves to the following qualitatively new phenomenon [57, Vol. 1, Ch. 5, p. 513]: surface instability does not occur at all concentrations of reinforcement and all relative stiffnesses. For example, as the external compressive load is continuously increased, internal instability may occur first or the critical loads for internal and surface instabilities may coincide.

This completes the brief discussion of results on near-surface fracture (near-surface instability) in laminated composite with polymer and metal matrices obtained within the framework of the piecewise-homogeneous material model. More details can be found in [57, Vol. 1, Ch. 5].

3.3.3.3. More Details on the Fracture Mechanics of Composite Laminates. Here we additionally briefly discuss the following issues of the fracture mechanics of composite laminates under compression: analysis of the continuum fracture mechanics of compressed composites (Sec. 3.3.2); development of a method for studying more complex buckling modes in composite laminates; drawing conclusions from a consistent analysis of the Dow–Gruntfest–Rosen–Schuerch theory.

3.3.3.3.1. Analysis of the Continuum Fracture Mechanics of Composites. As repeatedly indicated above, in solving various problems of stability in the mechanics of composites, the piecewise-homogeneous material model in which the TLTSDB is applied to the reinforcement and the matrix separately and the stress and displacement vectors are continuous at the interface is the most rigorous and accurate in solid mechanics. It is natural that this most rigorous and accurate model is the basis for estimating the accuracy of and validating any approximate theories and specific results they produce.

All the results on the theory of the fracture of composite laminates under compression outlined in Secs. 3.3.3.1 and 3.3.3.2 and in the monographs [30, 31, 35, 54, 57] were obtained using the most rigorous and accurate model. In this connection, the above results on the fracture mechanics of composite laminates under compression are the basis for estimating the accuracy of and validating approximate theories in the fracture mechanics of composite laminates under compression.

The continuum theory of fracture of composites compressed along the axes of material symmetry (Sec. 3.3.2) is based on a much more approximate model (compared with the above rigorous and accurate model)—homogeneous material with effective parameters and the TLTSDB (Sec. 2 the present paper). In this connection, the results (Secs. 3.3.3.1 and 3.3.3.2) on the theory of fracture of composite laminates under compression obtained using the rigorous and accurate model can be used to

estimate the accuracy of and validate the continuum theory of fracture of laminated composites compressed along the axes of material symmetry (Sec. 3.3.2).

One of the major results of the continuum theory of fracture of composites compressed along the axes of material symmetry, which is detailed in the monographs [54, Ch. 2] published in 1990 and [57, Vol. 1, Ch. 2] published in 2008 and briefly outlined in Sec. 3.3.2 is the determination of the theoretical ultimate compressive strength. In the case of polymer-matrix composites (as materials with low shear stiffness) for a plane problem (Fig. 3.25) in the plane $x_1 0x_2$ under uniaxial compression along the $0x_1$-axis, the theoretical ultimate strength $(\Pi_1^-)_T$ was estimated as follows ([57, Vol. 1, Ch. 2, formulas (2.60) and (2.61)]:

$$(\Pi_1^-)_T \le G_{12}, \quad (\Pi_1^-)_T \approx G_{12}, \tag{3.12}$$

where G_{12} is the modulus of a composite modeled by an orthotropic material (continuum approximation).

It should be noted that expressions (3.12) apply to a composite of arbitrary structure with the $0x_1$-axis (Fig. 3.25) being the axis of material symmetry. Since the continuum theory (Sec. 3.3.2) is validated against the rigorous and accurate theory for composite laminates (Secs. 3.3.3.1 and 3.3.3.2), the shear modulus G_{12} (3.12) for composite laminates is determined from the expression

$$G_{12} = G_r G_m (S_r G_m + S_m G_r)^{-1}, \tag{3.13}$$

where G_r and G_m are the shear moduli of the reinforcement and the matrix; S_r and S_m are the volume fractions of the reinforcement and the matrix in the case of isotropic layers. Note that expression (3.13) is derived from the strict consideration of the situation in Fig. 3.25 for a static plane problem using the long-wave method in the theory of wave propagation with reference to the classical linear theory of isotropic elasticity. Currently, expression (3.13) is well-known and standard. Thus, using the continuum theory of fracture (Sec. 3.3.2) for composite laminates in the plane case (Fig. 3.25), we obtain the theoretical ultimate strength for uniaxial compression:

$$(\Pi_1^-)_T = G_r G_m (S_r G_m + S_m G_r)^{-1}. \tag{3.14}$$

In [57, Vol. 1, pp. 20–21], conditions in which the continuous model or theory (homogeneous anisotropic body with effective properties or parameters) can be applied to composites are formulated. To this end, two geometrical parameters were introduced: parameter L characterizing the mechanical processes under consideration (variation of the mechanical fields with the space variables) and parameter h^* characterizing the average center-to-center distances of neighboring particles in the internal structure of the composite. The parameter L is the minimum distance at which the stress and strain fields change considerably in static problems, is the wavelength in wave-propagation problems, and is the buckling mode wavelength in stability problems. Now the condition of applicability of the homogeneous anisotropic material model with effective parameters (continuum model, continuum theory) can be represented as

$$L >> h^*. \tag{3.15}$$

When a composite laminate with alternating layers considered in Sec. 3.3.3 in the plane case (Fig. 3.25) loses stability in a periodic buckling mode along the $0x_1$-axis (Fig. 3.25), the following quantities are used instead of L and h^* in (3.15), according to [57, Vol. 1, p. 305]: $L \sim l$, where l is the half-wavelength (along layers) of the buckling mode; $h^* \sim 2(h_r + h_m)$, where $2(h_r + h_m)$ is the total thickness of the reinforcement layer and matrix layer. With the parameters chosen and formula (3.15), the applicability condition for the continuum model for a plane problem (Fig. 3.25) can be represented as

$$2(h_r + h_m) << l, \tag{3.16}$$

whence the wave numbers α_r and α_m can be found as

$$\alpha_r = \pi \frac{h_r}{l} << 1, \qquad \alpha_m = \pi \frac{h_m}{l} << 1. \tag{3.17}$$

Note that the characteristic determinants whose elements also depend on the wave numbers α_r and α_m (3.17) were obtained for composite laminates (Sec. 3.3.3) for all four buckling modes shown in Figs. 3.27–3.30 using the piecewise-homogeneous material model [57, Vol. 1, Ch. 3]. In [57, p. 314], the concept of asymptotically exact continuum theories of internal fracture (internal instability) of composite laminates was introduced.

The continuum theory of internal fracture based on the homogeneous material model effective average parameters (properties) is asymptotically exact if follows from the theory based on the piecewise-homogeneous material model as the wave numbers α_r and α_m tend to zero, in view of (3.16) and (3.17):

$$\alpha_r = \pi\frac{h_r}{l} \to 0, \qquad \alpha_m = \pi\frac{h_m}{l} \to 0. \tag{3.18}$$

Certainly, the asymptotic accuracy of the continuum theory for composite laminate in the plane case (Fig. 3.25) can be proved only for the four buckling modes shown in Figs. 3.27–3.30 for which the characteristic determinants were found using the piecewise-homogeneous material model (Sec. 3.3.2.1). To this end, it is necessary to expand all the elements of the characteristic determinants into series in powers of α_r and α_m (3.18) and to calculate the first term of this series expansion of the whole characteristic determinant.

In the monograph [57, Vol. 1, p. 316], it was rigorously proved that in the plane case (Fig. 3.25) of polymer-matrix composite laminates, the continuum theory of internal fracture (Sec. 3.3.2.1) is asymptotically exact and corresponds to the buckling mode of the first kind (flexural mode, Fig. 3.27). In this case, the expression for the theoretical ultimate strength in uniaxial compression (3.122) obtained in the monograph [57, Vol. 1, p. 316] coincides with expression (3.14) obtained using the continuum theory of internal fracture (Sec. 3.3.2.1).

The above proof indicates that the continuum theory of internal fracture (Sec. 3.3.2.1) does not describe fracture associated with buckling modes of the second, third, and fourth kind (Figs. 3.28–3.30) because of the following. In analyzing buckling modes of the second, third, and fourth kind in conditions (3.18), the results that are obtained that do not have direct physical meaning (see [54, Ch. 3] and [57, Vol. 1, pp. 304–312] for more details).

In the monographs [30] published in 1971 and [31] published in 1973 and in the papers [216] published in 1969, [179] published in 1982, and [177] published in 2001, it was found out numerically that the buckling modes of the third (Fig. 3.29) and fourth (Fig. 3.30) kinds do not lead to critical loads lower than those caused by the buckling modes of the first (Fig. 3.27) and second (Fig. 3.28) kinds [54, Ch. 3; 57, Vol. 1, Ch. 3]. Thus, in analyzing the asymptotic accuracy of the continuum theory of internal fracture (internal instability) outlined in Sec. 3.3.2.1, it is sufficient to consider the buckling modes of the first (Fig. 3.27) and second (Fig. 3.28) kinds analyzed in Sec. 3.3.3.1 using the piecewise-homogeneous model.

It should be noted that the piecewise-homogeneous material model and the TLTSDB were also used to analyze laminated polymer-matrix composites (brittle fracture) in the spatial case and laminated metal-matrix composites (ductile fracture) in the plane and spatial cases. In all the cases, the results obtained were the same as for composite laminates with polymer matrix in the plane case (see [54, Ch. 3; 57, Vol. 1, Ch. 3] for more details).

Thus, we have proved the following general statement.

Statement. For composite laminates with polymer or metal matrix, the continuum theory (Sec. 3.3.2.1) of internal fracture based on the homogeneous material model with effective parameters and the TLTSDB has the following properties:

(i) it is asymptotically exact and corresponds to the buckling mode of the first kind (bending mode, Fig. 3.27);

(ii) it does not describe internal fracture caused by the buckling mode of the second kind (tensile mode, Fig. 3.28).

Since the microbuckling of a composite laminate and start of fracture occur at the lower critical load (of the two critical loads corresponding to the buckling modes of the first (Fig. 3.27) and second (Fig. 3.28) kinds), the analysis can be continued. It is reasonable to consider the following three typical cases.

First Case. The buckling mode of the first kind occurs, while the buckling mode of the second kind does not. In this case, the continuum theory describes fracture.

Second Case. Either buckling mode of the first or the buckling mode of the second kind can occur. As follows from Tables 3.1 and 3.2 of the monographs [54, pp. 182–183] and [57, Vol. 1, pp. 300–301], the critical loads calculated using the piecewise-homogeneous material model (Sec. 3.3.3.1) and the TLTSDB for the buckling modes of the first (Fig. 3.27) and second (Fig. 3.28) kinds differ substantially in the examples considered in [54] and [57, Vol. 1]. Thus, in this case, the continuum theory also allows obtaining the reliable value of the theoretical ultimate strength. Apparently, it is expedient to increase the number of numerical examples for analysis.

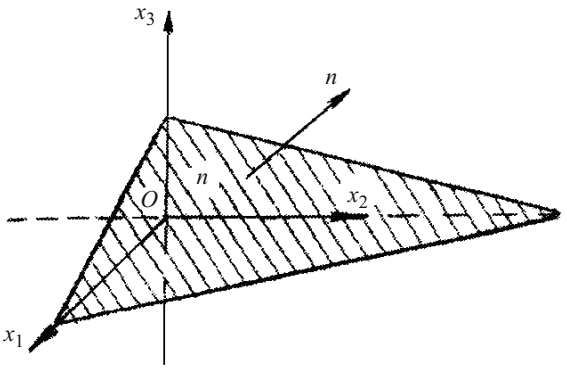

Fig. 3.32

Third Case. The buckling mode of the second kind occurs, while the buckling mode of the first kind does not. According to the statement above, the continuum theory of internal fracture under compression (Sec. 3.3.2.1) does not describe the internal fracture of composite laminates under compression. To ascertain whether expression (3.14) can be used to determine the theoretical ultimate strength of composite laminates in the third case, it is expedient to numerically analyze some composite laminates using the approach of Sec. 3.3.3.1 and the piecewise-homogeneous material model for the buckling mode of the second kind (Fig. 3.28, tensile mode).

This completes the analysis of the continuum theory of internal fracture of composites compressed along the axes of material symmetry outlined in Sec. 3.3.2.1 for composite laminates compressed along layers (Figs. 3.25 and 3.26).

3.3.3.3.2. Method of Analysis of Complex Buckling Modes in Composite Laminates. In analyzing the stability of composite laminates using the piecewise-homogeneous material model and the TLTSDB (Sec. 2), the following factors were separated out in all the buckling modes: $\sin \pi l_1^{-1} x_1$ in the plane case (Fig. 3.25) and $(\sin \pi l_1^{-1} x_1)(\cos \pi l_2^{-1} x_2)$ in the spatial case (Fig. 3.26), where l_1 and l_2 are the half-wavelengths of the buckling modes along the layers. Thus, the infinite-fiber model was used assuming that each ply buckles in the same periodic (in phase or antiphase) mode along plies. In these buckling modes, planes with equal phase (in the coordinate x_1 in the plane case (Fig. 3.25) and in the coordinates x_1 and x_2 in the spatial case (Fig. 3.27), generally along the layers) are perpendicular to the layers. Buckling modes that are periodic along the layers are more complex, but planes with equal phase are located arbitrarily relative to the plane of layers.

For more accurate characterization of the buckling modes, use is made of the concept of plane Π that consists of points of the buckled composite that are in phase in the coordinates along the layers. The plane Π is in an arbitrary position defined by a unit normal vector n (a Fig. 3.32), and the buckling mode is periodic along the layers (in x_1 in the plane case (Fig. 3.25) and in x_1 and x_2 in the spatial case Fig. 3.26)). The first octant of the plane Π in Fig. 3.32 is hatched and is defined by a unit vector n with the following components:

$$n_1, n_2, n_3, \quad n_1^2 + n_2^2 + n_3^2 = 1. \tag{3.19}$$

In [376], the system of static TLTSDB equations for composite laminates was explicitly solved for the buckling modes mentioned above and it was shown that this approach leads to characteristic determinant of finite order with elements represented in closed form. It should be noted that the statement (in Sec. 3.3.1) that the second approach is general and is consistent with the standard and rigorous method of analysis of the buckling phenomenon (analysis of the behavior of small perturbations in linearized three-dimensional dynamic problems) also applies to the buckling modes discussed above. Since the sufficient applicability conditions of the Euler method are satisfied in this case, only the static TLTSDB equations were solved in [376].

3.3.3.3.3. Conclusions from Consistent Analysis of the Dow–Gruntfest–Rosen–Schuerch Theory. The coining of the term Dow–Gruntfest–Rosen–Schuerch theory was discusses in the final part of Sec. 3.1.2. The results obtained with this theory are assigned to the first approach, which was briefly characterized in Sec. 3.1.2. Note that Sec. 3.1.2 formulates five groups of main assumptions typical for the first approach.

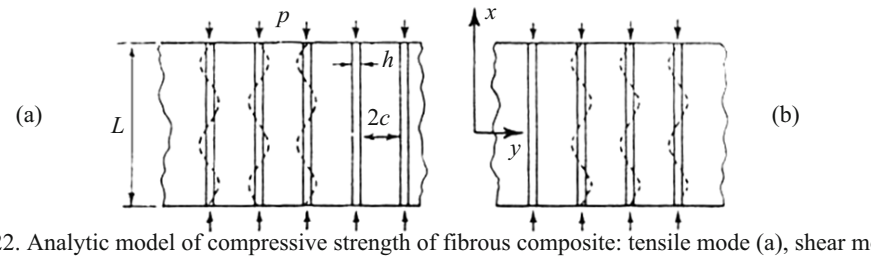

Fig. 3.22. Analytic model of compressive strength of fibrous composite: tensile mode (a), shear mode (b)

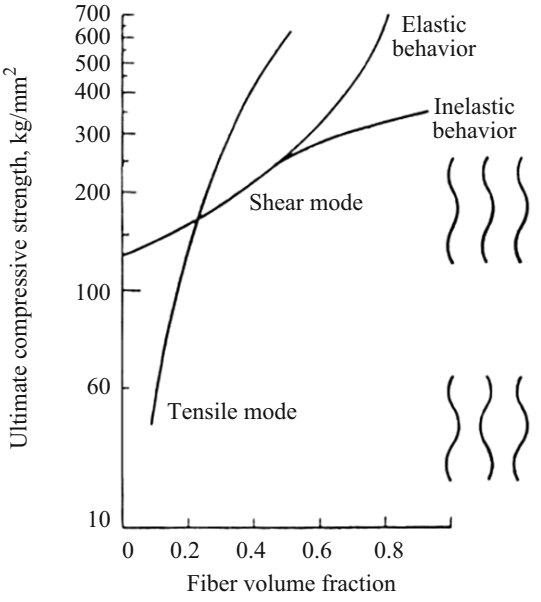

Fig. 3.23. Compressive strength of fiberglass-reinforced plastic

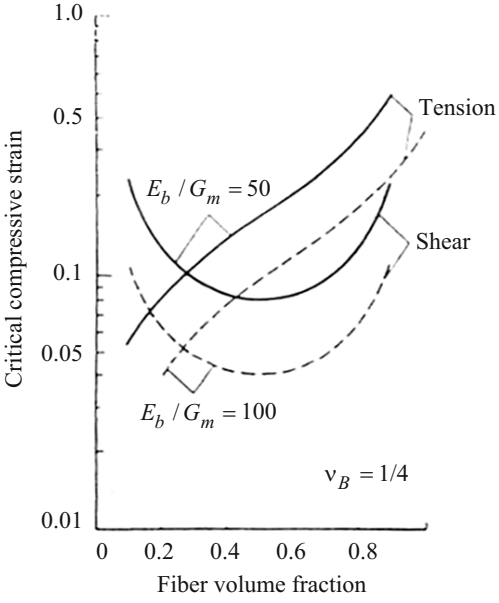

Fig. 3.24. Critical compressive strain of fibrous compositions

Fig. 3.33

A typical representative of the first approach, as already mentioned in Sec. 3.1.2, is the paper [551] published in English in 1965 and in Russian as [161] in 1967, which was apparently the first to report theoretical results and was included in multivolume encyclopedias on fracture [160] and on composites [127]. In this connection, we will follow [551, 161] in discussing the Dow–Gruntfest–Rosen–Schuerch theory. This theory should be discussed comparing with the second approach, which, as already mentioned in Sec. 3.1.3.1, does not use the five groups of assumptions. The Dow–Gruntfest–Rosen–Schuerch theory was analyzed in the monograph [54, pp. 206–214] of 1990, the monograph [57, Vol. 1, pp. 328–335] of 2008, and the review [65, pp. 22–26] of 2016. This analysis was based on results for composite laminates obtained with the second approach and partially outlined here. In this connection, Sec. 3.3.3.3.3 formulating conclusions from the analysis is included in Sec. 3.3.3. The major results of [551, 161] are presented below in Fig. 3.33 which includes Figs. 3.22–3.24 from [161].

For convenient analysis, the following indices are used to refer to the reinforcement (fibers, plies, etc.) and the matrix (binder): “r” and “m” in the present review; *B* and *M* in the paper [161] and in Fig. 3.33, which includes Figs. 3.22–3.24 from [161], which is a translation into Russian of [551].

From the discussion and analysis of the results of [551, 161], which are reported in [54, 57], the following brief conclusions can be drawn.

1. A fibrous composite is modeled by a laminated composite because the plane case in the plane $x0y$ (Fig. 3.33) is considered though the terms for fibrous composites are used. The way of modeling is justified in no way.

2. The theory being discussed has qualitative contradictions, of which two will be formulated below.

2.1. The theory [551, 161] does not permit (describes) microbuckling in shear mode for any composite (for any ratios between stiffness and geometrical characteristics). Note that the shear mode (Fig. 3.33) corresponds to the buckling mode of the first kind (Fig. 3.27). This conclusion follows (according to the approaches outlined near Fig. 3.3 in Sec. 3.1.1) from the expression [161, p. 96; B. 26], which suggests that the function $p = p(\alpha)$ (3.2) is monotonic, as the curve *B* in Fig. 3.2. This conclusion was formulated in more detail in [54, pp. 207–209].

The second approach allows proving that microbuckling in shear or bending mode can occur depending on the ratio between the stiffness and geometrical characteristics of the composite. For example, buckling in shear or bending mode occurs at low concentration of reinforcement [54, p. 209].

Thus, we have formulated the first qualitative contradiction of the theory [551, 161].

2.2. When the concentration of reinforcement is high, the theory [551, 161] leads to physically an incorrect result for the shear or tensile mode. For example, from expression (3.29) [161, p. 82] it follows that the theoretical ultimate compressive strength tends to infinity as $\nu_B \to 1$ (in [161], ν_B denotes the volume fraction of the reinforcement).

With the help of the second direction, it was rigorously proved that in the above situation, the theoretical ultimate compressive strength tends to a finite value [57, Vol. 1, p. 189, expression (2.71)]. This result also follows from expression (3.14) for $S_r \to 1$ and $S_m = 1 - S_r \to 0$, where $S_r \sim \nu_B$.

Thus, we have formulated the second qualitative contradiction of the theory [551, 161].

3. The theory being discussed has quantitative errors, of which two will be formulated below.

3.1. The results of the theory [551, 161] and the results of the second approach for layered composites differ considerably at low and high concentrations (volume fractions) of the reinforcement (plies, fibers, etc.). This conclusion was formulated in [54, p. 210].

3.2. The results of the theory [551, 161] and the results of the second approach for laminated composites can differ by a factor of three and more at low concentrations of the reinforcement. This conclusion was formulated in [54, p. 211].

Thus, the Dow–Gruntfest–Rosen–Schuerch theory [551, 161] and its quantitative results have significant qualitative contradictions and quantitative errors compared with a theory as accurate as usually adopted in solid mechanics (the second approach based on the TLTSDB). To validate specific results obtained using the Dow–Gruntfest–Rosen–Schuerch theory, it is necessary to conduct additional studies.

It should be noted that the above brief conclusions from the analysis of [551, 161] correspond to the review [65, p. 24] published in 2016. The fullest exposition of the analysis and conclusions can be found in the monograph [54, pp. 206–214] published in 1990.

It should be pointed out the conclusions from the analysis of [551, 161] and five groups of assumptions (Sec. 3.1.2) give an insight into the first approach.

This completes the discussion of the results related to composite laminates and piecewise-homogeneous material model (Sec. 3.3.3).

3.3.4. Unidirectional Fibrous Composites. Piecewise-Homogeneous Material Model. Here we will briefly discuss the mechanics of fracture of compressed fibrous composites with polymer and metal matrices based on the piecewise-homogeneous material model. The TLTSDB (Sec. 2) is applied to each fiber of the reinforcement and matrix, and continuity conditions for stresses and displacements are prescribed at the cylindrical interfaces. The basic results were obtained for brittle and ductile fracture. In the latter case, the generalized concept of increasing load outlined in Sec. 2 was used. In line with the basic approach outlined in Sec. 3.3.1, it is necessary to analyze the static equations and boundary conditions of the TLTSDB (Sec. 2) for a piecewise-homogeneous material (eigenvalue problem). Here we discuss results on unidirectional fibrous composites with interfacial defects for which the continuity conditions for the stress and displacement vectors are satisfied at all cylindrical interfaces. The basic results were obtained for microbuckling [57, Vol. 1, Ch. 4] and for near-surface buckling [57, Vol. 1, Ch. 6]. These results were partially included in the monographs [30, 31, 54], and briefly in the review [65]. The results for unidirectional fibrous composite being discussed were preliminarily published in articles most of which are included in the list of references to the present review and in the list of papers related to second approach given in the prologue to Sec. 3 (see [30, 31, 54, 57] for more details on the published articles). Note that the results (characteristic determinants) for fibrous composites are formulated in a unified general form for theories 1, 2, and 3 as termed in Secs. 2.2 and 2.4.

We will briefly discuss (following the brief review [65]) the basic results on the fracture mechanics of unidirectional fibrous composites compressed along fibers obtained using the piecewise-homogeneous material model and the TLTSDB.

3.3.4.1. Internal Fracture. The internal fracture (internal instability) of an unbounded unidirectional fibrous composite (Fig. 3.1) is analyzed using the general solutions of the static TLTSDB equations and the procedure outlined in Sec. 3.1.1, taking into account the approach outlined near Fig. 3.3. It is assumed that shortenings along fibers in the matrix and fibers (in a subcritical state under compression along fibers) coincide (Remark 3.8).

An inhomogeneous stress state depending on space variables in the cross-sectional plane can occur in unidirectional fibrous composites compressed along fibers (Fig. 3.1), unlike composite laminates compressed along plies (Fig. 3.2). A

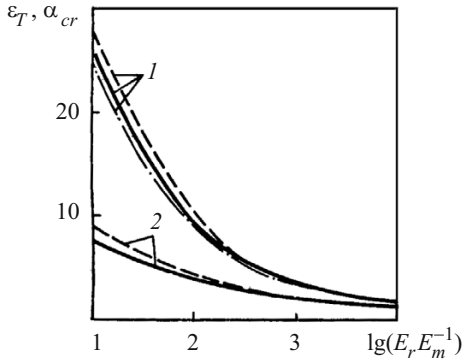

Fig. 3.34

homogeneous subctitical state can occur when (i) the fibers and the matrix are incompressible and (i) Poisson's ratios of the fibers and the matrix are equal ($\nu_r = \nu_m$). If Poisson's ratios of the fiber and matrix are different ($\nu_r \neq \nu_m$), the subcritical state will be inhomogeneous. This suggests that it is necessary to take into account (in buckling problems for unidirectional fibrous composites) the inhomogeneity of the subcritical state when $\nu_r \neq \nu_m$. This issue for one fiber was examined in [57, Vol. 1, Ch. 4, Sec. 1, pp. 391–396]. Quite accurate results were obtained numerically for an inhomogeneous subcritical state. For example, Fig. 3.34 shows the dependence of $10\varepsilon_T$ (ε_T is the theoretical ultimate compressive strain) and $\alpha_{cr} = \pi R / l_{cr}$ (critical wave number $\alpha = \pi R / l$, R is the fiber cross-sectional radius, l is the buckling half-wavelength (along the fibers)) on $\lg(E_r \cdot E_m^{-1})$. Curves *1* correspond to α_{cr}, curves *2* to $10\varepsilon_T$; the solid curves correspond to $\nu_r = 0.2$ and $\nu_m = 0.4$ (inhomogeneous subcritical state), the dashed curves to $\nu_r = \nu_m = 0.2$ (homogeneous subcritical state), and the dash-and-dot curves to $\nu_r = \nu_m = 0.4$ (homogeneous subcritical state). Note that the solid and dash-and-dot lines for $10\varepsilon_T$ practically coincide in Fig. 3.34. The values $\nu_r = 0.2$ and $\nu_m = 0.4$ represent the case of the maximum difference between Poisson's ratios of typical reinforcements and matrices, according to [57, Vol. 1, Tables 0.1 and 0.2, p. 67 and p. 68].

Analyzing Fig. 3.34 and [57, Vol. 1, Table 4.1, p. 395], we conclude that when $E_a \cdot E_m^{-1} \geq 20$, tolerating an error 5% is sufficient to neglect the inhomogeneity of the subcritical state caused by the difference between Poisson's ratios of the reinforcement and the matrix and to assume that $\nu_r = \nu_m = 0.3$. This conclusion allows applying the general solutions of the static TLTSDB equations (Secs. 2.5.1 and 2.5.2) for homogeneous subcritical stress states. All the results discussed below were obtained in this way.

For unidirectional fibrous composites compressed along the fibers (Fig. 3.1), various problems arise depending on the structure of the composite in the cross-sectional plane and the design models used. Figure 3.35 (cross-sectional plane) shows the following design models.

1. One fiber (Fig. 3.35*a*); applied to fibrous composites with so low volume fraction of fibers that neighboring fibers do not interact.

2. Two fibers (Fig. 3.35*b*); applied to fibrous composites with so low volume fraction of fibers that two neighboring fibers can interact upon buckling due to the irregularity of the structure.

3. A periodic row of fibers (Fig. 3.35*c*); applied to fibrous composites of periodic structure such that upon buckling, fibers of the same row interact, whereas fibers in neighboring rows do not interact (rather short distances between fibers in the same row, rather long distances between neighboring rows).

4. Several periodic rows of fibers (Fig. 3.35*d*); applied to fibrous composites of periodic structure such that upon buckling, fibers in the same row interact, rows of fibers within a group of rows interact, and different groups of rows do not interact.

5. Doubly periodic array of fibers (Fig. 3.35*e*); applied to fibrous composites of doubly periodic structure with so short distances between neighboring fibers that upon buckling, the interaction of fibers should be described by the doubly periodic model.

The number of problems for unidirectional fibrous composites is determined by not only the number of design models (five models in Fig. 3.35), but also by the necessity of analyzing various buckling modes depending on cross-sectional

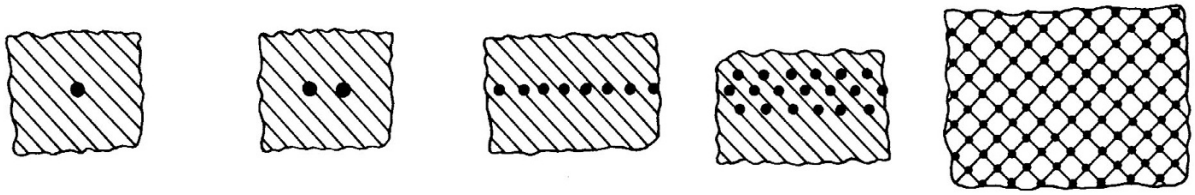

a *b* *c* *d* *e*

Fig. 3.35

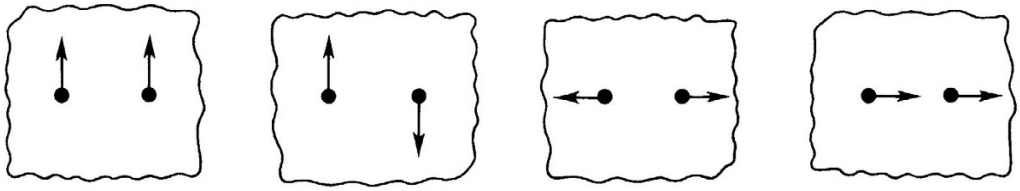

a *b* *c* *d*

Fig. 3.36

symmetry. Certainly, after analyzing various buckling modes, it is necessary to minimize all the eigenvalues (usually the first eigenvalues for each buckling mode) to determine the critical shortening along the fibers.

Figure 3.36 shows (in the cross-sectional plane), as an example, various buckling modes for two fibers (Fig. 3.35*b*): in-phase out-of-plane buckling modes (Fig. 3.36*a*); antiphase out-of-plane buckling modes (Fig. 3.36*b*); antiphase in-plane buckling modes (Fig. 3.36*c*); in-phase in-plane buckling modes (Fig. 3.36*d*).

The general method for solving such problems, which was used to solve all problems of the internal fracture of unidirectional fibrous composites under uniaxial compression within the framework of the second approach, involves the following steps:

– application of the general solutions of the static TLTSDB equations (Sec. 2) in circular cylindrical coordinates to fibers and matrix;

– representation of the solution as the sum of solutions in local cylindrical coordinates in the form of Fourier series with undetermined coefficients, including special circular cylindrical functions;

– derivation of characteristic equations in the form of infinite characteristic determinants and explicit calculation of their elements;

– proving that these infinite characteristic determinants are normal for noninteracting fibers, which allows replacing infinite determinants with finite determinants to find the roots, i.e., to apply the method of truncation;

– proving the practical convergence of the method by comparing the roots obtained with increase in the order of truncated determinants.

This method helped to obtain numerous results on the internal fracture of compressed unidirectional fibrous composites with polymer and metal matrices (see [57, Vol. 1, Ch. 4] for a more detailed and consistent exposition of these results). Currently, these results appear the most accurate and rigorous. Moreover, the method allows refining results obtained for noninteracting fibers.

Example. Let us briefly discuss experimental and theoretical ultimate strengths for a VKA-1 metal-composite (unidirectional fibrous composite with aluminum matrix reinforced with 50% of boron fibers 140 μm in diameter; $S_r = S_m =$ 0.5). The boron aluminum specimens are shown in Fig. 3.37. Figure 3.38 shows the magnified internal structure of boron aluminum composite in cross section. These results were reported in [95] and detailed in [57, Vol. 1, Ch. 4, pp. 486–488]. Theory 3, as termed in Sec. 2.2, was used for theoretical studies. Ductile fracture, which, according to Remark 3.7, is considered the stage when the whole matrix is in plastic state, was considered as well. In this connection, relation (3.8) was used to describe the plastic deformation of the matrix (3.8) modeled by an incompressible isotropic plastic material. The unidirectional fibrous boron aluminum composite under consideration uses AD-1 aluminum as matrix for (with reference to annealed and unannealed

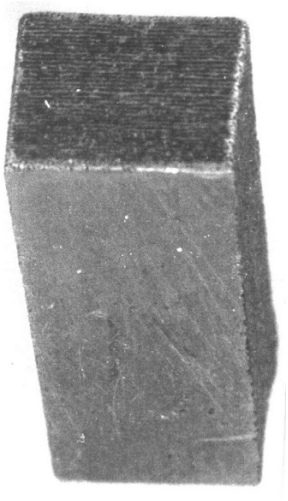

Fig. 3.37

Fig. 3.38

specimens) the parameters A_m and k_m, appearing in (3.8) were determined (see [57, Vol. 1, Ch. 4, pp. 486–488] for more detail). For example, the following was determined [95]:

$$A_m = 130 \text{ MPa}, \quad k_m = 0.43 \quad \text{for annealed matrix (aluminum)},$$

$$A_m = 70 \text{ MPa}, \quad k_m = 0.25 \quad \text{for unannealed matrix (aluminum)}. \tag{3.20}$$

Interestingly, the values of A_m and k_m for unannealed aluminum (3.20) coincide with the numerical values in the third approximation in (3.9). In fact, two metal-composites were considered: annealed and unannealed. In experiments, 32 annealed specimens and 14 unannealed specimens were destroyed to determine their experimental ultimate strengths. The theoretical ultimate strengths were determined using the continuum theory of fracture (Sec. 3.3.2.1), the piecewise-homogeneous material model for fibrous unidirectional composites (Sec. 3.3.4.1), and the doubly periodic design model (Fig. 3.35*e*). The results are summarized in Table 3.1 [57, Vol. 1, Ch. 4, Table 4.10, p. 487]. It can be seen that the continuum theory of fracture is in agreement with the average experimental results, while the piecewise-homogeneous material model is in agreement with the maximum experimental results.

More details on the internal fracture of unidirectional fibrous composites can be found in [57, Vol. 1, Ch. 4]. It should be noted that to determine the theoretical ultimate compressive strength of boron aluminum composite in the case of ductile fracture using the continuum theory of fracture (Sec. 3.3.2.1), the first approximation was used, as in Fig. 3.23.

Comparing the theoretical and experimental results (Table 3.1) on the ultimate strength in uniaxial compression of unidirectional boron aluminum composites along the fibers allows us to draw the following conclusions.

1. The theoretical ultimate compressive strength predicted by the continuum theory of fracture (Sec. 3.3.2) is close to experimental values: the difference is 11% for annealed materials and 14.4% for unannealed materials.

2. The theoretical ultimate compressive strength predicted by fracture mechanics based on the piecewise-homogeneous material model (Sec. 3.3.4.1) is close to its maximum experimental values: the difference is 1% for annealed materials and 15% for unannealed materials.

This completes the discussion of results on the internal fracture of unidirectional fibrous composites compressed along fibers.

3.3.4.2. Near-Surface Fracture. Let us briefly discuss results on the near-surface fracture of unidirectional fibrous composites obtained using the piecewise-homogeneous material model (see [57, Vol. 1, Ch. 6] for more details).

To study surface instability, a fibrous unidirectional composite occupying a half-space with the boundary surface parallel to the fibers is considered (Fig. 3.1). In this connection, the cross-section of the composite is a half-plane (Fig. 3.39) whose structure depends on which of the typical design models is used. Figure 3.39 shows five typical design models that can be described in a similar way as in Sec. 3.3.4.1. Note that the full circles in Fig. 3.39, as well as in Figs. 3.35 and 3.36, represent fiber

TABLE 3.1

Material	$(\Pi_3^-)_{ex}$, MPa			$(\Pi_3^-)_T$, MPa	
	max	min	Average	Continuum theory	Piecewise-homogeneous material model
Annealed	965	501	665	736	958
Unannealed	1716	1049	1282	1467	1972

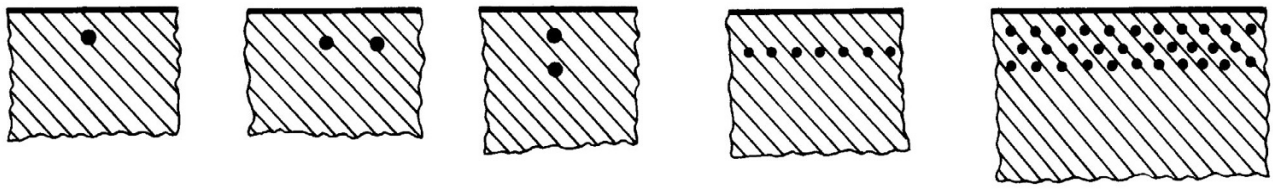

a *b* *c* *d* *e*

Fig. 3.39

cross-sections. The surface instability of unidirectional fibrous composites is studied by analyzing buckling modes that decay with distance from the boundary of the lower half-space (Fig. 3.39), which is determined by an additional condition. The solution is formed by adding a term in the form of a Fourier transform to the solution in 3.3.4.1 to satisfy the boundary conditions on the boundary of the lower half-space. With such a candidate solution, the method described before the Example in Sec. 3.3.4.1 was used.

Specific results on near-surface fracture were obtained for unidirectional fibrous composites with polymer and metal matrices. More details can be found in [57, Vol. 1, Ch. 6].

3.3.4.3. Method of Analysis of Complex Buckling Modes in Unidirectional Fibrous Composites. In studying the stability of unidirectional fibrous composites (Sec. 3.4.4.1 and Sec. 3.3.4.2) modeled by a piecewise-homogeneous material based on the TLTSDB (Sec. 2), the factor $\sin \pi l^{-1} x_3$ is separated out in all buckling modes, where the coordinate x_3 is measured along the fibers or plies and l is the buckling half-wavelength along fibers. Thus, the infinite-fiber model was used assuming that each fiber buckles in the same periodic mode along fibers. That such buckling modes occur was confirmed by experiments on composites with polymer (epoxy resin) matrix reinforced with glass fibers (Fig. 3.5) or with carbon fibers (Fig. 3.6).

The planes of equal phase in such buckling modes (along the x_3-axis; along fibers) are perpendicular to the $0x_3$-axis (perpendicular to the fibers). In this connection, it may be considered that fracture propagates along these planes. In a sense, the validation of the above procedure regarding buckling modes is the rigorous proof (Sec. 3.3.2.1), based on the continuum theory of fracture (Sec. 3.3.2), of the fact that brittle fracture propagates along planes perpendicular to the line of action of compressive loads. Note that the continuum theory of fracture (Sec. 3.3.2) assumes compression in the direction of preferred reinforcement (along fibers or plies). Nevertheless, the use of the continuum theory to prove an element of the piecewise-homogeneous material model is insufficiently logical and consistent because the continuum theory of fracture is approximate and less accurate than the piecewise-homogeneous material model.

In this connection, it appears reasonable to develop a method that would allow analyzing more general buckling modes in unidirectional fibrous composites than the buckling modes addressed in Secs. 3.3.4.1 and 3.3.4.2. Certainly, along with development of this method, it is necessary to analyze specific classes of problems to formulate general conclusions.

A method for studying more general buckling modes was proposed in [319] for unidirectional fibrous composites (Fig. 3.1) with the most complex doubly periodic structure (Fig. 3.35*e*) uniaxially compressed along the fibers. The method employs the infinitely long wave model (along the axis $0x_3$) where compression is along the $0x_3$-axis and buckling modes are periodic along the $0x_3$-axis, but the planes Π in Fig. 3.32 with equal phase along $0x_3$ (in the buckling mode) are in an arbitrary position

defined by an unit normal vector n to the plane Π. Explicit solutions to the static TLTSDB equations corresponding to an arbitrary position of the plane Π and to the most complex doubly periodic structure (Fig. 3.35*e*) was found in [319] in circular cylindrical (local for each fiber) coordinates for unidirectional fibrous composites. The use of this method leads to a characteristic equation in the form of an infinite determinant. It was also proved that the infinite determinant is normal for noninteracting fibers, which means that it is possible to truncate the infinite determinant to find the roots numerically. Practical convergence can be achieved by increasing the order of the truncated determinant and comparing the results obtained. It should be noted that the statement (in Sec. 3.3.1) that the second approach is general and is consistent with the standard and rigorous method of analysis of the buckling phenomenon (analysis of the behavior of small perturbations in linearized three-dimensional problems) also applies to the buckling modes discussed above. Since the sufficient applicability conditions of the Euler method are satisfied in this case, only the static TLTSDB equations were solved in [319].

The approach from [319] allows a changeover to simpler periodic structures for unidirectional fibrous composites (Fig. 3.35*c*, *d*). Specific results were only obtained for an elementary periodic structure shown in Fig. 3.35*c*, which is one periodic row of fibers in an infinite matrix. The design model in Fig. 3.35*c* applies to unidirectional fibrous composites of periodic structure such that upon buckling, fibers of the same row interact, whereas fibers in neighboring rows do not interact (rather short distances between fibers in the same row, rather long distances between neighboring rows). The results being discussed were reported in [405] of 2002, [406] of 2005, (preliminarily) in [425] of 1991, and briefly in [65, pp. 43–46]. In the publications cited above, the following conclusion was drawn: the minimum critical stress corresponds to the buckling mode in which the plane Π (Fig. 3.32) is perpendicular to the fibers. This conclusion is in agreement with the experimental results presented in Sec. 3.2.1 and the methods of studying internal fracture in composite laminates (Sec. 3.3.3.1) and unidirectional fibrous composites (Sec. 3.3.4.1) using the piecewise-homogeneous material model and the TLTSDB (Sec. 2).

We have briefly discusses results on the mechanics of brittle and plastic internal and near-surface fracture of unidirectional fibrous composites compressed along the fibers of circular cross section obtained using the piecewise-homogeneous material model and the TLTSDB (Sec. 2). Results on unidirectional fibrous composites with fibers of noncircular cross section were obtained in [82, 409, 410, 538, 539, etc.].

This completes the discussion of results on Problem 1 (fracture in composites compressed along reinforcement).

Conclusions to Sec. 3. It should be noted that Sec. 3 devoted to problem 1 is large because of the following:

1. The author of the present review and his followers have studied problem 1 for 50 years now (the first papers [25, 26] were published in 1969).

2. Significant results on problem 1 were reported in monographs, articles, and conference reports. The main publications in the list of references were listed in the prologue to Sec. 3.

3. The results of problem 1 obtained at the Department of Continuum Dynamics and Stability at the S. P. Timoshenko Institute of Mechanics have been recognized by the world's scientific community. An example is the following publication:

A. N. Guz (guest editor), "Micromechanics of composite materials: Focus on Ukrainian research," *Appl. Mech. Reviews (Special Issue)*, **45**, No. 2, 13–101 (1992).

This special issue was included as [534] in the list of references to the present review.

In this connection, the results on problems 2–8 will be analyzed briefly.

4. Problem 2. Short-Fiber Model in the Theory of Stability and Fracture/Failure Mechanics of Compressed Composites. We will briefly (compared with problem 1) discuss the basic results on problem 2 obtained at the Department Dynamics and Stability of Continua of the S. P. Timoshenko Institute of Mechanics since 1999. We will also discuss some related experimental results.

The major results are presented in the monograph [64] of 2015, the review [65] of 2016, and the articles [66, 67, 252–254, 362–368, 504, etc.] (see [64, 65] for more detailed references).

A doctoral dissertation on this problem was defended by V. A. Dekret.

Composites are reinforced with either relatively long (Problem 1) or relatively short fibers. Experiments on short-fiber reinforced composites under compression revealed the phenomenon of microbuckling with buckling modes that are not periodic along the fiber axis and are typical for short fibers in the matrix. The theory of stability under compression in the case corresponding to fracture mechanics describing the beginning (start) of fracture was developed using the TLTSDB with accuracy typical for solid mechanics. The major results were obtained by the author and his followers, including results on a plane problem for composites of various structures.

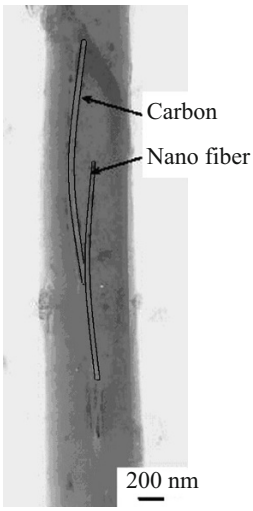

Fig. 4.1

4.1. Experimental Results on Microbuckling in Compressed Composites. Short Fibers. It should be noted that, as for long fibers (Sec. 3.2.1), microbuckling is not observed in homogeneous materials. It is only typical for composites (as for structurally inhomogeneous materials whose internal structure is described at different scales during analysis). The infinite-fiber model is, obviously, applicable to relatively long fibers (reinforcements). It may be a priori expected that the microbuckling modes in a composite reinforced with relatively short fibers is considerably different from the buckling modes in Figs. 3.4–3.6 corresponding to the infinite-fiber model. Let us consider, as an example, the experimental results on the stability of relatively short carbon nanofibers in a polymer matrix published in [554] in 2004. Figure 4.1 [554] shows buckling modes of two short carbon nanofibers, the scale in nm being indicated in the lower left corner of the figure. The buckling modes in Fig. 4.1 have nothing in common with those in Figs. 3.4–3.6. The buckling modes in Figs. 3.4–3.6 are sinusoidal (along the fibers) and have a great number of periods, while the buckling modes of short nanofibers in Fig. 4.1 can be approximated by sinusoids with one half-period. In this case, the critical loads and strains are strongly dependent on the boundary conditions at the ends of fibers.

Thus, the experimental results in Fig. 4.1 may be considered to validate the finite-fiber model.

We may now conclude that the infinite-fiber and finite-fiber models are experimentally validated, but they are applicable to different types to composites. The infinite-fiber model is, obviously, applicable to relatively long fibers (reinforcements). The finite-fiber model is applicable to relatively short fibers (reinforcements). Note that the conclusions drawn from Figs. 3.4–3.6 and Fig. 4.1 apply only to the phenomenon of microbuckling in composites.

4.2. Problem Statement. Here we consider composites reinforced with short fibers. It is assumed that these composites have axes of material symmetry; It is very difficult to create structural members from materials that do not have axes of material symmetry. Therefore, the above assumption is quite reasonable. The axes of material symmetry are provided by appropriate layup of short fibers.

When a composite is compressed along the axes of material symmetry, start (beginning) of fracture is determined by microbuckling (internal instability) or near-surface instability, according to the general concept of internal fracture (Sec. 3.1.1) and the general concept of near-surface fracture (Sec. 3.1.3.2). Thus, fracture mechanics is based on the theory of internal and near-surface buckling of composites.

We will briefly discuss the basic results obtained by the author and his followers on the fracture mechanics (in the above sense) of short-fiber-reinforced composites under compression using the piecewise-homogeneous material model and the TLTSDB.

Figures 4.2*a–f* show the simples design models related to problem 2 (short-fiber model in the theory of stability and fracture mechanics of compressed composites) when the composite is compressed at infinity ($x_1 = \pm\infty$) by forces of intensity $P = \text{const}$.

1. One short fiber (Fig. 4.2*a*); applied to composites with so low volume fraction of reinforcement that neighboring fibers do not interact neither in subcritical state nor upon buckling. In this case, one fiber in an infinite (in coordinates x_1, x_2, x_3) matrix is considered and buckling modes that decay with distance from the fiber (as $x_1, x_2, x_3 \to \pm\infty$) are analyzed.

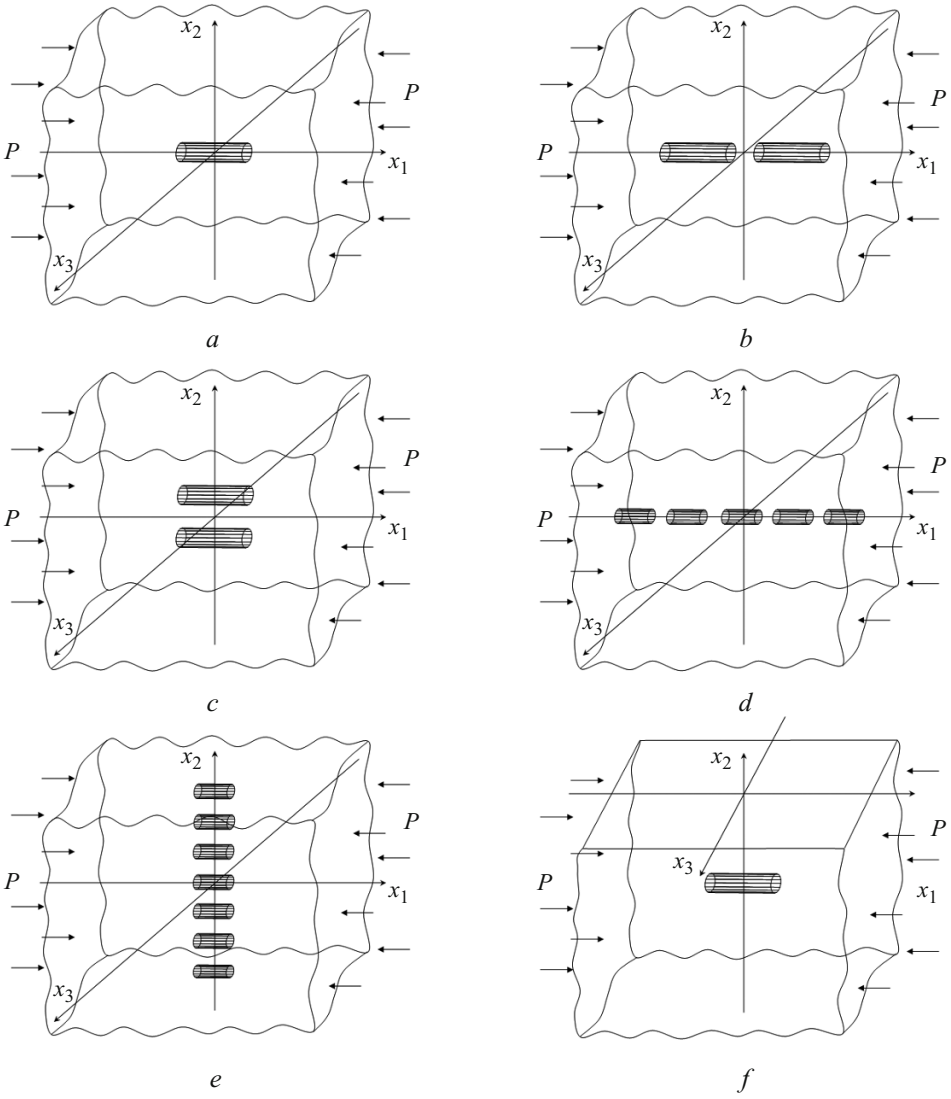

Fig. 4.2

2. Two collinear short fibers (Fig. 4.2*b*); applied to composites with so low volume fraction of reinforcement that two neighboring fibers can interact in subcritical state and upon buckling due to the irregularity of the structure. In this case, two fibers in an infinite (in coordinates x_1, x_2, x_3) matrix is considered and buckling modes that decay with distance from the fiber (as $x_1, x_2, x_3 \to \pm\infty$) are analyzed.

3. Two parallel short fibers (Fig. 4.2*c*); applied to composites with so low volume fraction of reinforcement that two neighboring fibers can interact in subcritical state and upon buckling due to the irregularity of the structure. In this case, two fibers in an infinite (in coordinates x_1, x_2, x_3) matrix is considered and buckling modes that decay with distance from the fiber (as $x_1, x_2, x_3 \to \pm\infty$) are analyzed.

4. A periodic row of collinear short fibers (Fig. 4.2*d*); applied to composites of periodic structure such that neighboring fibers of the same row interact, whereas fibers in neighboring rows do not interact (rather short distances between fibers in the same row, rather long distances between neighboring rows) in subcritical state or upon buckling. In this case, a periodic (in coordinate x_1) row of fibers in an infinite (in coordinates x_2 and x_3) matrix is considered and buckling modes that decay with distance from the row of fibers (as x_2 and $x_3 \to \pm\infty$) and are periodic in coordinate x_1 are analyzed.

5. A periodic (along the $0x_2$-axis) row of parallel short fibers (Fig. 4.2*e*); applied to composites of periodic structure such that neighboring fibers of the same row interact, whereas fibers in neighboring rows do not interact (rather short distances between fibers in the same row, rather long distances between neighboring rows) in subcritical state or upon buckling. In this

case, a periodic (in coordinate x_2) row of fibers in an infinite (in coordinates x_1 and x_3) matrix is considered and buckling modes that decay with distance from the row of fibers (as x_1 and $x_3 \to \pm\infty$) and are periodic in coordinate x_2 are analyzed.

6. One short fiber near a free surface (Fig. 4.2*f*); applied to composites with so low volume fraction of reinforcement that neighboring fibers do not interact neither in subcritical state nor upon buckling. Due to the irregularity of the structure, there are fibers located near the free surface $x_2 = 0$ and interacting with it in subcritical state and upon buckling. In this case, one fiber in a semi-infinite matrix (in the lower half-space ($x_2 \le 0$)) that interacts with the boundary of the lower half-space (certain boundary conditions on the boundary $x_2 = 0$ in a subcritical state and homogeneous boundary conditions during buckling are satisfied) is considered, and buckling modes that decay with distance from the boundary of the half-space and the fiber (as $x_2 \to -\infty$) and with distance from the fiber only (as x_1 and $x_3 \to \pm\infty$) are analyzed.

It should be noted that the sixth design model (Fig. 4.2*f*) is the simplest one for studying near-surface fracture. Certainly, the number of simple design models for studying near-surface fracture can be increased by adding the boundary of the half-space in the design models in Figs. 4.2*b–e*.

When the TLTSDB is used, the above design models are the simplest in the fracture mechanics of short-fiber reinforced composites under compression modeled by a piecewise-homogeneous material. The problems arising in this case are three-dimensional (spatial) TLTSDB problems. As indicated in Sec. 3.3.1, it was strictly proved that the sufficient conditions for the applicability of the static method of stability analysis (Sec. 2.4.2) are satisfied; therefore, the buckling problems are reduced to three-dimensional eigenvalue problems, i.e., the Euler method is used. Thus, using the second approach is fully consistent with the standard and rigorous method of studying buckling by analyzing the behavior of small perturbations in linearized three-dimensional dynamics.

As already mentioned, the formulated problems of the fracture mechanics of short-fiber reinforced composites compressed along fibers (Figs. 4.2*a–f*) are three-dimensional static TLTSDB problems. For composites, there are also two-dimensional static TLTSDB problems for which design models are two-dimensional analogs of three-dimensional static problems, and the design models in Figs. 4.2*a–f* are two-dimensional problems (plane strain) for ribbon-reinforced composites.

Ribbon-Reinforced Composites. Such composites are usually reinforced with thin ribbons of various shape. Here we will consider composites reinforced with parallel long flat ribbons of constant cross section located.

Reinforcing ribbons are assumed infinite along the $0x_3$-axis ($-\infty < x_3 < +\infty$, the $0x_3$-axis is perpendicular to the plane of the figure). In this case, it is possible to solve two-dimensional problems (plane strain) in the plane $x_1 0x_2$, considering the cross section of the ribbon to be reinforcement (dark color in Figs. 4.3*a–f*). Figures 4.3*a–f* show six design models in the plane $x_1 0x_2$ visually corresponding to Figs. 4.2*a–f* where reinforcements (cross sections of ribbons) are shown by dark rectangles. Let us briefly describe the design models in Figs. 4.3*a–f*, following the analogy with Figs. 4.2*a–f*.

1. One reinforcement element (Fig. 4.3*a*); applied to composites with so low volume fraction of reinforcement that neighboring elements do not interact neither in subcritical state nor upon buckling. In this case, one element in an infinite (in coordinates x_1 and x_2) matrix is considered and buckling modes that decay with distance from the element (as $x_1, x_2 \to \pm\infty$) are analyzed.

2. Two collinear reinforcement elements (Fig. 4.3*b*); applied to composites with low volume fraction of reinforcement where two neighboring elements can interact in subcritical state and upon buckling due to the irregularity of the structure. In this case, two collinear elements in an infinite (in coordinates x_1 and x_2) matrix is considered and buckling modes that decay with distance from two neighboring elements (as $x_1, x_2 \to \pm\infty$) are analyzed.

3. Two parallel reinforcement elements (Fig. 4.3*c*); applied to composites with low volume fraction of reinforcement where two neighboring elements can interact in subcritical state and upon buckling due to the irregularity of the structure. In this case, two parallel elements in an infinite (in coordinates x_1 and x_2) matrix is considered and buckling modes that decay with distance from two neighboring elements (as $x_1, x_2 \to \pm\infty$) are analyzed.

4. A periodic row of collinear reinforcement elements (Fig. 4.3*d*); applied to composites of periodic structure such that neighboring elements of the same row interact, whereas elements in neighboring rows do not interact (rather short distances between elements in the same row, rather long distances between neighboring rows) in subcritical state or upon buckling. In this case, a periodic (in coordinate x_1) row of collinear elements in an infinite (in coordinate x_2) matrix is considered and buckling modes that decay with distance from the row of elements (as $x_2 \to \pm\infty$) are analyzed.

5. A periodic (along the $0x_2$-axis) row of parallel reinforcement elements (Fig. 4.3*e*); applied to composites of periodic structure such that neighboring elements of the same row interact, whereas elements in neighboring rows do not interact (rather

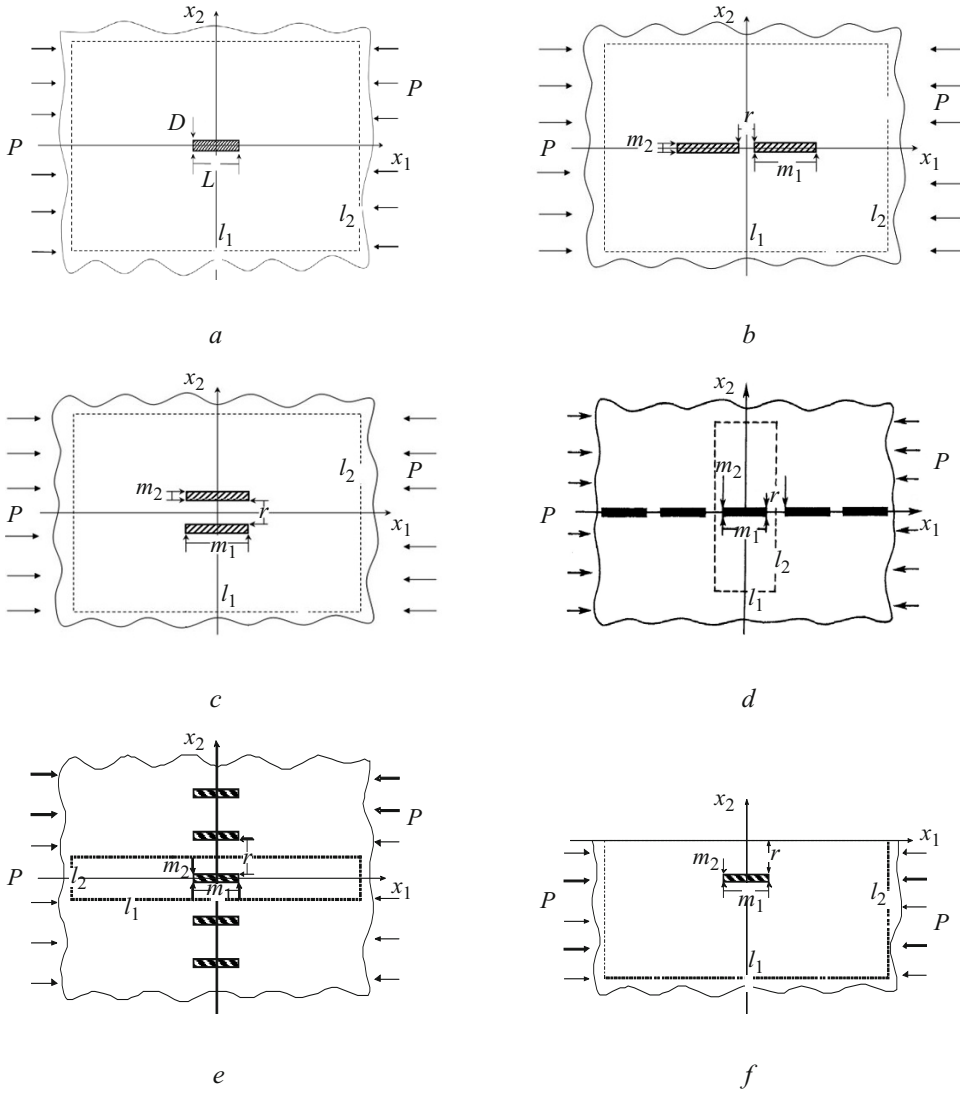

Fig. 4.3

short distances between elements in the same row, rather long distances between neighboring rows) in subcritical state or upon buckling.

In this case, a periodic (in coordinate x_2) row of parallel elements in an infinite (in coordinate x_1) matrix is considered and buckling modes that decay with distance from the row of elements (as $x_1 \to \pm\infty$) are analyzed.

6. One reinforcement element near a free surface (Fig. 4.3*f*); applied to composites with so low volume fraction of reinforcement that neighboring elements do not interact neither in subcritical state nor upon buckling. Due to the irregularity of the structure, there are reinforcement elements located near the free surface $x_2 = 0$ and interacting with it in subcritical state and upon buckling. In this case, one element in a semi-infinite matrix (in the lower half-plane ($x_2 = 0$)) that interacts with the boundary of the lower half-space (certain boundary conditions on the boundary $x_2 = 0$ in a subcritical state and homogeneous boundary conditions during buckling are satisfied) is considered, and buckling modes that decay with distance from the boundary of the half-plane and the reinforcement element (as $x_2 \le 0$) and with distance from the element only (as x_1 and $x_2 \to -\infty$) are analyzed.

It should be noted that the sixth design model (Fig. 4.3*f*) is the simplest one for studying near-surface fracture in the plane case. Certainly, the number of simple design models for studying near-surface fracture can be increased by adding the boundary of the half-plane in the design models in Figs. 4.3*b–e*.

When the TLTSDB is used, the above design models are the simplest in the fracture mechanics of composites with short reinforcement elements under compression modeled by a piecewise-homogeneous material. The problems arising in this case

are two-dimensional TLTSDB problems. As indicated in Sec. 3.3.1, it was strictly proved that the sufficient conditions for the applicability of the static method of stability analysis (Sec. 2.4.2) are satisfied; therefore, the buckling problems are reduced to two-dimensional eigenvalue problems, i.e., the Euler method is used. Thus, using the second approach is fully consistent with the standard and rigorous method of studying buckling by analyzing the behavior of small perturbations in linearized two-dimensional dynamics.

Section 3.3.3 outlined results on internal and near-surface fracture of composite laminates in the plane (Fig. 3.25) and spatial (Fig. 3.26) cases, considering layers of reinforcement and matrix to be very long (infinite). If reinforcement layers are short (finite) in the plane case (Fig. 3.25), we arrive at the design models shown in Figs. 4.3*a–f*. Thus, for plane problems in the plane $x_1 0 x_2$, the terms "reinforcement element" (used in describing the models in Fig. 4.3*a–f* to refer to the cross section of ribbon reinforcement) and "short layer" (which can be used to refer to the reinforcement in composite laminate (Fig. 3.35)) are equivalent. Hence, we may say that design models in Figs. 4.3*a–f* apply to plane problems for composite laminates reinforced with short layers aligned along the $0x_1$-axis.

Thus, we have formulated problems for composites reinforced with unidirectional short fibers and short layers, compressed along the reinforcement, and modeled by a piecewise-homogeneous material. Sections 2 and 3 discussed results on related problems obtained using various design models and the piecewise-homogeneous material model. In this connection, it makes sense to classify the design models used.

4.3. Classification of Design Models. On Analogies. Let us briefly consider the classification of the design models used in Secs. 2 and 3. Note that the piecewise-homogeneous material model uses formulas for different homogeneous deformable bodies to describe the deformation of the matrix and each reinforcement element, the continuity conditions (depending on the problem statement) for the stress and displacement vectors being satisfied at the interfaces between the reinforcement and the matrix performance. For this model, it is not necessary to use three-dimensional rigorous formulas of classical models of solid mechanics to describe the deformation of the matrix and each reinforcement element. It is possible to use simplified or complicated formulas, associated design models, and interface conditions.

Here we will discuss three types of general design models use in the fracture mechanics of unidirectional fibrous and laminated composites under compression.

4.3.1. Model of Infinite Fibers and Layers in the First Approach. Consider long fibers and layers as reinforcement. In the design models, fibers and layers are considered infinitely long, and buckling modes periodic (sinusoidal) along fibers and layers are analyzed. It is obvious that a three-dimensional (spatial) problem statement should be used for fibrous composites and a two-dimensional (plane) problem statement should be used for laminated composites.

The above features of the first approach are manifested in analyzing the well-known and publications [551, 161], which are included in the fundamental collective books on fracture [160] and on composites [127]. The analysis of and conclusions from [551] and [161] are briefly discussed in Sec. 3.3.3.3.3. Actually, the studies [551, 161] use a plane problem statement in the plane $x0y$ (Fig. 3.33 corresponds to Figs. 3.22 in [551, 161]) and reinforcement elements are called as fibers. Actually, the reinforcements in Fig. 3.33 are ribbons of the same cross section as in composite laminates.

Thus, the papers [551, 161] address a plane problem for composite laminate, and specific results (Fig. 3.33) were also obtained for a plane problem. We will use a terminology for fibrous composites, although fibrous composites should be studied using a three-dimensional (spatial) problem statement corresponding to, for example, Figs. 4.2*a–f*. Thus, the approximate approach proposed in [551, 161] consists in the following:

(i) the plane case is considered for laminated composites;

(ii) quantitative results obtained for laminated composites are used to analyze phenomena occurring in fibrous composites;

(iii) terminology typical for fibrous composites is used, where reinforcement elements are called fibers in the plane case (in which reinforcement elements are ribbons).

Note that this approximate approach disregards the issue of analogy between laminated and fibrous composites. Moreover, the results obtained in [551, 161] using the first approach are approximate. The accuracy of results was addressed in Sec. 3.3.3.3.3.

4.3.2. Model of Infinite Fibers and Layers in the Second Approach. Consider long fibers and layers as reinforcement. In the design models, fibers and layers are considered infinitely long, and buckling modes periodic (sinusoidal) along fibers and layers are analyzed, which corresponds to the experimental results (Figs. 3.4–3.6). It is obvious that a three-dimensional (spatial)

problem statement should be used for fibrous composites and a two-dimensional (plane) problem statement should be used for laminated composites.

The results obtained using the piecewise-homogeneous material model and the TLTSDB for elastic and plastic bodies with general constitutive equations are discussed in Sec. 3.3.4 for fibrous composites in three-dimensional (spatial) problem statement (see [57, Vol. 1, Chs. 4 and 6] for the fullest discussion of the results). The results obtained using the piecewise-homogeneous material model and the TLTSDB for elastic and plastic bodies with general constitutive equations are discussed in Sec. 3.3.3 for laminated composites in three-dimensional (Fig. 3.26) and two-dimensional (Fig. 3.25) problem statements (see [57, Vol. 1, Chs. 3 and 5] for the fullest discussion of the results).

From the results for fibrous and the laminated composites obtained using the model of infinitely long fibers and layers and the piecewise-homogeneous material model within the framework of the second approach (Sec. 3.1.3), it follows that there is no need to question the analogies between fibrous and laminated composites. This is so because all the results discussed in Sec. 4.3.2 were obtained using three-dimensional (spatial) problem statement and the TLTSDB for fibrous and laminated composites with polymer and metal matrix, which underlie the second approach (Sec. 3.1.3). For composite laminates (Fig. 3.25), however, a two-dimensional problem statement was used, which follows from the three-dimensional (spatial) statement. Thus, using the second approach is fully consistent with the standard and rigorous method of studying buckling by analyzing the behavior of small perturbations in linearized three-dimensional dynamics. Moreover, the piecewise-homogeneous material model and the TLTSDB underlie the second approach, which is the most rigorous approach in the fracture mechanics of composites under compression and in solid mechanics.

The above considerations apply to all the results discussed in Sec. 4.3.2.

4.3.3. Model of Short Fibers and Layers in the Second Approach. Unlike Secs. 4.3.1 and 4.3.2, here we consider composites reinforced with short reinforcement elements to which the model of infinite fibers and layers is inapplicable. In this case, buckling modes behave differently (as follows from experimental studies (Fig. 4.2))—they are not periodic along the reinforcement axis under compression along the reinforcement.

Remark 4.1. A typical feature of the problems solving using the model of Sec. 4.3.3 is an inhomogeneous subcritical state (three-dimensional in the general case of fibrous and laminated composites and two-dimensional in the special case of composite laminates).

Here we address models for fibrous and laminated composites.

Fibrous composites are considered to have an infinite matrix reinforced with short fibers. The simplest design models for studying internal fracture (internal instability) and near-surface fracture (near-surface instability) are presented in Figs. 4.2*a–f*. The problems being considered are reduced to three-dimensional static TLTSDB eigenvalue problems (due to the use of the second approach). A typical feature of the problems is the dependence of the coefficients of the associated systems of differential equations on three space variables.

Remark 4.2. Specific results for fibrous composites reinforced with short fibers for the design models in Fig. 4.2*a–f* can be obtained using numerical methods and computer mechanics. Such results have not been obtained yet either with the first approach or with the second approach.

For laminated composite, it is possible to consider two-dimensional problems (plane strain) in the plane $x_1 0 x_2$ in Fig. 4.3*a–f* for ribbon-reinforced composites. In this case, the reinforcement is long flat ribbons of constant cross-section parallel along the $0x_3$-axis (which is perpendicular to the plane of Fig. 4.3*a–f*). In this situation, we consider two-dimensional problems in the cross-sectional plane for an infinite two-dimensional matrix reinforced with short reinforcement elements corresponding to the cross section of ribbons. The simplest design models for studying internal fracture (internal instability) and near-surface fracture (near-surface instability) are presented in Figs. 4.3*a–f*. The problems being considered are reduced to two-dimensional static TLTSDB eigenvalue problems (due to the use of the second approach). A typical feature of the problems is the dependence of the coefficients of the associated systems of differential equations on two space variables.

Remark 4.3. Specific results for laminated composites reinforced with short reinforced elements for the design models in Fig. 4.3*a–f* can only be obtained using numerical methods and computer mechanics.

Such results have been obtained for a plane problem (plane strain) using the second approach/ These results are reported in the publications cited in the prologue to Sec. 4.

Remark 4.4. The above results were obtained for a plane problem (Figs. 4.3*a–f*). However, considering the approximate approach to studying fibrous composites mentioned in Sec. 4.3.1 and proposed in [551, 161], the results obtained for a plane problem [64, 67, 252–254, 362–368, 504] can be used to analyze the phenomena occurring in fibrous composites

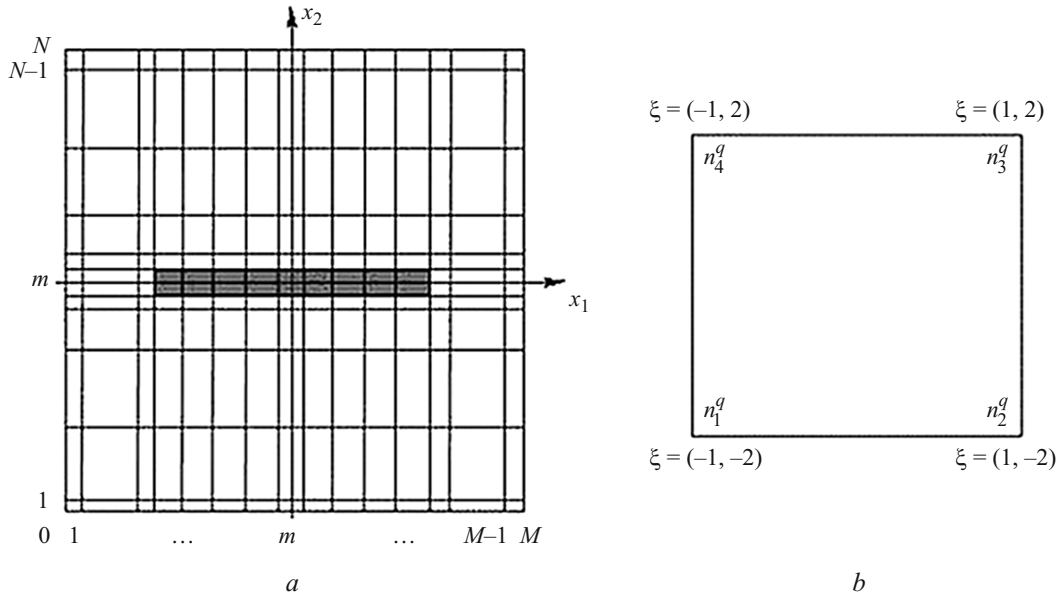

a *b*

Fig. 4.4

(Figs. 4.2*a–f*). These publications related to a plane problem (plane strain) use terminology typical for fibrous composites. The reinforcement elements shown in Figs. 4.3*a–f* are called short fibers although, actually, these elements correspond to the cross section ribbon reinforcement. This remark can apply to plane problems of the mechanics of brittle fracture of composites with short reinforcements under compression considered below.

4.4. Statement of Plane Problems of the Mechanics of Brittle Fracture of Composites with Short Reinforcement Elements under Compression. Section 4 gave a little attention to various aspects of the model of short fibers (generally, short reinforcement elements) in the theory of stability and in the fracture mechanics of compressed composites reinforced with such elements. In [64, 65], this model is called finite-fiber model. Other names for this model can also be proposed.

4.4.1. Problem Statement. Here we will briefly discuss statements of plane problems and methods for solving them for brittle fracture using the design models in Figs. 4.3*a–f*. The major results on problem statements and problem-solving methods are presented in [64–67, 252–254, 362–368, 504, etc.]. These results may be considered to be pioneering in rigorous study for composites with short reinforcement elements in the theory of stability and brittle fracture under compression.

The principles of the approach to problem statement and, naturally, its applicability conditions are formulated below.

1. The brittle fracture of composites compressed along the reinforcements is analyzed. In this connection, the reinforcement elements, according to Remark 4.4, will hereafter be called fibers, and matrices will be modeled by linear elastic isotropic bodies. Such modeling is valid for relatively short period of action of external loads and for moderate temperatures.

2. Theory 3 (as termed in Sec. 2.2) is used. The subcritical state is determined using a geometrically linear theory. This assumption is considered valid for relatively stiff fibrous composites that undergo fracture at relatively small strains.

3. The external loads are assumed dead. As already mentioned in Secs. 3 and 4, the sufficient applicability conditions for the static TLTSDB method (Euler method) are satisfied and the problems being discussed are reduced to two-dimensional static eigenvalue problems, the coefficients of the associated system of differential equations depending on two variables (x_1 and x_2 according to Figs. 4.3*a–f*).

4. The reinforcement and the matrix are assumed perfectly bonded (the stress and displacement vectors are continuous at the interfaces) in either determining the subcritical state or solving buckling problems.

5. For the design models in Figs. 4.3*a–f* used to study internal and near-surface fracture, appropriate conditions of damping at infinity are satisfied. For a periodic system of fibers, the appropriate periodicity conditions are satisfied as well. These conditions were detailed in Sec. 4.2 for each of the design models in Figs. 4.3*a–f*.

6. A plane problem (plane strain) is solved using the TLTSDB in Lagrangian coordinates (x_1, x_2), which coincide with Cartesian coordinates in the reference (first, undeformed) state.

The above principles follow from [64, 65].

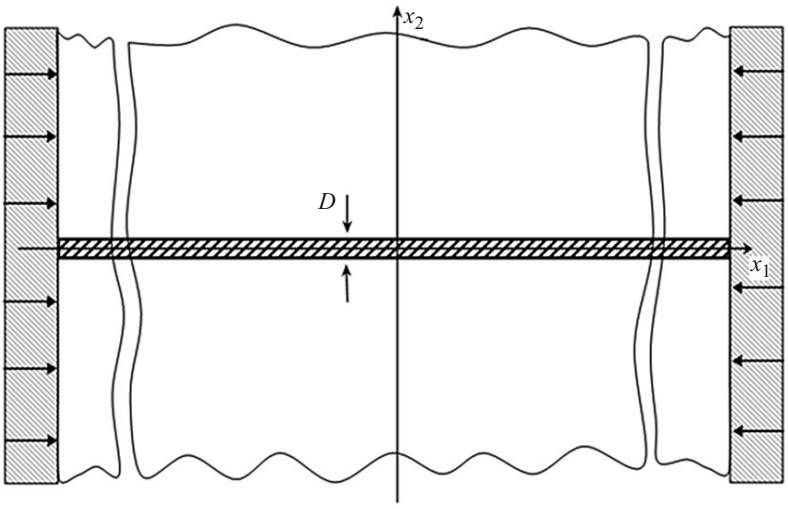

Fig. 4.5

4.4.2. On Numerical Method of Solving the Problems of Sec. 4.4. As mentioned in Remark 4.3, two-dimensional static eigenvalue problems with variable coefficients in the differential equations depending on the two variables x_1 and x_2 (Figs. 4.3*a–f*) can only be solved using numerical methods and computer mechanics. In what follows, we will briefly discuss the numerical analysis of such problems. The above principles should be considered in combination with the design models in Figs. 4.3*a–f*. We will follow the review [65] (see [64] for more details).

The problems formulated are solved using the finite-difference method, the variational difference method, and the concept of reference schemes. This approach was detailed in the review [504] with reference to wide classes of problems of composite mechanics. Following [65], we will consider the basic stages in the implementation of the numerical method [504] for the design model in Fig. 4.3*a*. The infinite domain (in the design model) is replaced by a finite rectangular domain with side lengths $l_1 \times l_2$. Note that the same finite rectangle $l_1 \times l_2$ is shown in all the design models in Fig. 4.3. To determine the subcritical state and to solve the TLTSDB problem, the condition of decay at infinity is replaced by similar conditions of decay on the boundary of the rectangle. The dimensions of the external rectangle $l_1 \times l_2$ are chosen by way of computational experiments so that their further increase does not affect the results. The rectangle $l_1 \times l_2$ is covered by straight lines parallel to the $0x_1$- and $0x_2$-axes to form a doubly nonuniform difference mesh $\overline{\omega} = \omega \cup \gamma$, where ω is the set of internal nodes and γ is the set of boundary nodes. The mesh is shown in Fig. 4.4*a* and its cell in Fig. 4.4*b*. The mesh is such that the material can be considered homogeneous within each cell. The mesh can be refined where the material properties change sharply, as at the interfaces between the matrix and fibers. It is assumed that near the interfaces between the matrix and fiber, the mesh can be refined until further refinement does not influence the result (critical load). Thus, the mesh consisting of internal and boundary nodes is a set of rectangular cells that have mechanical and geometric characteristics of the composite component (matrix or fiber) contained in them.

Discrete problems over the mesh $\overline{\omega}$ are formulated using the variational difference method and the concept of reference schemes. The components of reference schemes are determined by approximating and minimizing the appropriated functional on a cell template. When applying this procedure to buckling problems, the variational principles of the TLTSDB are used. Summing the values of reference schemes at each node of the mesh, we arrive at difference problems that are discrete analogs of the corresponding continuous problems.

Difference problems in operator form are then formulated to determine the subcritical state (using the classical linear theory of elasticity) and to solve the buckling problem (using theory 3, as termed in Sec. 2.2). The difference operators of the buckling problems preserve the properties of self-adjointness and positive definiteness of the respective differential operators. Thus, the buckling problem is solved by solving the appropriate finite-difference equations, which can be represented as a generalized algebraic eigenvalue problem.

To solve algebraic problems, direct and iterative methods well known in the theory of difference schemes are used, such as the Cholesky method, the conjugate-gradient method, the subspace-iteration method, the gradient-descent method.

This completes the brief discussion of the numerical method of solving the problems formulated in Secs. 4.4.2 and Sec. 4.2.

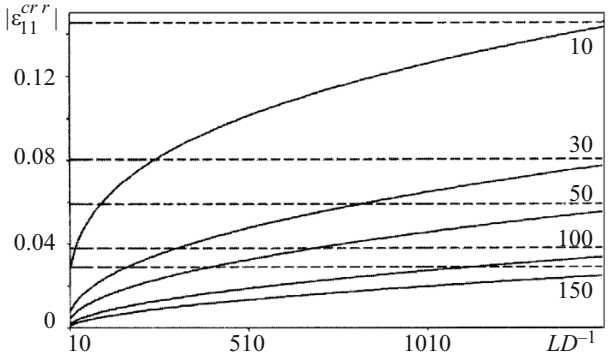

Fig. 4.6

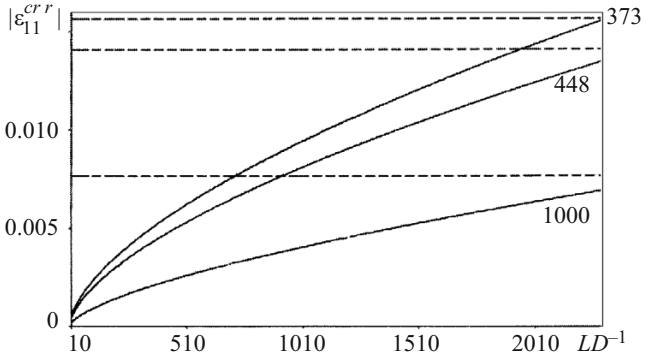

Fig. 4.7

4.5. Results on Plane Problems of the Mechanics of Brittle Fracture of Composites Reinforced with Short Fibers under Compression. Here we will briefly discuss specific results on plane problems of the mechanics of brittle fracture of short-fiber reinforced composites under compression. These results were obtained using the problem statements from Sec. 4.4.1, the method outlined in Sec. 4.4.2, and the design models in Fig. 4.3*a–f*.

Remark 4.5. The concept of imaginary buckling modes was introduced in [64–67, 252–254, 362–368, 504]. In this connection, it is reasonable to accurately define this concept because it will be used below.

Imaginary buckling modes are predicted (before computational experiments) general patterns of deformation of a fiber and the matrix surrounding it during buckling following from physical considerations and the relative stiffness and geometric characteristics of the fiber and the matrix.

Thus, imaginary buckling modes do not always correspond to the eigenfunctions of the problem and characterize the expected general pattern of deformation of a fiber and the matrix surrounding it. Imaginary buckling modes are sometimes convenient for analysis of specific results.

Example. Let us consider the case where the fiber is much stiffer then the matrix. Then, during buckling of the composite, the behavior of a fiber is similar to that of a perfectly rigid body. In this case, the only imaginary buckling mode of a fiber and the matrix surrounding is rigid-body turn of the fiber.

Remark 4.5 should be assigned to the prologue of Sec. 4.5.

4.5.1. Asymptotic Passage to the Infinite-Fiber Model. Here we will use the design model in Fig. 4.3*a* for one fiber, where: L is the fiber length; D is the cross-sectional diameter (see [65, 363] for more details). It is obvious that when $LD^{-1} \to \infty$, the design model in Fig. 4.5 corresponding to the infinite-fiber model follows from the design model in Fig. 4.3*a* corresponding to the short-fiber model. In Fig. 4.5, the upper and lower half-planes (matrix) are connected by an infinite strip (reinforcement) of width D. According to Remark 4.4, the strip models an infinite fiber in the plane case. The design model in Fig. 4.5 corresponds to Fig. 3.25 (when $h_m \to \infty$ and $2h_r = D$) in Sec. 3.3.3, which discussed results on composite laminates using the infinite-fiber model (or the infinite-layer model) and the second approach as termed in Sec. 3.1.3.

The results of the comparative analysis are the dependence of $|\varepsilon_{11}^{\mathrm{cr\,r}}|$ on the geometrical parameter LD^{-1}. In the case of the infinite-fiber model, this quantity is the critical strain along the $0x_1$-axis for both reinforcement and matrix, according to Remark 3.3.

In the case of the finite-fiber model, we have

$$\varepsilon_{11}^{\mathrm{cr\,r}} = \varepsilon_{11}^{\mathrm{cr\,r}}(x_1, x_2) \quad \text{for} \quad x_1 = 0 \ \text{ and } \ x_2 = 0 \tag{4.1}$$

for Fig. 4.3*a*. In this case, quantity (4.1) is the critical strain of the fiber along the $0x_1$-axis at the middle of the fiber. The critical strain of the matrix along the $0x_1$-axis determined at infinity can reach very different values. This situation should necessarily be taken into account when comparing results obtained using both models.

Figures 4.6 and 4.7 presents results for micro- and nanocomposites, respectively, with polymer matrix with the following mechanical parameters: $E_m = 2.68$ GPa, $\nu_m = 0.4$. The difference between micro- and nanocomposites is determined by the scale defined in [90, 423]. For microcomposites, the following values of the mechanical and geometrical parameters were

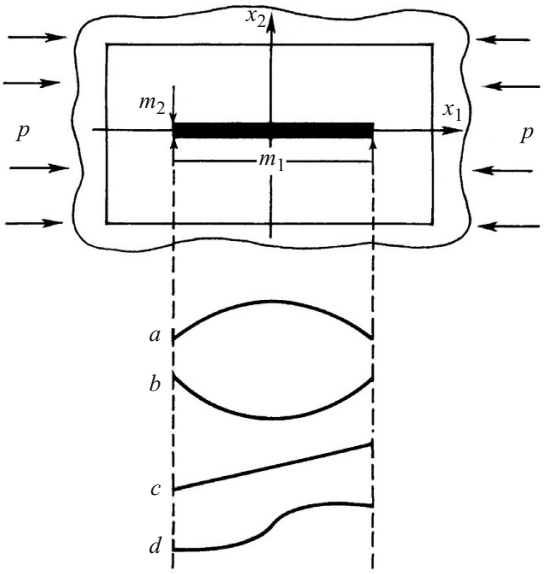

Fig. 4.8

used: $E_r \cdot E_m^{-1}$ = 10, 30, 50, 100, 150 (E_r and E_m are Young's moduli for the fibers and the matrix, respectively), $10 \le LD^{-1} \le 1510$. In Fig. 4.6, the curves are denoted by the values of $E_r \cdot E_m^{-1}$. For nanocomposites, the following values were used: $E_r \cdot E_m^{-1} = 285$, 373, 448, 500, 1000 and LD^{-1} ($10 \le LD^{-1} \le 2310$). In Fig. 4.7, the curves are denoted by the values of $E_r \cdot E_m^{-1}$. The solid lines correspond to the finite-fiber model, and the dashed lines to the infinite-fiber model.

It follows from Figs. 4.6 and 4.7 that for all values of $E_r \cdot E_m^{-1}$, as the geometrical parameter LD^{-1} increases within the specified range, the critical strains along the $0x_1$-axis calculated using the finite-fiber model asymptotically tend to the critical strains obtained using the infinite-fiber model. For the upper limits of the ranges of geometrical parameter, the critical strains are almost equal, which can be used to determine the limits of applicability of the infinite-fiber model depending on $E_r \cdot E_m^{-1}$ and LD^{-1}. Such results are analyzed in [65, 64, 363].

4.5.2. Results for One Fiber under Compression along It. The design model is shown in Fig. 4.3*a*.

For more accurate discussion of results, the design model (Fig. 4.3*a*) is shown in Fig. 4.8 in combination with the imaginary (as termed in Remark 4.5) buckling modes of one short fiber (Fig. 4.8) under compression along it.

In Fig. 4.8, as well as in the other figures of Sec. 4.5 related to imaginary buckling modes, the dark segments represent the centerlines of fibers (reinforcements) after buckling. It is assumed that the matrix surrounding the fiber deforms during buckling as described in principle 4 (Sec. 4.4.1) of the statement of plane problems of the mechanics of brittle fracture of composites with short reinforcement elements under compression. According to this principle, the reinforcement and the matrix are assumed perfectly bonded (the stress and displacement vectors are continuous at the interfaces) in either determining the subcritical state or solving buckling problems.

The imaginary buckling modes (*a* and *b* in Fig. 4.8) are symmetric about the vertical axis $0x_2$. Also, the modes *a* and *b* are equivalent (the critical loads are equal) due to the symmetry of the design model in Fig. 4.8 (upper part of the figure) about the horizontal axis $0x_1$. Symmetric buckling modes can be called flexural modes, similarly to the buckling mode of a strip under axial compression.

The imaginary buckling modes (*c* and *d* in Fig. 4.8) are antisymmetric about the vertical axis $0x_2$. The antisymmetric buckling mode (*c*) corresponds to a rigid-body turn of a fiber when the matrix does not ensure adequate support because of which a kind of a plastic hinge forms near the fiber ends during buckling. It is obvious such a buckling mode can occur when the matrix and the reinforcement differ considerably in stiffness, which is typical of production processes for composites. The antisymmetric buckling mode (*d*) corresponds a turn of a fiber accompanied by bending.

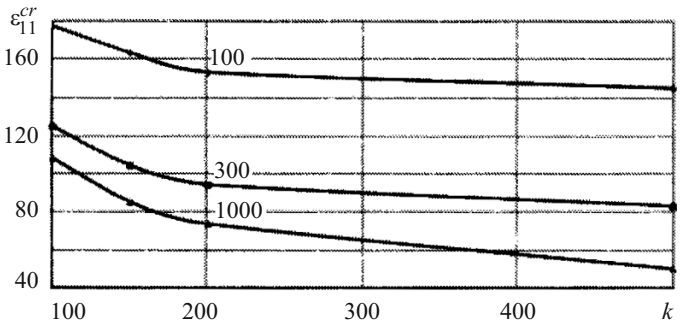

Fig. 4.9

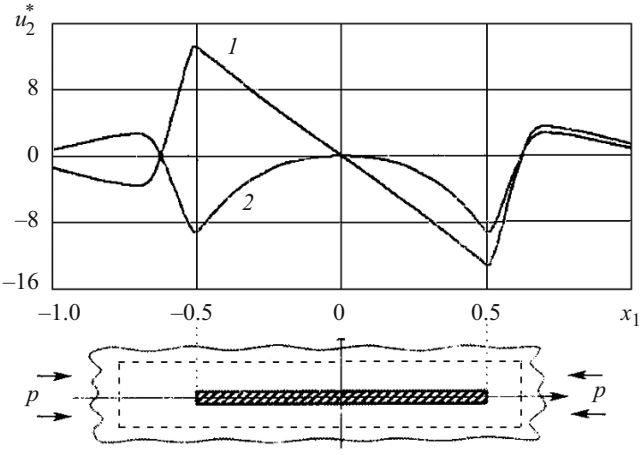

Fig. 4.10

The numerical solution of the buckling problem is presented in Fig. 4.9 as the dependence of critical strain $|\varepsilon_{11}^{\mathrm{cr}}|$ along the $0x_1$-axis (Fig. 4.8) for the matrix at infinity on the shape factor k of the reinforcement:

$$k = m_1 \cdot m_2^{-1} = L \cdot D^{-1}. \tag{4.2}$$

The following parameter values were used: $E_r \cdot E_m^{-1} = 100, 200, 300, 500, 1000$, $E_m = 2.75$ GPa, $\nu_r = \nu_m = 0.35$, $100 \le k \le 500$. Figure 4.9 gives the results only for three values: $E_r \cdot E_m^{-1} = 100, 300, 1000$. The mechanical characteristics (E_m and ν_m) of the matrix correspond to molding polyamide. The ultimate strain of this material corresponding to the ultimate strength is equal to 0.028. In all the curves in Fig. 4.9, the critical strain $\varepsilon_{11}^{\mathrm{cr}}$ for the matrix at infinity corresponding to buckling is much lower than the above ultimate strain. This situation suggests the possibility of fracture of the composite under compression because of microbuckling before the ultimate strength of the matrix is achieved.

Let us consider examples of numerical determination of the buckling mode. The buckling mode is characterized by the dimensionless displacement u_2^* along the vertical axis $0x_2$ divided by an amplitude factor:

$$u_2^*(x_1) = \left[u_2(x_1, x_2)\big|_{x_2=0} \right] \cdot \left[\left| \max\left\{ u_2(x_1, x_2)\big|_{x_2=0} \right\} \right| \right]^{-1}. \tag{4.3}$$

Figure 4.10 shows, in the upper part, buckling modes characterized by the function $u_2^*(x_1)$ (4.3) for a composite with parameters $E_r \cdot E_m^{-1} = 1000$, $E_m = 2.76$ GPa, $\nu_r = \nu_m = 0.35$. Curve *1* corresponds to $k = 10$ and curve *2* to $k = 30$, where k is defined by (4.2). Also Fig. 4.10 shows a portion of the design model in Fig. 4.8. The linear dimensions in the upper and lower parts of Fig. 4.10 along the horizontal axis $0x_1$ coincide; thus, the fiber ends correspond to $x_1 = \pm 0.5$ in the upper part. Hence, the curves in the upper part of Fig. 4.10 represent

a short fiber for $|x_1| \le 0.5$;

and the matrix for $0.5 \le |x_1| \le 1.0$.

The following conclusions can be drawn from the analysis of the numerically determined buckling modes shown in the upper part of Fig. 4.10:

1. When fibers are very short ($k = 10$, where k is defined by (4.2)), the buckling mode (curve *1*) occurs, which corresponds to the antisymmetric imaginary mode (Fig. 4.8*c*). In this case, the reinforcement element undergoes a rigid-body turn (see Sec. 4.5.2 for a more detailed description of the mode).

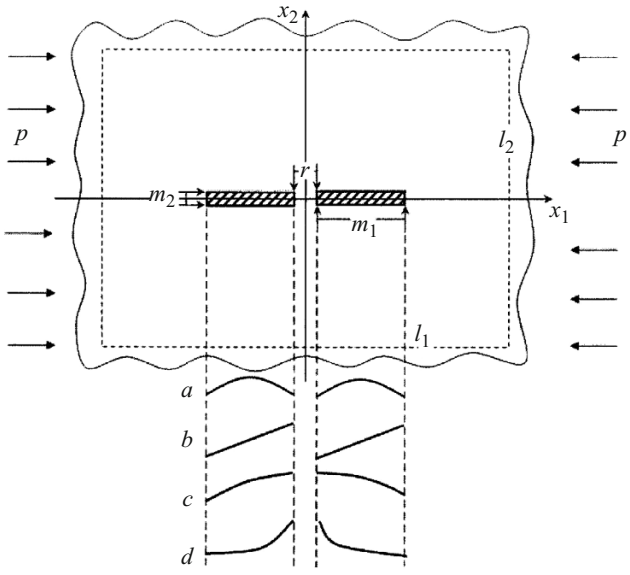

Fig. 4.11

2. When fibers are longer ($k \geq 30$, where k is defined by (4.2)), the buckling mode (curve *2*) occurs, which corresponds to the imaginary symmetric or flexural mode (Fig. 4.8*a*).

Thus, the above analysis and the conclusions from it suggest that the imaginary buckling modes considered in Remark 4.5 are useful for analysis of buckling modes determined numerically.

More details on results obtained using the design model in Fig. 4.3*a* can be found in [64–66, 366, 368, etc.].

4.5.3. Results for Two Collinear Fibers under Compression along Them. The design model is shown in Fig. 4.3*b*.

For more accurate discussion of the results, the design model (Fig. 4.3*b*) is shown in Fig. 4.11 in combination with the imaginary (as termed in Remark 4.5) buckling modes of two collinear short fibers (Fig. 4.11) under compression along them.

In Fig. 4.11, as well as in the other figures of Sec. 4.5 related to imaginary buckling modes, the dark segments represent the centerlines of fibers (reinforcements) after buckling. It is assumed that the matrix surrounding the fiber deforms during buckling as described in principle 4 (Sec. 4.4.1) of the statement of plane problems of the mechanics of brittle fracture of composites with short reinforcement elements under compression. According to this principle, the reinforcement and the matrix are assumed perfectly bonded (the stress and displacement vectors are continuous at the interfaces) in either determining the subcritical state or solving buckling problems.

The imaginary buckling modes *a*, *b*, *c*, and *d* shown in the lower part of Fig. 4.11 can be characterized as follows.

The flexural buckling mode (*a*) corresponds to the case where the fibers buckle almost independently of each other.

The buckling mode (*b*) is independent rigid-body turns of both fibers. This is possible when the fibers are rather stiff and the matrix does not provide the appropriate support, which results in the formation of a kind of plastic hinge at the fiber ends during buckling and when the fibers hardly interact.

The buckling mode (*c*) corresponds to the case where the two fibers buckle in the same flexural mode, which is possible when the fibers are quite flexible and close to each other.

The buckling mode (*d*) corresponds to the case where the two fibers undergo relatively rigid turn and bending. This is possible when the fibers are rather stiff and the matrix does not provide the appropriate support, which results in the formation of a kind of plastic hinge between the fibers during buckling.

The construction of imaginary modes can be continued considering the buckling modes in Fig. 4.11) as the first imaginary modes.

For the purpose of numerical analysis, the dimensionless parameter $r_1^* = r \cdot m_1^{-1}$ is introduced to characterize the dimensionless distance between ends of two neighboring fibers (Fig. 4.3*b*), the geometrical dimensions m_1, m_2, and r are indicated in Fig. 4.3*a*. The following parameter values were used: $E_r \cdot E_m^{-1} = 1000$, $\nu_r = \nu_m = 0.35$, $E_m = 2.76$ GPa,

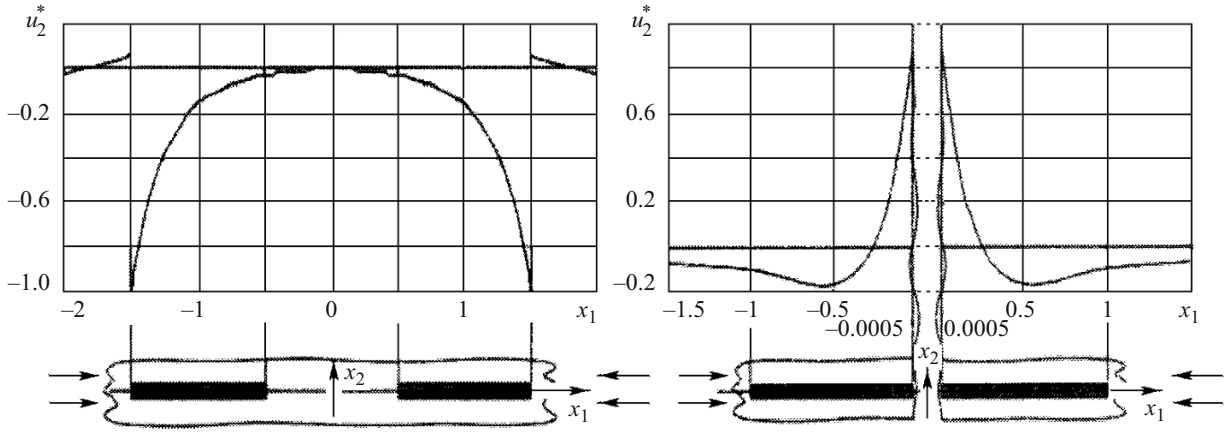

a *b*

Fig. 4.12

$k = m_1 \cdot m_2^{-1} = 100$, $0.001 \le r_1^* \le 32$. This value of $E_r \cdot E_m^{-1}$ can occur in technological processes due to the strong temperature dependence of E_m.

Figures 4.12*a* and *b* (for $r_1^* = 1$ and $r_1^* = 0.001$, respectively) show the distribution along the $0x_1$-axis of the dimensionless displacement u_2^* along the vertical axis $0x_2$ defined by (4.3). From Fig. 4.12*a* ($r_1^* = 1$), it follows that the buckling mode (the upper part of Fig. 4.12*a*) is similar to the imaginary buckling mode (*c*), which is shown in the lower part of Fig. 4.11 and called general flexural buckling mode.

From Fig. 4.12*b* ($r_1^* = 0.001$), it follows that the buckling mode (the upper part of Fig. 4.12*b*) is similar to the imaginary buckling mode (*d*), which is shown in the lower part of Fig. 4.11 and called mutual turn and bending of the fibers with a plastic hinge between them. The imaginary buckling modes *a*, *b*, *c*, and *d* shown by dark segments in the lower part of Fig. 4.11 apply only to fibers (the dark segments are limited by the vertical dotted straight lines representing the linear dimensions of the fibers). In this connection, the lines representing the buckling modes in Fig. 4.12*a*, *b* can be compared with only within the linear dimensions of the fibers. For example, such a comparison is possible for $0.5 \le |x_1| \le 1.5$ in Fig. 4.12*a* and for $0.0005 \le |x_1| \le 1.0$ in Fig. 4.12*b*.

The results of numerical analysis of the influence of interaction of two collinear short fibers (design models in Fig. 4.3*b* and 4.11) on the critical load ε_{11}^{cr} in a matrix at infinity (for $x_1 \to \pm\infty$) are presented in Fig. 4.13 as the dependence of ε_{11}^{cr} on dimensionless distance r_1^* between the ends in the range $0.001 \le r_1^* \le 32$. For more compact representation of discussed results in Fig. 4.13, the range ($0.001 \le r_1^* \le 32$) is divided in two parts ($0.001 \le r_1^* \le 0.01$) and ($0.1 \le r_1^* \le 32$) with different scales on the axis $0r_1^*$. The approach of the ends of two short cylinders in Fig. 4.13 corresponds to the curves in Fig. 4.13 when moving along the axis r_1^* from $r_1^* = 32$ to $r_1^* = 0.001$. For example, $|\varepsilon_{11}^{cr}|$ monotonically increases in the range from $r_1^* = 32$ to $r_1^* = 8$ and monotonically decreases in the range from $r_1^* = 8$ to $r_1^* = 0.001$. The buckling mode corresponds to the imaginary general flexural mode (*c*) in Fig. 4.11 in the range from $r_1^* = 32$ to $r_1^* = 0.005$ and to the imaginary mode (*d*) (mutual turn and bending of the fibers with a plastic hinge between them) in the range from $r_1^* = 0.005$ to $r_1^* = 0.001$. This nonmonotonic variation in the critical strain with distance between the neighboring reinforcement elements in a composite is a new mechanical effect.

This completes the discussion of results on two collinear short fibers under compression along them (see [64, 107, 367] for more details).

4.5.4. Results for Two Parallel Fibers under Compression along Them. The design model is shown in Fig. 4.3*c*. Below we will present, as an example, only one result obtained by the numerical method and related to the analysis of the influence of the interaction of two parallel short fibers (Fig. 4.3*c*) on the critical load ε_{11}^{cr} in a matrix at infinity (as $x_1 \to \pm\infty$).

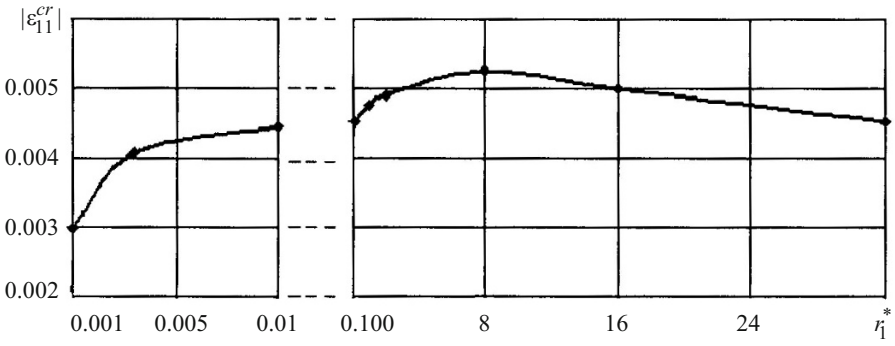

Fig. 4.13

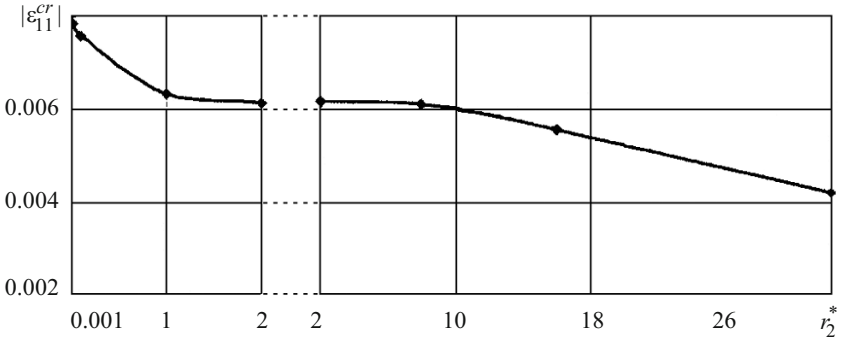

Fig. 4.14

The following parameter values were used: $E_r \cdot E_m^{-1} = 1000$, $\nu_r = \nu_m = 0.35$, $E_m = 2.76$ GPa, $k = m_1 \cdot m_2^{-1} = 100$. This value of $E_r \cdot E_m^{-1}$ can occur in technological processes due to the strong temperature dependence of E_m. The dependence of the critical load $\varepsilon_{11}^{\text{cr}}$ on the distance between two parallel short fibers under compression along them was analyzed numerically. In Fig. 4.3*c*, the distance between parallel fibers is denoted by *r*, and the dimensionless parameter $r_2^* = r \cdot m_1^{-1}$ is introduced. Figure 4.14 shows the dependence of $|\varepsilon_{11}^{\text{cr}}|$ on the parameter r_2^* in the range $0.001 \le r_2^* \le 32$. For more compact representation of the results, the range ($0.001 \le r_2^* \le 32$) is divided into two parts ($0.001 \le r_2^* \le 2$) and ($2 \le r_2^* \le 32$) with different scales on the $0r_2^*$-axis.

The two parallel short fibers in Fig. 4.3*c* approach each other with decrease in r_2^*, i.e., when moving on the $0r_2^*$-axis from $r_2^* = 32$ to $r_2^* = 0.001$. From Fig. 4.14, it follows that as the fibers approach each other (in moving from right to left on the $0r_2^*$-axis), a monotonic increase occurs, which is consistent with engineering considerations. This situation again demonstrates the new mechanical effect: nonmonotonic variation in the critical strain with distance between the reinforcement elements in the composite.

4.5.5. Results for a Periodic Row of Collinear Fibers under Compression along Them. The design model is shown in Fig. 4.3*d*. Principle 4 after Fig. 4.3*a–f* states that for the design model in Fig. 4.3*d* the conditions of decay at infinity are satisfied in the coordinate x_2 (as $x_2 \to \pm\infty$), while the periodicity conditions are satisfied in the coordinate x_1. In this connection, the use of the numerical method involves the following situation. As indicated in Sec. 4.4.2, for numerical purposes, the infinite domain is replaced by a finite rectangular domain $l_1 \times l_2$ shown by dashed lines in Fig. 4.3*d*. For a periodic row (Fig. 4.3*d*), the dimension l_1 of this rectangle is fixed from the periodicity conditions and only the dimension l_2 is changed to satisfy the conditions of decay at infinity (as $x_2 \to \pm\infty$), i.e., the value of l_2 is determined in a computational experiment.

If the structure is periodic (Fig. 4.3*d*) with period $T = m_1 + r$, it is possible to consider periodic (along the $0x_1$-axis) buckling modes with period multiple of the structure period $N(m_1 + r)$, where *N* is an integer. In this case, the dashed rectangle in Fig. 4.3*d* has dimensions $l_1 \times l_2$, where $l_1 = N(m_1 + r)$, and covers *N* short fibers.

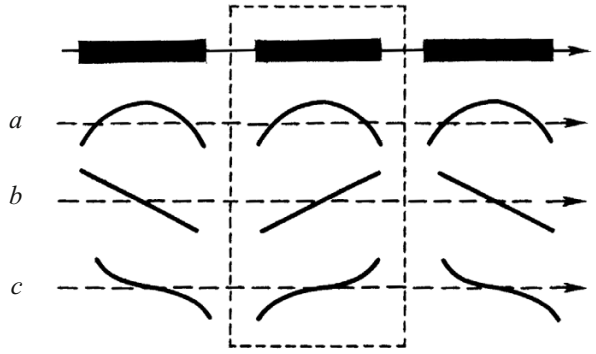

Fig. 4.15

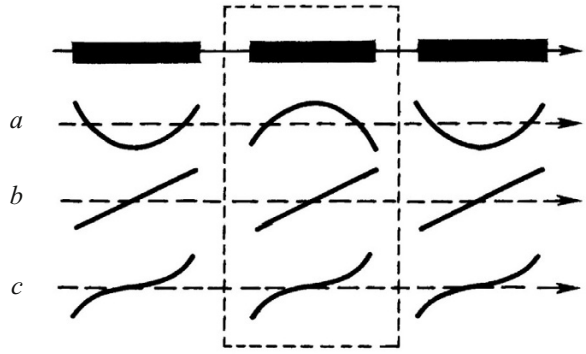

Fig. 4.16

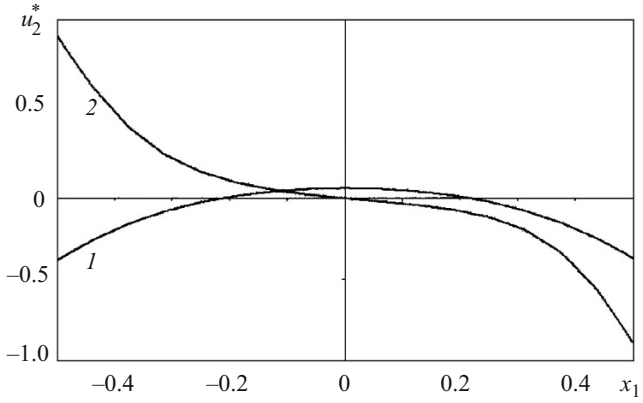

Fig. 4.17

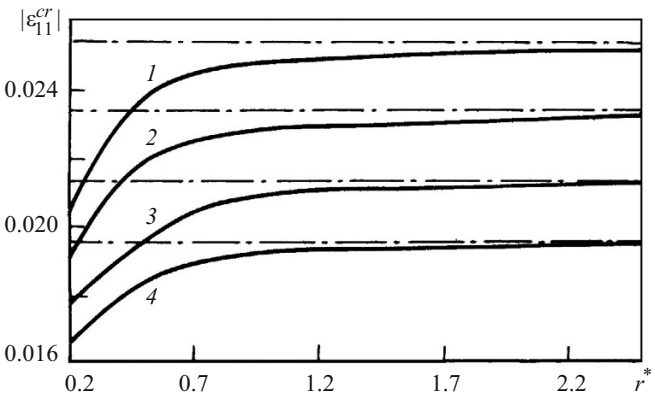

Fig. 4.18

Let us consider imaginary buckling modes for a periodic structure (Fig. 4.3*d*, dashed rectangle with one short fiber inside). Figure 4.15 shows imaginary buckling modes (*a*, *b*, *c*) that are symmetric about the vertical lines drawn through the middle of the segments between the ends of neighboring fibers. Figure 4.16 shows imaginary buckling modes (*a*, *b*, *c*) that are antisymmetric about these vertical lines. The buckling modes in Figs. 4.15*a* and 4.16*b*, *c* are periodic along the $0x_1$-axis with period equal to the structure period *T*, and the buckling modes in Figs. 4.15*b*, *c* and Fig. 4.16*a* are periodic along the $0x_1$-axis with period equal to 2*T*. In addition, it is possible to introduce the dimensionless parameter $r^* = r \cdot m_1^{-1}$ to characterize the distance between the ends of two neighboring fibers. The parameters m_1, m_2, and *r* are specified in Fig. 4.3*d*.

The buckling modes in Figs. 4.15 and 4.16 can also be characterized as follows.

The buckling mode in Fig. 4.15*a* can be considered similar to the flexural mode for far spaced, noninteracting fibers.

The buckling mode in Fig. 4.15*b* can be considered similar to the rigid-body turn of closely spaced fibers that are stiffer than the matrix so that it does not provide appropriate support, resulting in a plastic hinge between the fiber ends.

The buckling mode in Fig. 4.15*c* can be considered similar to the turn and bending of relatively stiff fibers (this mode may be considered to result from imposing bending on the buckling mode in Fig. 4.15*b*).

It is convenient to use these considerations on imaginary buckling modes when describing buckling modes obtained numerically. For example, Fig. 4.17 shows the buckling mode of a composite with specific parameters for the design model in Fig. 4.3*d*. These results were obtained by the numerical method briefly outlined in Sec. 4.4.2. Figure 4.17 corresponds to one fiber and uses dimensionless coordinate x_1 divided by the fiber length m_1 (Fig. 4.3*d*); therefore, $-0.5 \le x_1 \le 0.5$ in Fig. 4.17. Figure 4.17 shows the distribution of the dimensionless vertical displacement u_2^* defined by (4.3) over the $0x_1$-axis: for two distances between the ends of neighboring fibers characterized by the dimensionless parameter $r^* = r \cdot m_1^{-1}$:

(i) $r^* = 1$, the distance between the ends of two neighboring fibers is equal to the fiber length (curve *1*);

(ii) $r^* = 0.2$ (curve *2*).

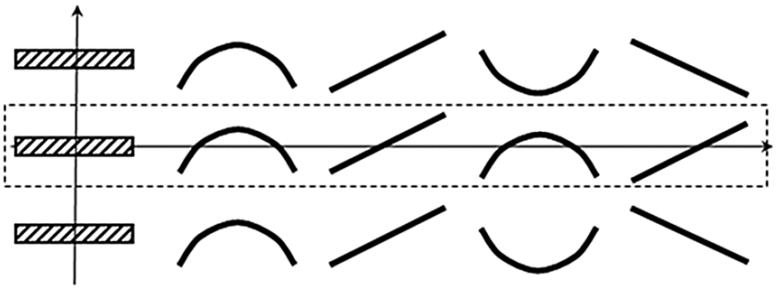

Fig. 4.19

From Fig. 4.17, it follows that the buckling mode (curve *1*, $r^* = 1$) is very similar to the imaginary buckling mode in Fig. 4.15*a* and the buckling mode (curve *2*, $r^* = 0.2$) is very similar to the imaginary buckling mode in Fig. 4.15*c*. Moreover, as the distance between collinear short fibers in a periodic row decreases, the buckling modes change. A similar situation took place in the case of two collinear fibers, as demonstrated by Figs. 4.10 and 4.12.

In what follows, we will discuss the dependence of $|\varepsilon_{11}^{cr}|$ (critical strain along the $0x_1$-axis in a matrix at infinity (as $x_1 \to \pm\infty$) according to Fig. 4.3*d* on $r^* = r \cdot m_1^{-1}$ (m_1, m_2, and r are specified in Fig. 4.3*d*). These results were obtained by the numerical method briefly outlined in Sec. 4.4.2. After finding the value of ε_{11}^{cr}, which is an eigenvalue, no numerical analysis was performed to find the associated eigenfunction from which the buckling mode is determined. The following parameter values were used: $E_r \cdot E_m^{-1} = 1000$, $\nu_r = \nu_m = 0.35$, $E_m = 2.76$ GPa, $k = m_1 \cdot m_2^{-1} = 100, 200, 300, 500$. The dimensionless distance r^* between the ends of two neighboring fibers changed in the range $0.2 \le r^* \le 4.5$. The results obtained are presented in Fig. 4.18, where curves *1*, *2*, *3*, *4* correspond to $k = 100, 200, 300, 500$. The dash-and-dot lines correspond to $|\varepsilon_{11}^{cr}|$ for the case of one fiber at the same values of k. From Fig. 4.18, it can be concluded that at distances between the ends of two neighboring fibers exceeding the fiber length ($r^* > 1$), the critical strain $|\varepsilon_{11}^{cr}|$ for a periodic row of collinear fibers under compression along them is very close to $|\varepsilon_{11}^{cr}|$ for one isolated fiber of the same length.

From this conclusion related to the mechanics of interaction of short fibers in a composite, it is possible to draw a conclusion on the creation of composites. In terms of compressive strength of short-fiber reinforced composites, the creation of composites with $S_r \ge 50\%$ (S_r is the volume fraction of fibers) may appear ineffective for such materials with inhomogeneous structure. It follows from Fig. 4.18 that for $r^* < 1$ ($r^* = 1$ is the distance between the ends of neighboring fibers equal to the fiber length; $S_r \approx 50\%$), $|\varepsilon_{11}^{cr}|$ decreases substantially, i.e., the ultimate strength decreases when $S_r > 50\%$.

In the case of composites of ordered structure (such as fibrous composites of doubly periodic structure in cross-sectional plane), the supporting effect of neighboring periodic rows of short fibers can prevent the decrease in $|\varepsilon_{11}^{cr}|$ with increase in S_r, which occurs (according to Fig. 4.18) in the range ($0.2 \le r^* \le 1$) upon approach of the ends. The approach of the ends of two neighboring fibers in a periodic row of collinear short fibers corresponds to the motion from right to left along the $0r^*$ axis in Fig. 4.18.

In the case of composites of disordered (irregular) structure, situations represented by Fig. 4.3*d* (one periodic row of fibers in infinite space; i.e., no interaction of fibers in neighboring rows) can occur in some parts of a composite. In such parts, the conclusion drawn in Fig. 4.18 on the mechanics of interaction of short fibers in a composite. Hence, the conclusion on the inefficiency of creation of materials with $S_r > 50\%$ also applies to such parts.

Certainly, this phenomenon exists but should be additionally studied.

This completes the discussion of results related to the design model in Fig. 4.3d (see [64, 65, 109, 252, 365] for more details).

4.5.6. Results for a Periodic Row of Parallel Fibers under Compression along Them. The design model is shown in Fig. 4.3*e*. The dimensionless parameter $r^* = r \cdot m_1^{-1}$ is additionally introduced. The parameters m_1, m_2, and r are specified in Fig. 4.3*e*. Principle 5 after Fig. 4.3*a–f* states that for the design model in Fig. 4.3*e* the conditions of decay at infinity are satisfied in the

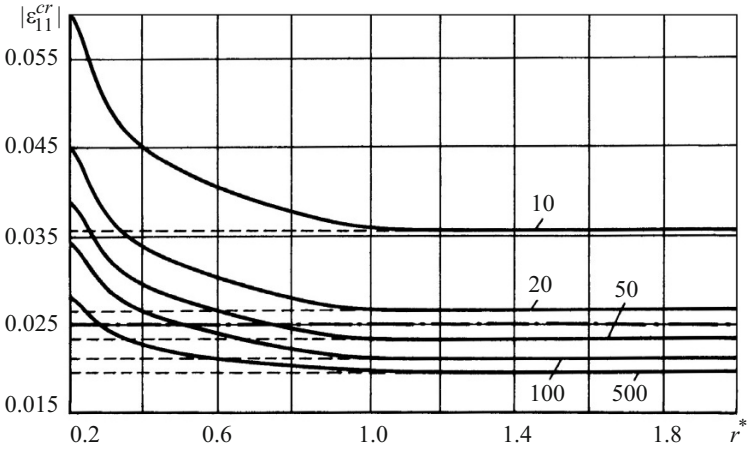

Fig. 4.20

coordinate x_1 (as $x_1 \to \pm\infty$), while the periodicity conditions are satisfied in the coordinate x_2. In this connection, the use of the numerical method involves the following situation. As indicated in Sec. 4.4.2, for numerical purposes, the infinite domain is replaced by a finite rectangular domain $l_1 \times l_2$ shown by dashed lines in Fig. 4.3*e*. For a periodic row (Fig. 4.3*e*), the dimension l_2 of this rectangle is fixed from the periodicity conditions and only the dimension l_1 is changed to satisfy the conditions of decay at infinity (as $x_1 \to \pm\infty$), i.e., the value of l_1 is determined in a computational experiment.

If the structure is periodic (Fig. 4.3*e*) with period $T = m_2 + r$, it is possible to consider periodic (along the $0x_2$-axis) buckling modes with period multiple of the structure period $N(m_2 + r)$, where N is an integer. The dashed rectangle covers N short fibers.

Let us consider imaginary buckling modes for a periodic structure (Fig. 4.3*e*, dashed rectangle with one short fiber inside). Figure 4.19 shows, as an example, the imaginary buckling modes *a*, *b*, *c*, *d*, which can be characterized as in Sec. 4.5.5. The imaginary buckling modes a and b in Fig. 4.19 have period $T = m_2 + r$ along the vertical axis, and the modes *c* and *d* in Fig. 4.19 have period $2(m_2 + r)$ along the vertical axis. This completes the discussion of the imaginary buckling modes as applied to the design model in Fig. 4.3*e*.

Following [253], we will discuss the dependence of $|\varepsilon_{11}^{\mathrm{cr}}|$ (critical strain along the $0x_1$-axis in a matrix at infinity (as $x_1 \to \pm\infty$) according to Fig. 4.3*e*) on $r^* = r \cdot m_1^{-1}$ (m_1, m_2, and r are specified in Fig. 4.3*e*), which is the relative distance between neighboring parallel fibers in an infinite periodic row of fibers along the $0x_2$-axis. The following parameter values were used [253]: $E_r = 1.2$ TPa, $E_m = 3.5$ GPa, $\nu_r = \nu_m = 0.4$, $k = m_1 \cdot m_2^{-1} = 10, 20, 50, 100, 500$, r^* varying in the range $0.2 \le r^* \le 4.5$. The results are presented in Fig. 4.20, where the figure near each curve indicate the value of *k*.

From Fig. 4.20, it may be concluded that with increase in the distance between neighboring fibers, which is greater than the fiber length ($r^* > 1$), $|\varepsilon_{11}^{\mathrm{cr}}|$ hardly changes and corresponds to the results obtained for one fiber in a matrix (Fig. 4.3*a*). The value of $|\varepsilon_{11}^{\mathrm{cr}}|$ for one fiber in a matrix is shown in Fig. 4.20 by a dashed line for each value of *k*. As the distance between neighboring fibers in a row of parallel fibers (Fig. 4.3*e*) decreases ($r^* < 1$), according to Fig. 4.20, the critical strain $|\varepsilon_{11}^{\mathrm{cr}}|$ along the $0x_1$-axis increases for all values of *k*. Thus, in the case of a periodic row of parallel fibers (Fig. 4.3*e*), the situation discussed in the final part of Sec. 4.5.5 (Fig. 4.3*d*) and occurring when $|\varepsilon_{11}^{\mathrm{cr}}|$ decreases for $r^* < 1$, which follows from the results in Fig. 4.18 for the design model in Fig. 4.3*d*.

This completes the discussion of results related to the design model in Fig. 4.3*e* (see [64, 65, 110, 253] for more details).

4.5.7. Results for One Fiber near a Surface under Compression along It. Analysis of Near-Surface Instability. The design model is shown in Fig. 4.3*f*. The dimensionless parameter $r^* = r \cdot m_1^{-1}$ characterizing the relative distance from the fiber to the boundary of the half-plane is additionally introduced. The parameters m_1, m_2, and r are specified in Fig. 4.3*f*.

As already mentioned in Sec. 4.2, the sixth design model (Fig. 4.3*f*) is the simplest design model for studying near-surface fracture within the framework of the second approach (Sec. 3.1.3) and piecewise-homogeneous material model in

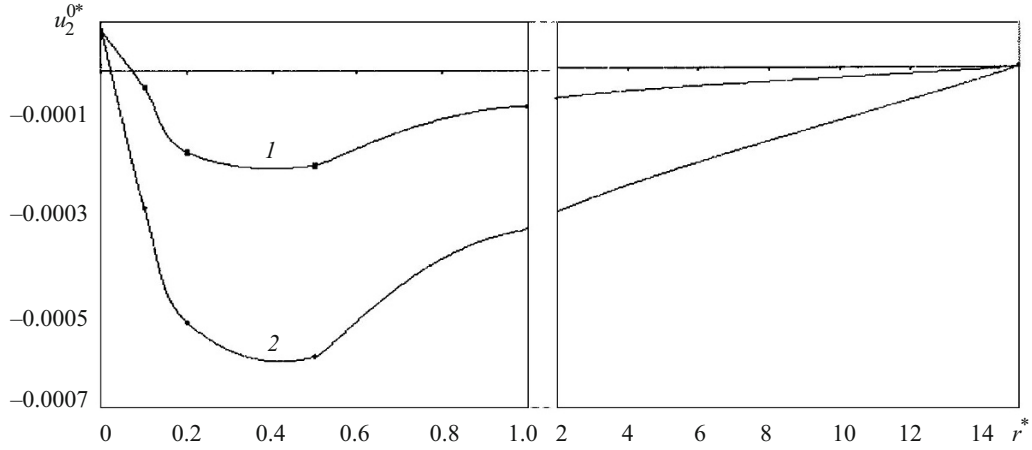

Fig. 4.21

the plane case. Certainly, the number of simple design models for studying near-surface fracture can be increased by adding the boundary of the half-plane in the design models in Figs. 4.3*b–e*.

In analyzing the design model in Fig. 4.3*f*, certain boundary conditions on the boundary $x_2 = 0$ of the half-plane (Fig. 4.3*f*) are prescribed. We consider boundary conditions for stresses on the unloaded free half-plane $x_2 = 0$ in determining the subcritical state. These are homogeneous boundary conditions for stresses for $x_2 = 0$ and conditions of decay at infinity as $x_1 \to \pm\infty$ and $x_2 \to -\infty$.

For numerical purposes, the semi-infinite domain (half-plane) is replaced by a finite rectangular domain $l_1 \times l_2$ shown in Fig. 4.3*f*. One of the sides of the rectangle coincides with the boundary of the half-plane, and the other three sides are shown by dashed lines in Fig. 4.3*f*. On the dashed sides, the conditions of decay as $x_1 \to \pm\infty$ and $x_2 \to -\infty$ are set. When applying the numerical method, the size of the rectangle is increased by changing the position of the dashed sides. The dimensions $l_1 \times l_2$ are chosen by way of computational experiments so that their further increase does not affect the results (critical load and critical strain).

Remark 4.6. Noteworthy a situation occurring in the mechanics of near-surface fracture whose initial stage (start) is near-surface buckling in a composite near the surface near which there is a reinforcement element of finite size (for example, a short fiber, Fig. 4.3*f*). Let us consider this situation for the simplest design model (Fig. 4.3*f*) related to near-surface fracture. When a uniformly distributed (in x_2) load of constant intensity acts at infinity (as $x_1 \to \pm\infty$), the distribution of the material near the short cylinder is asymmetric (about the centerline of the cylinder, for $x_2 = -(r + 0.5m_2)$ in Fig. 4.3*f*) because no material is present for $x_2 > 0$. Under these conditions, local bending due to the asymmetry in the distribution of the material occurs near the short fiber. This local bending increases with the compressive load. This situation occurs in the subcritical state. Hence, here the buckling mechanism is much more complex than the buckling of a rod under axial compression. Note that for the design model in Fig. 4.3*f*, a uniformly distributed (in x_2) load of constant intensity acting at infinity (as $x_1 \to \pm\infty$) is equivalent to constant compressive strain along the $0x_1$-axis (independent of x_2) at infinity (as $x_1 \to \pm\infty$).

Remark 4.7. The situation described in Remark 4.6 does not occur in studying the near-surface fracture of composites using the model of infinite reinforcement elements parallel to the free surface of composites. Such results obtained with the second approach (Sec. 3.1.3) and the piecewise-homogeneous material model are briefly outlined in Sec. 3.3.3.2 for laminated composites and in Sec. 3.3.4.2 for unidirectional fibrous composites. The matter is that identical compressive strains for the reinforcement and matrix are set at infinity (near the boundary surface), which is natural for the model of infinite long layers and fibers and which leads to a homogeneous subcritical state.

The publications [64, 65, 111, 254, etc.] report numerous quantitative results on the local bending of a short fiber obtained in determining the subcritical state using the design model in Fig. 4.3*f*. We will consider only two examples. The bending in the subcritical state for the design model in Fig. 4.3*f* is convenient to characterize by the difference of vertical displacements u_2^0:

$$u_2^{0*} = u_2^0|_{x_1=0} - u_2^0|_{x_1=0.5m_1}, \tag{4.4}$$

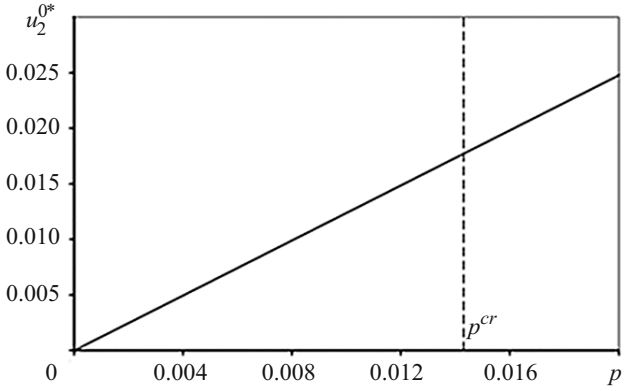

Fig. 4.22

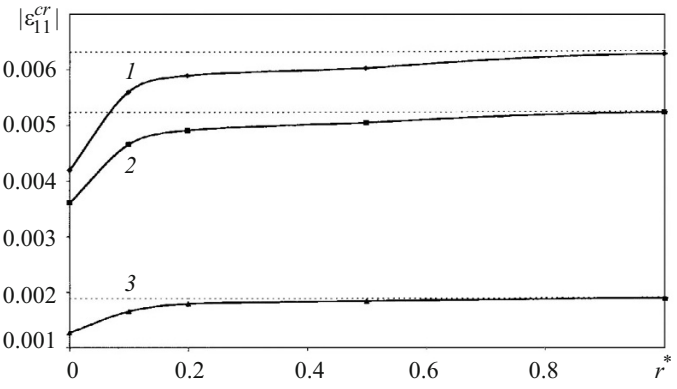

Fig. 4.23

where $u_2^0|_{x_1=0}$ is the vertical displacement (displacement u_2^0) along the vertical line passing through the center of the reinforcement element; $u_2^0|_{x_1=0.5m_1}$ is the vertical displacement (displacement u_2^0) along the vertical line passing through the end of the reinforcement element. Assuming that $x_2 = -(r + 0.5m_2)$ in (4.4), according to Fig. 4.3*f*, we obtain the difference of these vertical displacements:

$$u_2^{0*}|_{x_2=-(r+0.5m_2)} = \left(u_2^0|_{x_1=0} - u_2^0|_{x_1=0.5m_1} \right)\Big|_{x_2=-(r+0.5m_2)}. \tag{4.5}$$

Assuming that $x_2 = 0$ in (4.4), according to Fig. 4.3*f*, we obtain the difference of vertical displacements of points lying on the free surface and being the projection of the center of the reinforcement and the end of the reinforcement onto the free surface:

$$u_2^{0*}|_{x_2=0} = \left(u_2^0|_{x_1=0} - u_2^0|_{x_1=0.5m_1} \right)\Big|_{x_2=0}. \tag{4.6}$$

Figure 4.21 show the dependence of u_2^{0*} (4.4) on $r^* = r \cdot m_1^{-1}$ (Fig. 4.3*f*). Curve *1* corresponds to (4.5) and curve *2* to (4.6). The results in Fig. 4.21 were obtained for the range $0.0 \le r^* \le 15.0$ of the dimensionless distance to the free surface in Fig. 4.3*f*. The results in Fig. 4.21 were obtained for a composite with the following parameters: $E_r \cdot E_m^{-1} = 343$, $E_m = 3.51$ GPa, $\nu_r = \nu_m = 0.4$, $k = m_1 \cdot m_2^{-1} = 1000$.

From Fig. 4.21 it follows that over the range $0 \le r^* \le 15$, the difference of vertical displacements of the reinforcement center and end (curve *1*) is not zero, which is indicative of local bending. The difference $\to 0$ for $r^* \to 15$. Thus, when $r^* > 15$, local bending is absent and the numerical results correspond to one reinforcement in an infinite matrix (Fig. 4.3*a*, Sec. 4.5.2).

Figure 4.22 shows, for the subcritical state of a specific composite, the dependence of the difference of vertical displacements (4.5) on the compressive load at infinity, according to Fig. 4.3*f*. The dashed line represents the value of P^{cr} corresponding to buckling.

Figure 4.23 presents results on near-surface buckling for the design model in Fig. 4.3*f*. The following parameter values were used: $E_r \cdot E_m^{-1} = 343$, 1000, $E_m = 3.51$ GPa, $\nu_r = \nu_m = 0.4$, $k = m_1 \cdot m_2^{-1} = 200$, 1000 and for the range $0 \le r^* \le 15$ of the parameter $r^* = r \cdot m_1^{-1}$. The parameters m_1, m_2, and r are specified in Fig. 4.3*f*. In Fig. 4.23, the dashed lines represent the values of $|\varepsilon_{11}^{\text{cr}}|$ for one fiber in an infinite matrix (Fig. 4.3*a*, microbuckling). Curves *1*, *2*, and *3* in Fig. 4.23 correspond to composites with the following parameter values: $E_r \cdot E_m^{-1} = 1000$, $k = 1000$ (curve *1*); $E_r \cdot E_m^{-1} = 343$, $k = 200$ (curve *2*); $E_r \cdot E_m^{-1} = 1000$, $k = 200$ (curve *3*). As the parameter r^* (the distance from the fiber to the free surface in Fig. 4.3*f*) increases, curves *1*, *2*, and *3* in Fig. 4.23 asymptotically tend to the respective dashed lines from below and coincide with them for $r^* = 1$. Note that $r^* = 1$ corresponds to the distance from the fiber to the free surface (Fig. 4.3*f*) equal to the fiber length.

We may draw the following two conclusions for the composites under consideration.

1. When $r^* \geq 1$, there is no need to analyze near-surface instability because the corresponding value of $|\varepsilon_{11}^{cr}|$ practically coincides with the value of $|\varepsilon_{11}^{cr}|$ for internal instability (Fig. 4.3*a*, a fiber in an infinite matrix).

2. When $r^* \leq 1$, it makes sense to analyze near-surface instability because when $r^* \to 0$, it is possible to decrease $|\varepsilon_{11}^{cr}|$ to 30% compared with $|\varepsilon_{11}^{cr}|$ for internal instability (Fig. 4.3*a*, a fiber in an infinite matrix).

This completes the discussion of results related to the design model in Fig. 4.3*f* (see [64, 65, 111, 254, 368] for more details).

4.6. Conclusions to Sec. 4. Problem 2 (short-fiber model in the theory of stability and the fracture mechanics of compressed composites) began to be actively studied at the beginning of the 21th century. In this connection, much attention was given here to problem statement aspects which resulted in expansion of the amount of reviewed material.

For the short-fiber model, the general concept was accepted (when composites are compressed along fibers and layers, the beginning (start) of fracture is determined by microbuckling (internal or near-surface instability). This mechanism of start of fracture was confirmed experimentally.

The problem statements, approaches, and results discussed here are based on the piecewise-homogeneous material model and the TLTSDB. This general approach is apparently the most rigorous in solid mechanics. With this approach, specific results on Problem can be obtained only numerically because problems related to Problem 2 lead to inhomogeneous subcritical stress–strain states.

Spatial (three-dimensional) problems and plane (two-dimensional) problems were analyzed. These spatial problems address composites reinforced with short circular cylinders. The plane problems, when solved rigorously, address ribbon-reinforced composites. When treated approximately, results of solving these problems can be used to analyze phenomena occurring in composites reinforced with short fibers.

Currently, only brittle fracture in Problem 2 has been studied. The solution of problems on ductile fracture involves additional difficulties associated with the determination of the subcritical inhomogeneous state taking into account unloading zones changing during loading.

For Problem 2, it is important to analyze the influence of the shape of the ends of short fibers on the critical compressive strain, considering that $|\varepsilon_{11}^{cr}|$ is a criterion of fracture whose initial stage (start) is determined by buckling. This fracture criterion is of integral type because $|\varepsilon_{11}^{cr}|$ is determined in terms of the eigenvalue of the associated eigenvalue problem in the TLTSDB. Due to this, we may say that the effect of the shape of the ends of short fibers on $|\varepsilon_{11}^{cr}|$ will be weaker compared with local failure criteria, which are determined by some invariants of the stress tensor at the point of interest of the material. Nevertheless, it is important to analyze the influence of the shape of the ends of short fibers on $|\varepsilon_{11}^{cr}|$.

5. Problem 3. End Crushing of Composites under Compression. We will briefly (compared with problems 1 and 2) discuss the major results on problem 3 obtained at the Department Dynamics and Stability of Continua of the S. P. Timoshenko Institute of Mechanics. We will also discuss some related experimental results.

5.1. Introduction. The major results are reported in the monographs [54, Ch. 7, Sec. 4, pp. 568–589) and [57, Vol. 2, Ch. 11, Sec. 4, pp. 529–551], the reviews [329, 336, 347, 350] and [21] (in the list of references to [336]), the articles [51, 76, 304, 305, 317, 325], the conference reports [312, 314, 316, 320, 321, 323, 324], and some other publications that are not included in the list of references to the present review. The phenomenon under consideration was also termed as buckling of the ends in [304, 305], bearing strain in end faces in [312, 314], and end-crush fracture of compressed composites in [347, 350]. The phenomenon is also called brooming.

Note that Yu. V. Kokhanenko's dissertation is partially related to this research area. Kokhanenko's dissertational is devoted to a numerical method based on the finite-difference method, the variational difference method, and reference schemes (briefly described in Sec. 4.4.2). This numerical method is applied to piecewise-homogeneous materials, which corresponds to the piecewise-homogeneous material model in the mechanics of composites, including the TLTSDB. The list of references to this review includes publications reporting results obtained with this method, for example [64, 65, 76, 128, 129, 503, 504, etc.].

This completes the introduction to Sec. 5.

5.2. Experiments. Here we will address phenomena that occur at the ends of unidirectional fibrous or layered composites compressed along fibers or layers or composites of other structures compressed along the axes of material symmetry. In this connection, primary attention will be given to the fracture near the ends of composite specimens.

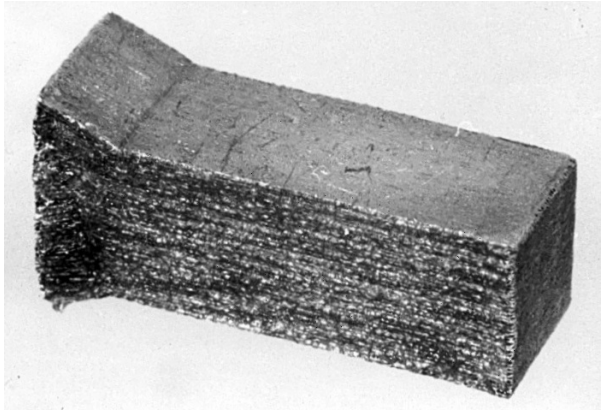

Fig. 5.1

Let us consider the fracture near the ends of metal-composite specimens for which experimental results were presented in the example in Sec. 3.3.4.1. The experimental results to be discussed were obtained for a metal-composite (unidirectional fibrous boron aluminum composite with 50% boron fibers, $S_r = S_m = 0.5$) VKA-1 with boron fibers 140 μm in diameter. The boron aluminum specimens before fracture are shown in Fig. 3.37. Figure 3.38 shows the magnified internal structure of boron aluminum composite in cross section. Figure 5.1 shows a specimen after ductile fracture. It can be seen that the left end of the specimen has been crushed, i.e., the fracture is local (near the left end). The damaged portion of the specimen looks like a broom, hence the name "brooming fracture."

The above results (Fig. 5.1) as well as other results on the ductile end-crush fracture of boron aluminum composites were reported in [95] and detailed in [57, Vol. 1, Ch. 4, pp. 486–488).

Among the various mechanisms of fracture in composites, the end-crush fracture mechanisms in composites under compression are frequent. In general, end-crush fracture (of specimens or structural members made of composites) is local failure of the material near the ends, most of the specimen being not affected. In this connection, the ultimate strength of the material against end-crush fracture is somewhat lower than the ultimate strength against fracture of the whole material (far from ends, internal fracture as termed in Sec. 3.3). When the ultimate compressive strength (fracture far from the ends) is determined experimentally, the end-crush fracture of specimens is usually prevented using special means. For example, specimens can be wrapped near the ends or inserted into rigid shells to tightly cover the ends. The latter method was applied to fiberglass-reinforced plastic specimens, as shown in Figs. 3.8–3.10.

Such prevention of end-crush fracture during experiments in laboratories does not mean that this and other phenomena will not occur in full-scale structures. Phenomena similar to end crushing are observed in various structural members such as various joints. In wood (as a structural material), these phenomena have long been known and were repeatedly observed and described by many researchers. It should be noted that end-crush fracture is also observed in a complex stress state when the external compressive loads applied to the ends reach certain limits.

Experiments on end-crush fracture are very complex and do not always lead to unambiguous results. This is because the results of experimental studies are usually an image of a specimen destroyed near the ends or a value of the ultimate strength corresponding to completed end-crush fracture. To study or describe this phenomenon, it is necessary to know the initial stage of fracture (to reveal its causes and mechanism). The complex pattern of end-crush fracture (final stage) can hardly be used to identify the initial-stage processes. A similar situation was observed in Sec. 3 in analyzing experimental results on problem 1.

Thus, it would be appropriate to develop a theory that would describe end-crush fracture using either the continuum approximation or the piecewise-homogeneous material model.

5.3. Theoretical Studies. Theoretical results on problem 3 can be found in the publications cited in the introduction (Sec. 5.1). Here we will briefly discuss theoretical results separately for the general concept, the piecewise-homogeneous material model, and the continuum approximation (model).

5.3.1. General Concept. We will consider composites of various structure modeled by orthotropic materials in the continuum approximation. It is assumed that these materials or specimens made of them have an end coinciding with one of the planes of orthotropy, and a normal compressive load is applied to the end. This situation can be considered as a design model that

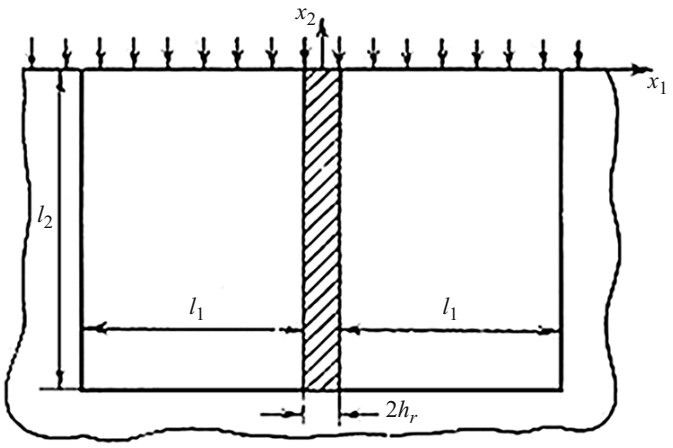

Fig. 5.2

also related to a specimen (Fig. 5.1, after fracture) made of a unidirectional fibrous composite with cross section loaded by an external normal compressive load.

General Concept. In the situation described above, the initial stage (start) of end-crush fracture is near-surface buckling near the loaded end. In analyzing the further development of this failure mechanism, it is necessary to consider its possible interaction with other failure mechanisms. The theoretical ultimate strength and theoretical ultimate strain corresponding to end-crush fracture are critical load and critical strain predicted by the TLTSDB.

The above general concept allows developing the mechanics of end-crush fracture under compression by analyzing near-surface instability near the loaded end using either the piecewise-homogeneous material model or the continuum theory. It is assumed that a dead load acts on the end; in this connection, the sufficient applicability conditions of the static TLTSDB method are satisfied for brittle and plastic fracture, according to Sec. 2.4.2. Thus, studies on end-crush fracture are fully consistent with the standard and rigorous method of studying buckling by analyzing the behavior of small perturbations in linearized three-dimensional dynamics.

Remark 5.1. Apparently, a factor responsible for the occurrence of end-crush fracture is certain boundary conditions at the ends. The matter is that the ends are compressed through rigid plates in the case of specimens and through rigid joints in the case if structural members. Due to the high stiffness of the plates and joints, the compressive strains of the reinforcement (fibers or layers) and the matrix at the ends are equal. This situation corresponds to the case where identical normal displacements are set as boundary conditions on the whole surface of the ends. If design or manufacturing features (for example, polishing of the surface of the support plate) provide low or no friction at the end under compression, then some parts of the composite at the end can slide freely over the support plate. It is in this situation that end-crush fracture appears to occur.

Thus, for occurrence of end-crush fracture, constant normal displacements and zero shear stresses on the end surface are the most favorable boundary conditions and constant normal displacements and zero tangential displacements on the end surface are the least favorable boundary conditions. Note that the least favorable boundary conditions correspond to the fixation of the ends in perfectly rigid shells (as in Figs. 3.9 and 3.10) when end-crush fracture does not occur.

Remark 5.2. When using the piecewise-homogeneous material model in the mechanics of end-crush fracture, it is possible to solve two-dimensional (plane) problems and three-dimensional (spatial) problems. When treated rigorously and consistently, plane problems (for plane strain) are solved for composites reinforced with parallel infinite ribbons of constant cross section perpendicular to the plane of the figure (as in Figs. 4.3*a–f*) and for laminated composites (as in Fig. 3.2). When interpreted approximately, the results on plane problems can be used to analyze phenomena that occur in unidirectional fibrous composites, similarly to the approximate approach briefly described in Sec. 4.3.1. When treated consistently, spatial problems are solved for unidirectional fibrous composites (as in Fig. 3.1).

This completes the formulation and discussion of the general concept and separate aspects related to the statement and analysis of problems on the mechanics of end-crush fracture of composites under compression.

5.3.2. Piecewise-Homogeneous Material Model. As an example of study of end-crush fracture based on the piecewise-homogeneous material models and the TLTSDB, we will briefly discuss the results obtained in [76] for the simplest

model in the mechanics of end-crush fracture. We will change the notation used in [76] to the notation adopted in the present review. We will use the general concept for brittle end-crush fracture and theory 3 (as termed in Sec. 2.2) for composite laminates (Fig. 3.2, infinite-layer model) with low concentration of reinforcement (the interaction between two neighboring layers during buckling can be neglected). Only the upper end (Fig. 5.2) will be considered.

The simplest design model corresponding to the above problem statement is presented in Fig. 5.2 for a plane problem in the plane $x_1 0 x_2$ where the $0x_3$-axis is perpendicular to the plane of Fig. 5.2. Since end-crush fracture is observed only near an end and neighboring reinforcement elements do not interact, the design model in Fig. 5.2 is reduced to the lower half-plane $x_2 \le 0$ with one reinforcement half-strip. Thus, it is necessary to consider a part of the lower half-plane containing a reinforcement element and to specify boundary conditions for $x_2 = 0$ and conditions of decay as $x_2 \to -\infty$ and $x_1 \to \pm\infty$. This part of the half-plane is shown by a wavy line and the boundary $x_2 = 0$ where $2h_r$ is the thickness of the reinforcement (layer), as in Fig. 3.2.

In analyzing brittle end-crush fracture, the reinforcement and matrix are modeled by linear elastic isotropic bodies. In this connection, the conventional constitutive equations and theory 3 will be used:

$$\sigma_{ij}^a = \delta_{ij}\lambda_a \varepsilon_{nn}^a + 2\mu_a \varepsilon_{ij}^a, \qquad \sigma_{ij}^m = \delta_{ij}\lambda_m \varepsilon_{nn}^m + 2\mu_m \varepsilon_{ij}^m,$$

$$2\varepsilon_{ij}^a = u_{i,j}^a + u_{j,i}^a, \qquad 2\varepsilon_{ij}^m = u_{i,j}^m + u_{j,i}^m. \tag{5.1}$$

where λ_r, μ_r, E_r, and ν_r are the elastic constants of the reinforcement; λ_m, μ_m, E_m, and ν_m are the elastic constants of the matrix (binder).

Let us briefly consider how to determine the subcritical state. We will restrict ourselves to the analysis of compression of an end through a rigid support plate, which is shown by arrows in Fig. 5.2. According to Remark 5.1, the compressive strains of the reinforcement and matrix ($\varepsilon_{22}^{r0} = \varepsilon_{22}^{m0}$) on the end surface $x_2 = 0$ (Fig. 5.2) are equal. The index "0" is used to refer to the subcritical state. Let us also assume that there is no friction between the specimen and the support plate on the end $x_2 = 0$ (Fig. 5.2). According to Remark 5.1, this condition is the most favorable boundary conditions for the occurrence of end-crush fracture. Thus, we have the following boundary conditions at the end ($x_2 = 0$) for the determination of the subcritical state:

$$\varepsilon_{22}^{a0} = c, \quad \sigma_{12}^{a0} = 0 \quad \text{for} \quad |x_1| \le h_a \quad \text{and} \quad x_2 = 0,$$

$$\varepsilon_{22}^{m0} = c, \quad \sigma_{12}^{m0} = 0 \quad \text{for} \quad |x_1| \ge h_a \quad \text{and} \quad x_2 = 0, \quad c = \text{const}. \tag{5.2}$$

With the boundary conditions (5.2) at the end $x_2 = 0$ (Fig. 5.2) and relations (5.1) for plane strain in the plane $x_3 = 0$ (Fig. 5.2, $\varepsilon_{33} \equiv 0$) the subcritical state is determined in the following analytical form:

$$\sigma_{11}^{a0} = 0, \quad \sigma_{12}^{a0} = 0, \quad \sigma_{22}^{a0} = 4\mu_a(\lambda_a + \mu_a)(\lambda_a + 2\mu_a)^{-1}\varepsilon_{22}^{a0},$$

$$\sigma_{11}^{m0} = 0, \quad \sigma_{12}^{m0} = 0, \quad \sigma_{22}^{m0} = 4\mu_m(\lambda_m + \mu_m)(\lambda_m + 2\mu_m)^{-1}\varepsilon_{22}^{m0},$$

$$\varepsilon_{22}^{a0} = \varepsilon_{22}^{m0} = c = \text{const}. \tag{5.3}$$

Let us briefly discuss, following [76], results on buckling problem according to the above problem statement for the subcritical state (5.3). This buckling problem is local (near the end $x_2 = 0$ in Fig. 5.2). The boundary conditions on the end surface consistent with conditions (5.2) for the subcritical state are given by

$$\varepsilon_{22}^a = 0, \quad \sigma_{12}^a = 0 \quad \text{for} \quad |x_1| \le h_a \quad \text{and} \quad x_2 = 0,$$

$$\varepsilon_{22}^m = 0, \quad \sigma_{12}^m = 0 \quad \text{for} \quad |x_1| \ge h_a \quad \text{and} \quad x_2 = 0. \tag{5.4}$$

Since the buckling problem is local, the conditions of decay with distance from the end ($x_2 \to -\infty$) are prescribed. And since composite laminates with low concentration of reinforcement (two neighboring layers do not interact during buckling) are considered, the conditions of decay as $x_1 \to \pm\infty$ are specified:

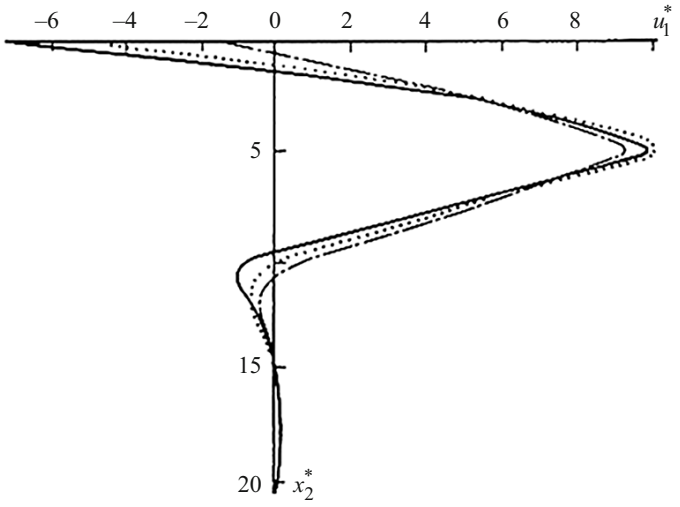

Fig. 5.3

$$\mathbf{u}^a \to 0 \quad \text{as} \quad x_2 \to -\infty,$$

$$\mathbf{u}^m \to 0 \quad \text{as} \quad x_2 \to -\infty \quad \text{or} \quad x_1 \to \pm\infty. \tag{5.5}$$

For the buckling problem, formulas (2.21)–(2.27) and (2.10)–(2.13) of theory 3 are used to formulate the continuity conditions for the stress and displacement vectors for $x_1 = \pm h_r$, taking expressions (2.10) and (2.23) into account.

The buckling problem for the lower half-plane $x_2 \le 0$ (Fig. 5.2) with the constitutive equations (5.1), the boundary conditions (5.4) on the boundary $x_2 = 0$, the conditions of decay (5.5), and the above-mentioned continuity conditions for the stress and displacement vectors for $x_1 = \pm h_r$ was solved by the numerical method briefly described in Sec. 4.4.2. The semi-infinite domain (lower half-plane) was replaced with a finite rectangular domain with the side lengths $2(l_1 + h_a) \times l_2$ shown in Fig. 5.2. The values of $l_1 \cdot h_r^{-1}$ and $l_2 \cdot h_r^{-1}$ were selected so that the final result (critical strain or stress) did not depend on them. It was established that for $l_1 \cdot h_r^{-1} \ge 10$ and $l_2 \cdot h_r^{-1} \ge 20$, further increase does not change the results. In this connection, all the results discussed below were obtained for $l_1 \cdot h_r^{-1} = 10$ and $l_2 \cdot h_r^{-1} = 20$. The results obtained are the buckling modes for the design model in Fig. 5.2 and the critical compressive stress σ_{22}^{r0} (in the reinforcement) or σ_{22}^{m0} (in the matrix) determined from the critical strain $\varepsilon_{22}^{r0} = \varepsilon_{22}^{m0}$ at the end. We will consider these results separately.

First, we will discuss the buckling modes determined for the design model in Fig. 5.2. The buckling mode is convenient to characterize by horizontal displacements (displacements along the $0x_1$-axis in Fig. 5.2). The horizontal displacement of points of the centerline of the reinforcement, i.e., the displacement $u_1^r(0, x_2)$, is especially characteristic. Figure 5.3 shows the variation of the dimensionless displacement $u_1^* = u_1^r(0, x_2) \cdot h_r^{-1}$ along the $0x_2^*$-axis, where $x_2^* = -x_2 \cdot h_r^{-1}$. Thus, Fig. 5.3 shows the variation in the dimensionless horizontal displacement u_1^* points of the centerline of the reinforcement with distance from the end. Figure 5.3 addresses composites with $\nu_r = \nu_m = 0.3$ and $E_r \cdot E_m^{-1} = 25$ (solid line), $E_r \cdot E_m^{-1} = 100$ (dashed line), $E_r \cdot E_m^{-1} = 1600$ (dash-and-dot line). It can be seen that the horizontal displacement u_1^* decreases with distance from the end as a rapidly damped wave, which is completely damped at $x_2^* \approx 15$, which corresponds to 7.5 thicknesses of the reinforcement. Also, $\max u_1^*$ is reached at $x_2^* \approx 5$ (2.5 thicknesses of the reinforcement) and is 5 thicknesses of the reinforcement. Note that the above numerical characteristics of the decrease in the horizontal displacement in the buckling mode apply only to the composites exemplified above.

Let us now consider the critical loads corresponding to buckling. The expressions for the critical values follow from (5.3):

$$(\sigma_{22}^{r0})^{\text{cr}} = E_r(1-\nu_r^2)^{-1}(\varepsilon_{22}^{r0})^{\text{cr}},$$

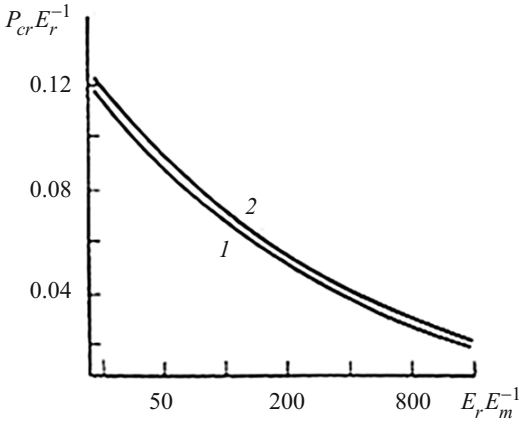

Fig. 5.4

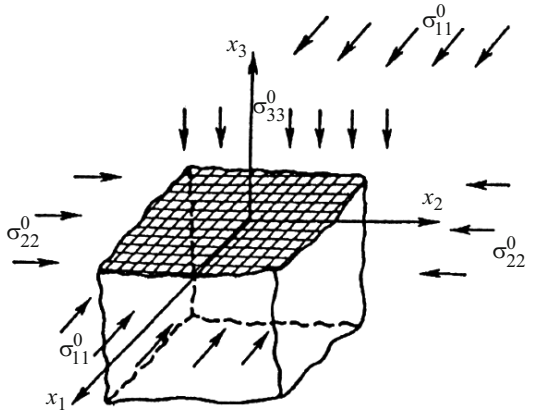

Fig. 5.5

$$(\sigma_{22}^{m0})^{\mathrm{cr}} = E_m (1-\nu_m^2)^{-1} (\varepsilon_{22}^{m0})^{\mathrm{cr}},$$

$$(\varepsilon_{22}^{r0})^{\mathrm{cr}} = (\varepsilon_{22}^{m0})^{\mathrm{cr}}. \tag{5.6}$$

In (5.6), $(\varepsilon_{22}^{r0})^{\mathrm{cr}}$ and $(\varepsilon_{22}^{m0})^{\mathrm{cr}}$ denote the critical compressive strains for the reinforcement and matrix at the end (Fig. 5.2), which are equal because the support plate is used. Figure 5.4 shows the dependence of

$$P_{\mathrm{cr}} \cdot E_r^{-1} = \left|(\sigma_{22}^{r0})^{\mathrm{cr}}\right| \cdot E_r^{-1} \tag{5.7}$$

on the parameter $E_r \cdot E_m^{-1}$ for $\nu_r = \nu_m = 0.3$ (curve *1*) and $\nu_r = 0.3$ and $\nu_m = 0.4$ (curve *2*). The logarithmic scale $\ln(E_r \cdot E_m^{-1})$ is used on the horizontal axis.

Remark 5.3. Noted that here we are discussing the results reported in [76] in connection with the following situation. The paper [76] was apparently the first to report on results on edge effects in the theory of stability of composites obtained using the piecewise-homogeneous material model and the TLTSDB. In the case of static problems for composites, many numerical results on edge effects obtained using a three-dimensional problem statement and the piecewise-homogeneous material model are presented in the 12-volume monograph [145, Vol. 1, Sec. III, Chs. 10–12, pp. 313–445], where the numerical method developed is also described in detail.

5.3.3. Continuum Approximation. Here we will briefly discuss results on brittle and ductile end-crush fracture of specimens or structural members made of composites modeled by homogeneous materials with effective parameters. The results being discussed are reported in a number of articles cited in the introduction (Sec. 5.1) and consistently reviewed in the monograph [57, Vol. 2, Ch. 11, Sec. 4, pp. 529–551).

The principles of the continuum theory of end-crush fracture of composites under compression are the following.

1. The general concept formulated in Sec. 5.3.1 is accepted: the initial stage (start) of end-crush fracture is near-surface buckling near the loaded end. The theoretical ultimate strength and theoretical ultimate strain corresponding to end-crush fracture are critical load and critical strain predicted by the TLTSDB.

2. The role of boundary conditions in end-crush fracture is the same as explained in Remark 5.1.

3. In studying the end crushing phenomenon, the effect of the lateral surfaces of a specimen or a structural member and the interaction of two opposite ends (long specimen) are disregarded, which makes it possible to analyze the lower half-space $x_3 \le 0$ (Fig. 5.5) where the end is cross-hatched.

4. In analyzing surface instability near the loaded end, the subcritical state is considered homogeneous. If the subcritical state is inhomogeneous, then local surface instability at each point of the end surface is analyzed (within a small neighborhood of this point). Thus, we again arrive at a homogeneous subcritical state.

5. The external normal compressive load applied to the end $x_3 = 0$ (Fig. 5.5) is dead. Thus, the applicability conditions for the static (Euler) method are satisfied for brittle and ductile fracture, according to Sec. 2.4.2.

6. Laminated and fibrous composites are considered. In laminated composites, plies are perpendicular to the end surface $x_3 = 0$. Fibrous composites are assumed unidirectionally or cross-reinforced provided that the primary reinforcement is aligned with the $0x_3$-axis (Fig. 5.5), i.e., perpendicular to the end surface $x_3 = 0$.

7. In the continuum approximation, such composites with polymer or metal matrix are modeled by homogeneous compressible orthotropic elastic or elastoplastic materials with effective constants whose axes of material symmetry coincide with the chosen coordinate axes (Fig. 5.5). In the transversely isotropic case, it is additionally assumed that the planes $x_3 = \text{const}$ are the planes of isotropy.

8. Only near-surface instability near the loaded end (cross-hatched in Fig. 5.5) when stresses and displacements decay as $x_3 \to -\infty$ is analyzed.

9. Theory 3 (as termed in Sec. 2.2) is used.

Principles 1–9 are used to develop a continuum theory of brittle and ductile end-crush fracture and a method for solving plane and spatial problems based on Fourier integrals. Specific results are obtained. These results are detailed in the monograph [57, Vol. 2, Ch. 11, Sec. 4, pp. 529–551]. We will briefly discuss only final results.

Denote

by $(\Pi_3^-)_{\mathrm{T}}^{\mathrm{br}}$ the theoretical ultimate strength against end-crush fracture under uniaxial compression along the $0x_3$-axis (Fig. 5.5);

by $(\Pi_3^-)_{\mathrm{T}}$ the theoretical ultimate strength against internal fracture under uniaxial compression along the $0x_3$-axis without crushing of the ends.

The final result obtained as a result of a rigorous analysis can be represented as

$$(\Pi_3^-)_{\mathrm{T}}^{\mathrm{br}} < (\Pi_3^-)_{\mathrm{T}}. \tag{5.8}$$

Inequality (5.8) is physically consistent and was repeatedly validated experimentally, suggesting that fracture of homogeneous materials starts on their surface. It should be noted that although Sec. 5 addresses composites, Sec. 5.3.3 considers the continuum approximation in which composites are homogeneous.

Despite the rigorously proved inequality (5.8), the quantities appearing in it differ insignificantly, which was also proved in the monograph [57, Vol. 2, Ch. 11, Sec. 4, pp. 529–551) for brittle and ductile end-crush fracture. To illustrate this situation, we will consider an example of brittle fracture.

Example. Consider a unidirectional fibrous composite with fibers directed along the $0x_3$-axis (Fig. 5.5) and disorder structure in the cross section ($x_3 = \text{const}$ in Fig. 5.5). If subject to brittle fracture, the composite is modeled by an elastic transversely isotropic material with isotropy planes being the planes $x_3 = \text{const}$ in Fig. 5.5. Using this modeling, the following expression (11.276) was derived in [57, Vol. 2, Ch. 11, Sec. 4, pp. 542–543]:

$$(\Pi_3^-)_{\mathrm{T}}^{\mathrm{br}} = (\Pi_3^-)_{\mathrm{T}}\left[1-\frac{G'^2}{EE'}(1-\nu^2)\left(1-\nu'^2\,\frac{E}{E'}\right)\right], \tag{5.9}$$

where E' is Young's modulus along the $0x_3$-axis; E is Young's modulus in the isotropy plane ($x_3 = \text{const}$); G' is the shear modulus along the fibers, $G' = G_{31} = G_{32}$. In the continuum approximation, the following conditions are satisfied for the unidirectional fibrous composite (as a material with low shear stiffness):

$$G' << E', \quad G' \approx E. \tag{5.10}$$

The relation below follows from (5.9) and (5.10):

$$(\Pi_3^-)_{\mathrm{T}}^{\mathrm{br}} \approx (\Pi_3^-)_{\mathrm{T}}. \tag{5.11}$$

A similar relation also holds for ductile fracture; however, the proof is much more awkward.

Conclusion. Relation (5.11) can be used to compare $(\Pi_3^-)_{\mathrm{ex}}^{\mathrm{br}}$ (experimental value of ultimate strength against end-crush fracture under uniaxial compression along the $0x_3$-axis) and $(\Pi_3^-)_{\mathrm{T}}^{\mathrm{br}}$, including two conditions.

One condition is that experimentally observed fracture must be end crushing (as the photograph in Fig. 5.1).

TABLE 5.1

Material VKA-1	Ultimate strength, MPa	
	$(\Pi_3^-)_{ex}^{br}$	$(\Pi_3^-)_T^{br}$
Annealed	665	736
Unannealed	1282	1467

The other condition is that $(\Pi_3^-)_{ex}^{br}$ is compared with $(\Pi_3^-)_T$ according to (5.11).

Let us apply the comparison procedure to annealed and unannealed unidirectional boron aluminum composite VKA-1, which was discussed in the example in Sec. 3.3.4.1. The first condition is satisfied by analyzing Fig. 5.1, while the second condition is satisfied by analyzing Table 5.1 [57, Vol. 2, p. 551, Table 11.8]. It should also be noted that the values of $(\Pi_3^-)_{ex}^{br}$ in Table 5.1 are averages over 32 annealed specimens and over 14 unannealed specimens (see [95] for more details).

This completes the brief analysis of results on problem 3 obtained at the Department of Dynamics and Stability of Continua of the S. P. Timoshenko Institute of Mechanics.